Universidad de Concepción
Dirección de Postgrado
Facultad de Ciencias Naturales y Oceanográficas

Sombras de surgencia en el golfo de Arauco: Formación y evolución en respuesta al forzamiento en distintas escalas de variabilidad

Tesis para optar al grado de
Doctor en Oceanografía

ZENEIDA ELIZABETH WONG CHANG
CONCEPCIÓN-CHILE
2022

Profesor Guía: Marcus Sobarzo Bustamante
Dpto. de Oceanografía, Facultad de Ciencias Naturales y Oceanográficas
Universidad de Concepción

Universidad de Concepción
Dirección de Postgrado

La Tesis de "*Doctorado en Oceanografía*" titulada *"SOMBRAS DE SURGENCIA EN EL GOLFO DE ARAUCO: FORMACIÓN Y EVOLUCIÓN AL FORZAMIENTO EN DISTINTAS ESCALAS DE VARIABILIDAD"*, de la Srta. *"ZENEIDA ELIZABETH WONG CHANG"* y realizada bajo la Facultad de Ciencias Naturales y Oceanográficas, Universidad de Concepción, ha sido aprobada por la siguiente Comisión de Evaluación:

Dr. Marcus Sobarzo
Profesor Guía
Universidad de Concepción _____

Dr. Fabián Tapia
Miembro Comité de Tesis
Universidad de Concepción _____

Dr. Gonzalo Saldías
Miembro Comité de Tesis
Universidad del Bío-Bío _____

Dr. John Largier
Miembro Comité de Tesis
Universidad de California, Davis _____

Dr. Iván Pérez
Evaluador Externo
Universidad de los Lagos _____

Dra. Pamela Hidalgo
Directora
Programas de Postgrados en Oceanografía
Universidad de Concepción _____

A mis padres Zeneida y Antonio quienes me dieron su amor,
paciencia y esfuerzos para culminar con éxito esta etapa académica.
A mis hermanos José y Rebeca por su apoyo, su cariño y sus palabras de aliento.

AGRADECIMIENTOS

El desarrollo de esta Tesis Doctoral se llevó a cabo gracias a la beca otorgada en mi primer año de estudios por la Red Doctoral en Ciencia, Tecnología y Ambiente (REDOC.CTA), el cual es un Convenio de Desempeño de MINEDUC, adjudicado por la Universidad de Concepción. Mi segundo, tercer y cuarto año fueron financiados por la Beca Doctoral para Extranjeros del Programa de Formación de Capital Humano Avanzado de CONICYT.

Quiero comenzar agradeciendo a Dios por haberme dado la oportunidad de cursar este programa de estudios, por haberme dado la fortaleza de seguir adelante y de contar con el apoyo de valiosas personas en cada etapa y cada uno de los desafíos, de diversa índole, que se presentaron a lo largo de este camino, obteniendo así este nuevo logro académico. También agradezco infinitamente a mis padres quienes me apoyaron incondicionalmente a pesar del dolor de ver a su primogénita alejarse de casa para estudiar en otro país.

Agradezco al Dr. Marcus Sobarzo por todo su apoyo y dedicación durante todo este proceso, desde que fui aceptada en el programa y solicité su respaldo para poder aplicar a la beca y luego aceptar ser mi profesor guía. Siempre mostró la mejor de las predisposiciones, ha sido un gran guía para mí en el ámbito académico, en cada paso, en cada escalón ha estado allí para apoyarme, guiarme, darme fuerzas y ánimo. Tanto él como su esposa Marcela me acogieron tan bien y supieron darme un gran soporte y apoyo en momentos claves de mi vida personal, ese cálido apoyo era lo que necesitaba para poder surgir y avanzar.

Agradezco a mis compañeros del programa con quienes formé lindas amistades y quienes fueron una gran compañía en el día a día, durante las horas de estudio y

concentración, y también durante las horas de relax y distracción en las que compartimos y aprendimos sobre la cultura y costumbres de los países de los cuales proveníamos. A los compañeros del laboratorio de Física costera con quienes formé maravillosas amistades y con quienes compartí muy gratos momentos.

También extiendo mis agradecimientos a Gonzalo Saldías quien me ayudó con la gestión de las pasantías en la Universidad Estatal de Oregón EE.UU., siendo un magnífico apoyo durante esas estadías, además de ser un notable apoyo en el proceso de elaboración de mi primera publicación. Agradezco al Dr. Ted Strub por recibirme en el College of Earth, Ocean, and Atmospheric Sciences de la Universidad Estatal de Oregón, y al Dr. John Largier por recibirme en el Bodega Marine Laboratory de la Universidad de California - Davis.

También quiero agradecer a mi amiga María Lucía quien ha estado ahí, con un abrazo, una sonrisa o una palabra de aliento siempre que lo he necesitado; y a mi amiga Ana Verónica, una mujer excepcional con quien he tenido las pláticas más largas y enriquecedoras, y quien no ha permitido que me rinda y me ha incitado a levantarme cuando mis fuerzas han mermado y he sentido que ya no podía más, una palabra, un consejo un gesto de amistad de su parte es capaz de devolverme al camino.

Quiero agradecer también a Fabiola Gaete por su maravillosa labor y por siempre estar atenta y presta a apoyar en lo que se requería, resolvió muchas de mis dudas y atendió un sin fin de peticiones, hasta lo último. Por último, mi agradecimiento a Mónica Sorondo una mujer maravillosa y ejemplar quien fue uno de mis primeros contactos en la Universidad desde la escuela de verano un año antes de comenzar mis estudios, y quien se preocupó de que mi estadía sea agradable y productiva; y sin importar los distintos caminos que depare el destino ella es una persona con la que siempre se puede contar.

Curriculum Vitae

Zeneida Elizabeth Wong Chang

Nacida el 13 de Diciembre de 1984, en Guayaquil, Ecuador

2002 - 2008: Oceanógrafa, Escuela Superior Politécnica del Litoral, Ecuador.
2013 - 2022: Doctor en Oceanografía, Universidad de Concepción, Chile.

PUBLICACIONES

- Wong, Z., Saldías, G. S., Largier, J. L., Strub, P. T., Sobarzo, M. (2021). Surface thermal structure and variability of upwelling shadows in the Gulf of Arauco, Chile. Journal of Geophysical Research: Oceans, 126(4), e2020JC016194.

- Mardones, P., Wong, Z., Contreras-Rojas, J., Muñoz, R., Hernández-Miranda, E. and Sobarzo, M. Upwelling Shadows driven by the Low-Level Jet along the Subtropical West Coast of South America: Gulf of Arauco, Chile. Artículo enviado a JGR: Oceans.

ÁREAS DE INVESTIGACIÓN

Principal: Oceanografía Física Costera.
Secundaria: Oceanografía Física.
Otras: Meteorología y clima

EXPERIENCIA DOCENTE

- Año 2005: Matemáticas I para Oceanografía y Acuacultura. Ayudante de curso - ESPOL.

- Año 2005: Matemáticas II para Oceanografía y Acuacultura. Ayudante de curso - ESPOL.
- Año 2006: Taller Náutico para Oceanografía y Acuacultura. Ayudante de curso - ESPOL.
- Año 2006: Matemáticas III para Oceanografía. Ayudante de curso - ESPOL.
- Año 2014: Ayudante curso de R. Ayudante en curso de Biología Marina - UdeC.
- Año 2015: Oceanografía Física para Biología Marina. Ayudante en curso de oceanografía - UdeC.

CRUCEROS OCEANOGRÁFICOS

- Abril 2009. BAE-ORION. Instituto Oceanográfico de la Armada, Ecuador.
  CRUCERO OCEANOGRÁFICO INSULAR. Oceanografía Física: manejo y procesamiento de datos del ADCP

- Sep-Oct 2008. BAE-ORION. Instituto Oceanográfico de la Armada, Ecuador.
  XI CRUCERO OCEANOGRÁFICO REGIONAL DEL PACÍFICO SUR ORIENTAL
  Proyecto: Caracterización de la corriente de Cromwell o Sub-corriente Ecuatorial (SCE) entre 92_00'W – 89_00'W – 0.5_N

ESTADÍAS DE INVESTIGACIÓN O ENTRENAMIENTO

- College of Earth, Ocean, and Atmospheric Sciences. Corvallis, Oregón, USA. Análisis y procesamiento de datos satelitales (Jul-Ago 2016).
- Visita Académica a Bodega Marine Laboratory UC-DAVIS (Bodega Bay, California, USA. Ago/2016).

RESUMEN

Sombras de surgencia en el golfo de Arauco: formación y evolución en respuesta al forzamiento en distintas escalas de variabilidad

Zeneida Elizabeth Wong Chang
Doctorado en Oceanografía
Universidad de Concepción, 2021
Dr. Marcus Sobarzo Bustamante, Profesor Guía

El estudio del golfo de Arauco (GA) ha tenido un particular interés debido a sus características físicas, biológicas, batimétricas, topográficas y especialmente por ser parte de una de las zonas de surgencia más importantes del centro-sur de Chile. Además, al ser una bahía semicerrada, protegida de los vientos favorables a surgencia, la dinámica del golfo incluye un proceso conocido como sombra de surgencia (SS), el cual consiste en una piscina de agua cálida localizada entre la costa y el agua fría de la surgencia costera (SC). Esto origina anomalías positivas de temperatura superficial del mar (TSM) de aproximadamente 2°C en la zona del GA que está más protegida del viento. Las SS han sido estudiadas en otras zonas de surgencia con distintos enfoques, los cuales proponen algunos de los principales mecanismos que explican el calentamiento costero superficial, tales como las variaciones espaciales en el campo de vientos favorables a surgencia y, durante periodos de relajación, la radiación solar entrante y la advección tienen un papel fundamental. También, un rotor del viento positivo (en el HN) crea un gradiente de presión y una corriente cercana a la costa con dirección hacia el polo dentro de la zona de surgencia. Debido a la importancia de estos sistemas, también se han estudiado algunos aspectos biológicos como las floraciones de algas nocivas.

El aporte de esta tesis doctoral se orientó a ampliar el conocimiento sobre el mecanismo de formación y evolución de los eventos de sombra de surgencia, específicamente dentro del Golfo de Arauco, evaluando las características radiativas y la variabilidad tanto del esfuerzo del viento como del rotor del viento en Chile centro-sur y su contribución en la sombra de surgencia. Además, se evalúan fenómenos atmosféricos de escala sinóptica y su impacto en las sombras de surgencia. Para ello, en esta tesis se utilizaron diversas fuentes de datos satelitales (GOES y GSST1) diarios de TSM, así como datos de flujo de calor y de vientos del producto de reanálisis ERA5; y como complemento se usaron datos de estaciones meteorológicas locales, así como información de corrientes y temperatura de anclajes dentro del área de estudio.

Se desarrolló un Índice de Sombra de Surgencia (USI) en base a diferencias de TSM entre el GA y la región costa afuera de Punta Lavapié (PL), la cual se destaca por ser un área de fuerte surgencia. Los resultados mostraron que las SS son más frecuentes en primavera/verano con vientos favorables a surgencia y acompañados de un intenso rotor ciclónico del estrés del viento. Según la época del año, las SS pueden desarrollarse en un ambiente frío (Ej. noviembre) o en un ambiente cálido (Ej. enero), lo que modifica la intensidad y duración de estos eventos. Estas dos últimas características también son afectadas por la radiación solar entrante que, sumada a la lenta circulación al interior del GA, causa la estratificación de la columna de agua, aumentando así el tiempo de residencia del agua cálida dentro del golfo. Períodos de relajación del viento favorable a surgencia conllevan al debilitamiento o desvanecimiento del gradiente de la SS. Una relajación corta resulta en la advección de agua fría de surgencia desde el norte hacia el interior del GA, mientras que períodos de relajación mayor a una semana resultan en el calentamiento de toda la región, desvaneciendo así la señal de la SS.

A través del análisis de fenómenos atmosféricos de escala sinóptica se propone que los anticiclones migratorios (ACM) que se desplazan de oeste a este al sur de Chile y que favorecen la formación e intensificación del chorro costero (CLLJ) responsable de gatillar

la surgencia costera al oeste de PL, induce un área cálida de baja presión conocida como bajas costeras (BC). La presencia de estas BC influye en el incremento la TSM dentro del GA. Una BC completamente desarrollada provoca el debilitamiento de los flujos convectivos netos que también contribuyen al incremento de TSM dentro del golfo, magnificando la SS. Hacia el norte de la BC se forma un gradiente en sentido opuesto dando paso a vientos desde el norte que disminuyen la intensidad del CLLJ retornando el sistema a sus condiciones iniciales. Por otro lado, las tasas de calentamiento observadas al interior del GA sugieren que la advección meridional solo explica parcialmente el incremento de temperatura en la SS.

Palabras claves: Sombra de surgencia, TSM, rotor del viento, chorro costero, anticiclones migratorios, bajas costeras, bahías semicerradas, Golfo de Arauco, Chile central, balance de calor.

ABSTRACT

Upwelling shadows in the Gulf of Arauco: Formation and evolution in response to different scales of variability

Zeneida Elizabeth Wong Chang
Doctorate in Oceanography
Universidad de Concepción, 2021
Dr. Marcus Sobarzo Bustamante, Advisor

The study of the Gulf of Arauco (GA) has been of particular interest due to its physical, biological, bathymetric, topographic characteristics and specially because it is part of one of the most important upwelling areas in south-central Chile. In addition, as it is a semi-enclosed bay, protected from upwelling favorable winds, the dynamics into the gulf includes a process known as upwelling shadow (US), which consists of a pool of warm water located between the coast and the cold water of the coastal upwelling (CU). This results in positive sea surface temperature (SST) anomalies of about 2°C in the section of the Gulf of Arauco that is most protected from the wind. US have been studied in other upwelling regions under various approaches, which have proposed some principal mechanisms that explain coastal surface warming such as spatial variations of upwelling favorable winds and, during relaxation periods, incoming solar radiation and advection play a fundamental role. Also, a wind stress curl (positive at NH) creates a pressure gradient and a subsequent nearshore current in a poleward direction within the upwelling zone. Due to the importance of these systems, some biological aspects such as harmful algal blooms have also been studied.

The contribution of this doctoral thesis is aimed at expanding the knowledge about the mechanism of formation and evolution of the US events, specifically within the GA, evaluating the radiative characteristics and the variability of both the winds stress and wind stress curl in south-central Chile, and its contribution to the US phenomenon. In addition, synoptic scale atmospheric phenomena and their impacts on US are evaluated. To do this, this thesis used various sources of satellite data (GOES \& GSST1) of daily SST, as well as heat fluxes and wind data from the reanalysis product ERA5; and as a complement, data from local meteorological stations were used, as well as data on currents and temperature from moorings deployed within the study area.

An upwelling shadow index (USI) was developed, based on SST differences between the GA and the region off Punta Lavapié (PL), which stands out for being an active upwelling area. The results showed that US are more frequent in spring/summer with upwelling favorable winds and a strong cyclonic wind stress curl. Depending on the time of the year, US can take place in a cold environment (e.g., November) or in a warm environment (e.g., January), which modifies intensity and duration of these events. These last two characteristics are also affected by the incoming solar radiation that, added to the slow circulation inside the GA, causes the stratification of the water column, thus increasing the residence time of the warm water within the gulf. Relaxation periods of upwelling favorable winds lead to the weakening or vanishing of the US thermal gradient. Brief relaxations cause an advection of cold upwelled water from the north into the GA, while relaxation periods longer than a week result in the heating of the entire region, thus fading the US signal.

Through the analysis of synoptic-scale atmospheric phenomena, it is proposed that migratory anticyclones (MA) that drift eastward in Southern Chile, and that favor the formation and intensification of the coastal low-level jet (CLLJ) that triggers coastal upwelling off PL, lead to a warm low-pressure area known as a coastal low (CL). The presence of these CLs influences the increase in SST within the GA. A CL in its mature

state causes a weakening of the net convective fluxes that also contribute to the SST increasing and consequently enhancing the US. North of the CL, a pressure gradient in the opposite direction is generated, diminishing the CLLJ and returning the system to its initial condition. On the other hand, the warming rates observed within the GA suggest that meridional advection of warm water only partially explain the temperature increase in the US.

Keywords: Upwelling shadow, SST, wind stress curl, coastal low-level jet, migratory anticyclones, coastal lows, semi-enclosed bays, Gulf of Arauco, central Chile, heat balance.

INDICE

INDICE DE FIGURAS

1. INTRODUCCIÓN

1.1. Anticiclón del Pacífico Sur

El anticiclón del Pacífico Sur (APS) es un centro de alta presión atmosférica formado sobre la cuenca del océano Pacífico sur en respuesta a la celda de Hadley, encargada de distribuir el calor desde el Ecuador hacia latitudes medias (Inzunza, 2012). En promedio el centro del APS se encuentra en torno a 30°S y 100°O (Figura 1). Al ser un centro de alta presión, el aire fluye desde el centro hacia afuera (bajas presiones) y con rotación antihoraria, debido a la dirección de la fuerza de Coriolis en el hemisferio sur. Su presencia intensifica los vientos alisios en el Ecuador y los vientos que fluyen de sur a norte paralelos a la costa forzando el sistema de corrientes de Humboldt (Strub et al., 1998; Inzunza, 2012; Ancapichún, 2012; Ancapichun, 2015). La dinámica de este anticiclón incluye ciclos a escala estacional, interanual, e interdecadal (Ancapichún, 2012; Ancapichun, 2015). Además, un tren de ondas de altas y bajas presiones (en latitudes medias en el hemisferio sur) asociado con un mayor calentamiento de la región de la Zona de convergencia Subtropical durante el verano austral (DEF) resulta en anomalías positivas de la presión atmosférica a nivel del mar que se proyectan sobre el centro del APS causando un aumento de su área y fortaleciendo los asociados al mismo (Fahad et al., 2020), lo que podría explicar la variabilidad del APS a escala sinóptica.

El APS se caracteriza por presentar gran estabilidad atmosférica y es considerado un sistema semipermanente ya que la intensidad y ubicación de las isóbaras cambian de acuerdo a las variaciones de temperatura a lo largo del año, resultando en un desplazamiento estacional de su centro entre 25°S y 35°S (Figura 2). Además, presenta una intensidad máxima dos veces en el año. Durante el mes de mayo se ubica alrededor de 26°S y 86°O presentando su máxima intensidad frente a La Serena (29.91°S, 71.27°O), mientras que entre los meses de febrero y marzo el APS alcanza su posición más austral (~37°S, ~108°O aproximadamente) con su máxima intensidad frente a la costa centro-sur

de Chile (Ancapichún, 2012; Ancapichun, 2015), favoreciendo la formación e intensificación de los vientos favorables a surgencia en esta región (Rutllant et al., 2004; Ancapichun, 2015; Weidberg et al., 2020). El proceso de subsidencia que forma parte del anticiclón limita la formación de nubes por lo cual el APS se relaciona inversamente con el régimen de precipitación a lo largo de Chile, es decir a mayor intensidad del anticiclón, menor precipitación (Rutllant y Fuenzalida, 1991; Barrett, 2017).

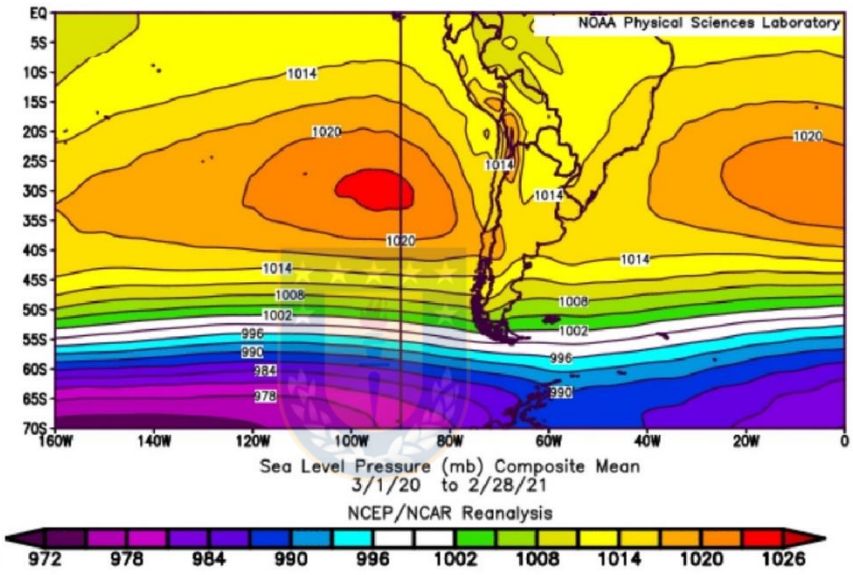

Figura 1 Anticiclón del Pacífico. Compuesto promedio (Mar/2019 a Feb/2020) de la presión a nivel del mar, en milibares. (Fuente: NCEP/NCAR Reanalysis - https://psl.noaa.gov/data/composites/day/)

A escala interanual e interdecadal, la intensidad y posición del APS son influenciadas por patrones climáticos de mayor escala. El Niño-Oscilación del Sur (ENOS) representa casi el 50% de variabilidad interanual en la región. Este patrón climático se correlaciona de forma inversa con el APS, de modo que durante fases positivas del ENOS (eventos El Niño) los valores de presión del anticiclón disminuyen (Ancapichun, 2015), reduciendo su intensidad y con ello debilitando también los eventos de surgencia costera, ya que al profundizarse la termoclina debido al ENOS, el agua que

asciende a la superficie es menos fría de lo normal (Blanco et al., 2002). Por el contrario, durante fases frías del ENOS (La Niña), el APS se intensifica fortaleciendo las surgencias costeras que advectan aguas más frías hacia la superficie.

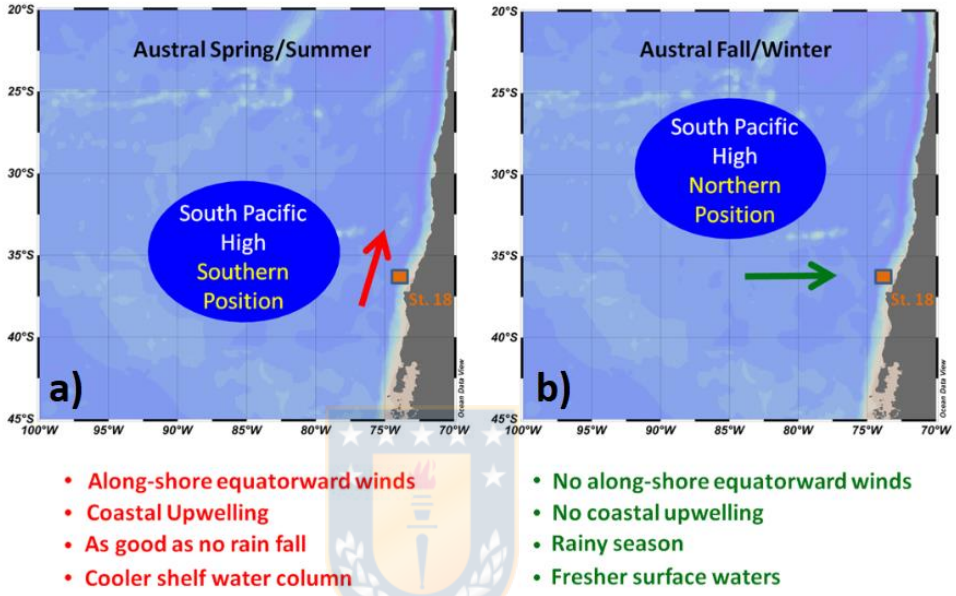

Figura 2 Anticiclón del Pacífico Sur. a) Posición típica de verano/primavera austral del APS con vientos costeros frente a la costa de Chile centro-sur. b) Posición típica de otoño/invierno austral del APS con vientos zonales frente a la costa de Chile centro-sur. El recuadro naranja marca la ubicación de la estación 18 del Centro COPAS de la Universidad de Concepción. Fuente: Schneider et al. (2017).

A escala de toda la cuenca del Pacífico (con mayor énfasis en el Pacífico Norte) se ha definido un patrón de variabilidad climática parecido a un evento El Niño de larga duración conocido como Oscilación Decadal del Pacífico (ODP) que, al igual que el ENOS, varía entre una fase fría y una fase cálida. En referencia al Pacífico Sur, la fase cálida está caracterizada por anomalías positivas de temperatura superficial del mar (TSM) en la costa oeste de América del Sur, con respuestas del anticiclón a estos cambios similares a los eventos ENOS. Tanto el ENOS como la ODP afectan el campo de presiones del APS provocando anomalías en la magnitud y dirección de los vientos a gran escala.

1.2. Anticiclones Migratorios

Los anticiclones migratorios (ACM) se forman a nivel superficial en respuesta a la circulación en la tropósfera libre, es decir por sobre la capa límite marina (alturas mayores a 1000 m). Los niveles de presión varían a lo largo de la atmósfera, tanto horizontal como verticalmente, generando gradientes de presión en ambas direcciones. La altura de un nivel específico de presión se conoce como altura geopotencial. De acuerdo con la ecuación hipsométrica (Wallace y Hobbs, 2006), la distribución espacial de las líneas de igual altura geopotencial (i.e. isohipsas) depende de las variaciones de temperatura. Por lo tanto, en latitudes con mayor temperatura la altura geopotencial aumenta, mientras que en zonas frías esta altura disminuye (Figura 4). Esto conlleva a la formación de ondas de altura geopotencial, principalmente en latitudes medias (donde el gradiente térmico horizontal en la atmósfera es mayor), las cuales presentan dorsales y vaguadas (Holton, 1973; Wallace y Hobbs, 2006). Estas dorsales también se conocen en la literatura como "midlevel ridges"(Rutllant, 1994; Garreaud et al., 2002).

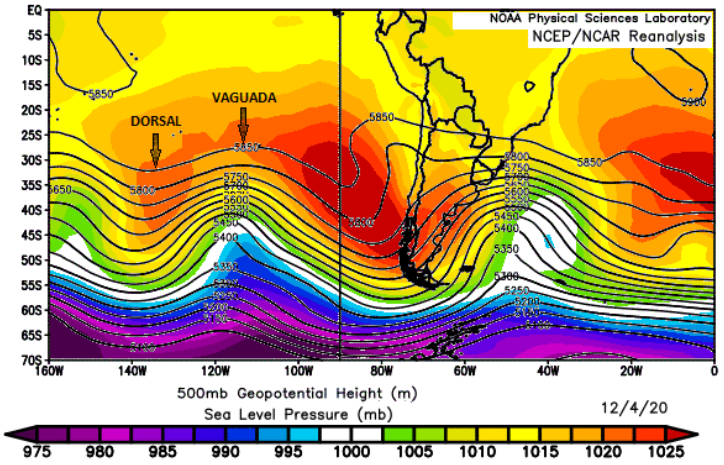

Figura 3 Presión superficial a nivel del mar (escala de colores) y contornos de y contornos de altura geopotencial (isohipsas) de la isobara de 500 mb (líneas negras), para el día 4 de diciembre de 2020. La altura de las isohipsas es menor hacia los polos (~5100 m) y aumenta hacia el Ecuador (~5900 m). Fuente: NCEP/NCAR Reanalysis - https://psl.noaa.gov/data/composites/day/). Nota: Se unificó imágenes de ambas variables.

La circulación en altura (mayor a 1000 m) está definida por el balance geostrófico de los vientos respecto a los gradientes asociados a estas ondas de altura geopotencial. Los vientos geostróficos son paralelos a las isóbaras y por efecto de la vorticidad absoluta (relativa más planetaria) tienen una tasa de rotación distinta en los ejes de vaguadas y dorsales, de modo que experimentan una rotación lenta en la dorsal y una rotación rápida en la vaguada. En la Figura 4 se puede observar cómo esta diferencia en la velocidad de rotación crea zonas de divergencia (alta presión) en la pre-vaguada causando un ascenso de aire y formando una zona de baja presión a nivel superficial. En la pre-dorsal, por otra parte, al pasar de una velocidad de rotación lenta a una rápida, se crea una zona de convergencia, obligando al aire a descender, formando un área de alta presión a nivel superficial (Holton, 1973; Wallace y Hobbs, 2006). Estos procesos de conservación de la vorticidad y advección vertical son los que contribuyen a la formación de los sistemas de bajas y altas presiones a nivel superficial, también conocidos como ciclones y anticiclones migratorios, respectivamente.

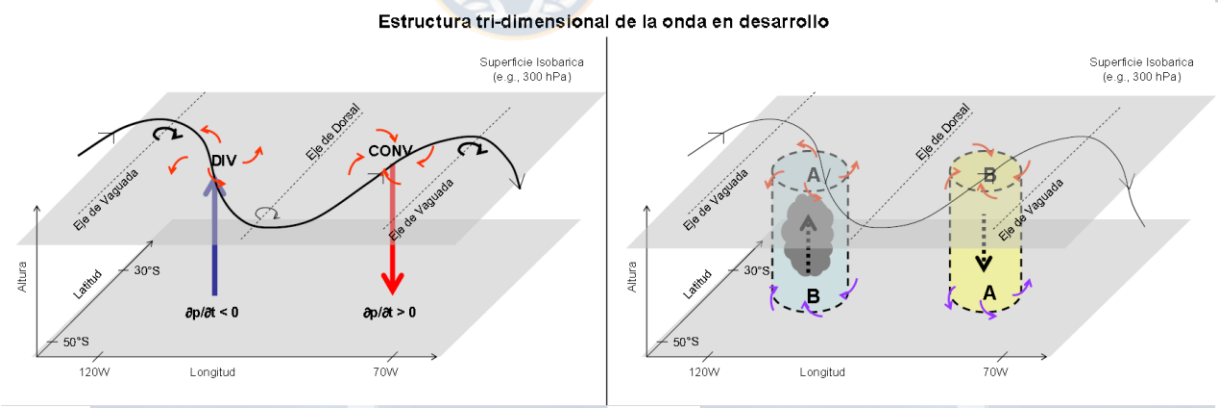

Figura 4. Esquema de formación de los sistemas de altas y bajas migratorias (Fuente: Curso Meteorología Sinóptica: Ciclogénesis y Frontogénesis. Universidad de Chile, Dpto. de Geofísica. Prof. René Garreaud Salazar)

En las costas de Chile, el paso de los anticiclones migratorios ha sido asociado con la intensificación de eventos de surgencia costera al fortalecer los vientos que la originan (Renault et al., 2012; Aguirre et al., 2019). También los anticiclones migratorios se

consideran forzantes de los chorros costeros de bajo nivel o CLLJ (por sus siglas en inglés) (Renault et al., 2012; Rahn y Garreaud, 2014; Aguirre et al., 2021), y se han asociado con la formación de vientos del este, ladera abajo en la zona centro y sur de Chile (Rutllant y Garreaud, 2004; Montecinos et al., 2017).

1.3. Bajas Costeras

La baja costera (BC) es un fenómeno de baja presión y de escala sinóptica que se desarrolla frente a las costas de Chile centro-sur. Su origen se debe en gran parte a un marcado calentamiento adiabático de la troposfera inferior (Garreaud et al., 2002; Garreaud, 2003) asociado al paso de anticiclones migratorios hacia el sur de 40°S. La BC se desplaza de norte a sur cerca de la costa entre 27°S y 37°S, extendiéndose hasta 42°S durante el verano austral (Rutllant, 1994; Rutllant y Garreaud, 1995; Garreaud et al., 2002), alcanzando una extensión aproximada de 500 y 1000 km en dirección costa afuera y a lo largo de la costa, respectivamente (Rutllant, 1994; Rutllant y Garreaud, 1995; Garreaud et al., 2002). Algunos de los factores que complementan la generación de este fenómeno incluyen la posición del APS y el chorro costero de bajo nivel asociado, la orientación de la línea de costa y la presencia de la cordillera de los Andes, que se levanta por sobre los 4000 m de altura. Estos dos últimos aspectos orográficos les dan características únicas respecto a las costas de Sudáfrica, donde también se forman BC (Rutllant, 1994; Garreaud et al., 2002).

Estos eventos se forman típicamente por el paso de los anticiclones migratorios (ACM, descritos en la sección 1.2) alrededor de 40°S, lo cual provoca un aumento de la presión atmosférica a nivel del mar (PANM). Cuando estos ACM llegan a la costa de Sudamérica, se presentan anomalías negativas del gradiente de presión a lo largo de la costa hacia el Ecuador, pasando de un gradiente hacia el polo a un gradiente hacia el Ecuador. Considerando que durante el verano austral el APS se encuentra en su posición más al sur, el arribo del ACM resulta en un alargamiento del APS hacia el este, ingresando

al continente (Figura 5b) y dejando un centro de baja presión entre el APS y la cordillera de los Andes, representado por la L en la Figura 5 b (Garreaud et al., 2002).

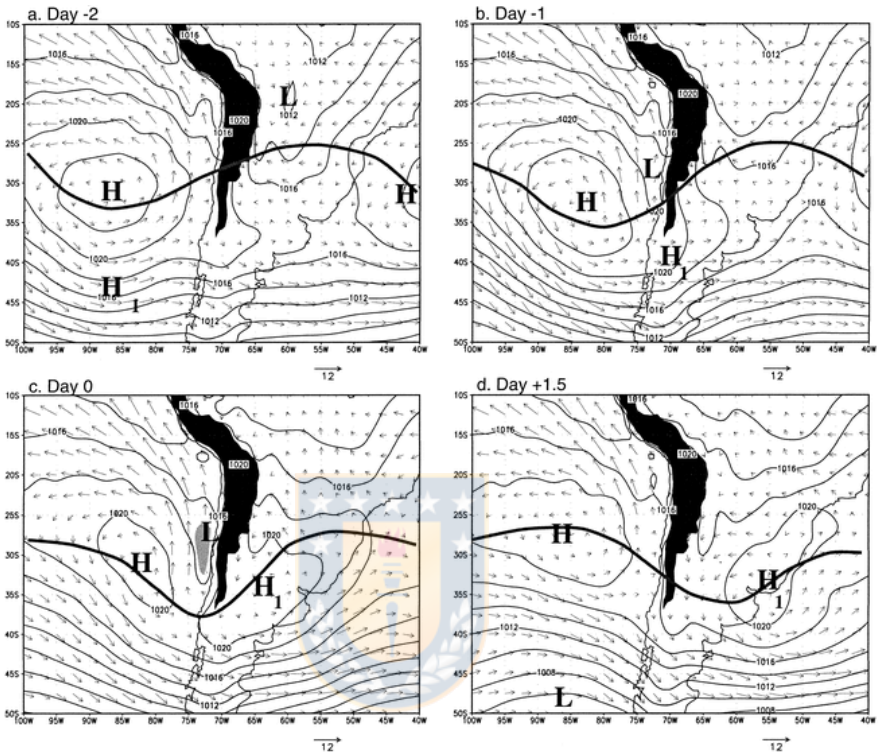

Figura 5. Compuestos de la presión a nivel del mar (contornos cada 2 hPa) y vientos a los 1000 hPa (flechas) en los días a) -2, b) -1, c) 0, y d) +1.5. La línea gruesa y sólida es la altura geopotencial de 5680m a 500 hPa. En el fondo de cada panel se muestra la referencia del vector de viento (en m/s). El área negra indica elevaciones de terreno mayores a 2000 m. Centros de alta y baja presión se indican por las letras H o L respectivamente. H1 indica el centro del anticiclón migratorio. El sombreado claro en el día 0 indica presión de nivel mar menores a 1016.5 hPa (Garreaud et al., 2002)

Cuando el ACM se desplaza hacia el noreste de los Andes se forma una estructura entre el APS y el ACM (Figura 5c) que intensifica más el gradiente de PANM tanto en sentido zonal como meridional. Estos gradientes también afectan la intensidad y dirección de vientos. Debido a la presencia de la cordillera de los Andes, que impide que el aire fluya libremente en los niveles bajos, el viento está solo en balance semigeostrófico (Garreaud et al., 2002), de modo que el viento que no puede circular zonalmente, lo hace

meridionalmente fortaleciendo aún más los vientos del sur que están asociados al chorro costero a lo largo de la costa entre 150-200 m sobre la superficie. Sin embargo, por sobre la cordillera los vientos se encuentran en balance geostrófico con las anomalías de altura geopotencial permitiendo el libre flujo desde el este (Garreaud et al., 2002). El desbalance a nivel superficial es complementado por un flujo de aire que desciende por la cordillera. Al descender esta capa de aire experimenta mayor presión del entorno, se comprime y se calienta adiabáticamente (Figura 6), acentuando el gradiente de presión con dirección hacia el polo, lo que mejora tanto el flujo del este a bajo nivel como el calentamiento adiabático, dando paso a la formación de una BC completamente desarrollada (BCD de aquí en adelante) que se extiende más al sur de 35°S (Garreaud et al., 2002; Garreaud, 2003).

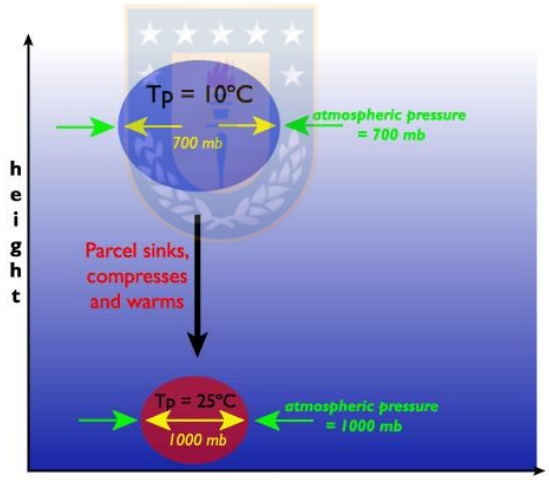

Figura 6. Esquema referencial del enfriamiento y calentamiento adiabático. Cuando el aire es obligado a ascender, se expande y disminuye su temperatura; si es obligado a descender su temperatura aumenta debido a la compresión. Fuente: https://geography.name/the-adiabatic-process/

La presencia de este flujo proveniente del este inhibe la formación de nubes estratocúmulus propia de la costa subtropical de Sudamérica. Este tipo de nubes definen el borde superior de la capa límite marina (CLM), que también es afectada por la presencia de la BCD. Antes de la BCD, la CLM es una capa mezclada homogéneamente entre la superficie y los 950 hPa (~ 520 a 610 m de altura cerca de la costa de Chile entre 35°S y

39°S), de características frías, con valores de temperatura potencial alrededor de 10°C y cielos nublados. Durante la BCD (Día 0 en la Figura 5), una región de cielos despejados se expande costa afuera debido al flujo hacia el oeste (Figura 7), cuyo calentamiento adiabático asociado genera una disminución de la presión superficial. Estas condiciones causan la reducción de la CLM, al punto de desaparecer completamente el día 0, presentándose así un calentamiento generalizado a lo largo de la tropósfera, con las mayores diferencias (~ 6°C) entre 900 hPa y 800 hPa (Garreaud et al., 2002).

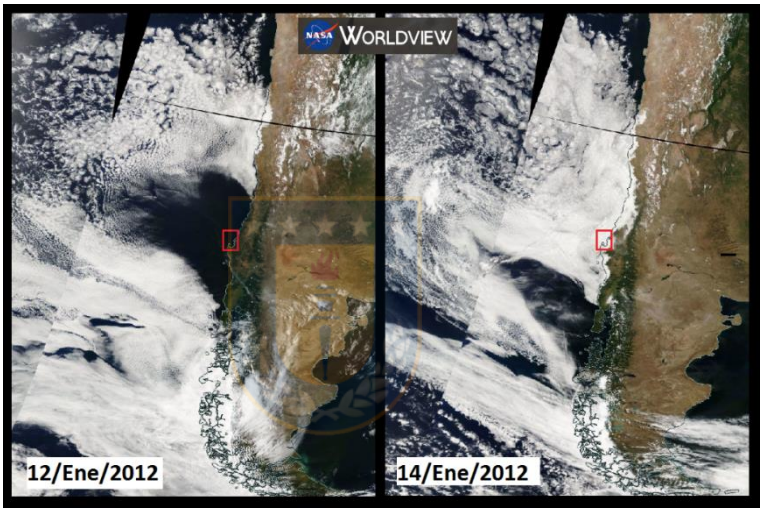

Figura 7. Imágenes satelitales de nubosidad durante una BC (izquierda) y después de la misma (derecha). El recuadro rojo indica ubicación del golfo de Arauco. Fuente: https://worldview.earthdata.nasa.gov/

Hacia el norte de 25°S, la presencia de la BCD genera al mismo tiempo un gradiente de presión hacia el Ecuador, el cual por balance geostrófico forma un flujo hacia la costa que es bloqueado por la cordillera. Estas condiciones dan inicio a la recuperación de la CLM. A medida que el ACM continúa desplazándose hacia el este, hacia el norte de Argentina/sur de Brasil, el gradiente de presión hacia el sur de Chile comienza a disminuir. Eventualmente el gradiente entre los subtrópicos y las latitudes medias vuelve a estar orientado hacia el Ecuador y los vientos a gran escala nuevamente fluyen hacia la costa terminando así la BC y permitiendo que el sistema recupere sus condiciones iniciales. El chorro costero disminuye su intensidad, los cielos despejados son cubiertos nuevamente

por los estratocúmulos (Figura 7) que se desplazan de norte a sur y la CLM vuelve a estar homogénea a lo largo de la tropósfera inferior (Garreaud et al., 2002).

1.4. Surgencia Costera

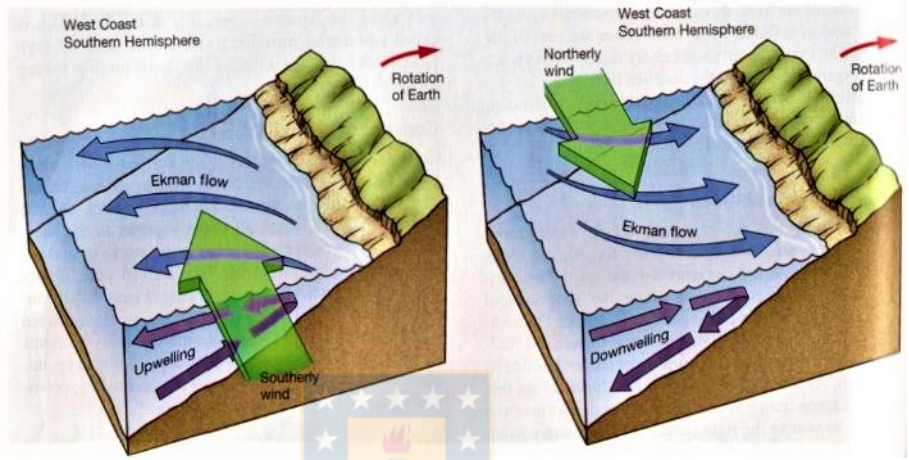

Figura 8. Esquema del proceso de surgencia y de hundimiento costero en el hemisferio sur. Adaptación de Thurman y Trujillo, 2004

Las regiones de borde oriental de los giros subtropicales que están más alejadas de la costa, se caracterizan por presentar un flujo débil y poco profundo. Sin embargo, corrientes de corto periodo o cercanas a la plataforma presentan un flujo fuerte que es independiente del régimen de los giros, esta circulación en el océano es gobernada por el esfuerzo del viento a lo largo de la costa (Tomczak y Godfrey, 2003; Talley, 2011). En Chile, los vientos que se dirigen hacia el Ecuador, por efecto de la fuerza de Coriolis generan transporte Ekman costa afuera del agua costera superficial, induciendo la surgencia costera (Stewart, 2008; Talley, 2011) (Figura 8). Además de los vientos, la configuración de la línea de costa junto con la topografía del fondo marino asociado también influye en la formación de la surgencia (Talley, 2011).

El agua cálida superficial que ha sido advectada costa afuera es reemplazada por agua subsuperficial más fría (por ejemplo ~ 100 m de profundidad en la zona frente a PL).

En la Figura 9 se muestra un esquema de la surgencia para el hemisferio sur. La distancia costa afuera del frente de advertida surgencia se relaciona directamente con el ancho de la plataforma continental, para el caso de Chile-central, varía entre 5 km en 38°S y ~105 km a la altura de 35.5°S Letelier et al. (2009). Sin embargo, la surgencia puede extenderse a más de 200 o 300 km hacia debido a la presencia de remolinos, meandros, filamentos y el chorro costero Letelier et al. (2009). La duración e intensidad del viento juegan un rol importante, a mayor intensidad del esfuerzo del viento se generará un mayor transporte de Ekman costa afuera (Bakun, 1991; Tomczak y Godfrey, 2003; Stewart, 2008; Talley, 2011). El agua fría de la surgencia es rica en nutrientes, lo cual promueve la alta productividad biológica en estas áreas (Stewart, 2008; Talley, 2011). Debido a sus condiciones frías, el agua de surgencia modifica el clima a lo largo de la costa (Talley, 2011).

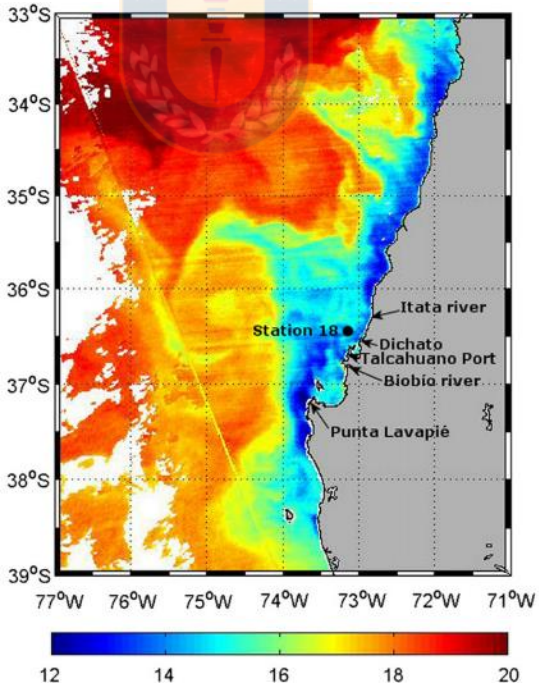

Figura 9. Evento de surgencia costera frente a las costas de Chile. Imagen satelital de TSM durante el verano austral (21/mar/2005). Fuente: Sobarzo et al. (2007).

A nivel global existen cinco regiones de surgencia costera que forman parte de los Sistemas de Corrientes de Borde Oriental. El sistema de surgencia chileno forma parte de

uno de ellos (Strub et al., 1998), destacando la zona costera adyacente al golfo de Arauco como una de las regiones de surgencia más importantes de la costa chilena debido a la combinación de vientos provenientes del suroeste y a la batimetría local (Figueroa y Moffat, 2000). Varios estudios a lo largo de la costa de Chile se han centrado en el proceso de surgencia y en la dinámica costera asociada (Fonseca, 1985; Figueroa y Moffat, 2000; Sobarzo y Djurfeldt, 2004; Aiken et al., 2008; Letelier et al., 2009; Bravo et al., 2013).

El régimen de vientos frente a las costas de Chile está gobernado por el desplazamiento del APS (Sobarzo et al., 2007). Durante el verano austral el APS alcanza su posición más hacia el sur (Letelier et al., 2009; Ancapichun, 2015) lo cual resulta en una mayor variabilidad de los vientos, principalmente entre los 30°S y 40°S (Letelier et al., 2009). La formación del chorro costero de bajo nivel asociado al paso de ACM alrededor de 40°S fortalece, aún más, los vientos paralelos a la costa que fluyen hacia el Ecuador. La intensificación de estos vientos da paso a la formación de la surgencia costera en esta zona (Rutllant et al., 2004; Sobarzo et al., 2007; Aguirre et al., 2012; Ancapichun, 2015) (Figura 9).

1.5. Sombra de Surgencia

Las sombras de surgencia se caracterizan por presentar anomalías positivas de TSM al interior de bahías orientadas hacia el Ecuador y que están protegidas parcial o totalmente del viento (Figura 10). Graham (1993) definió este fenómeno sobre la base de patrones superficiales particulares de TSM que mostraron anomalías positivas hacia la costa del frente de surgencia, en el extremo más protegido de la bahía de Monterey (36°N, 122°O) (bahía orientada hacia el Ecuador). La presencia de esta agua cálida presentó buena correlación con la fase activa de la surgencia (Graham y Largier, 1997) y fue explicada debido al calentamiento ocasionado por el aumento del tiempo de residencia de dichas aguas en áreas someras cerca de la orilla (Figura 11). La sombra de surgencia se puede reconocer por la presencia de un fuerte gradiente de temperatura superficial

transversal a la costa, con anomalías positivas de TSM (~ >2°C) y agudos gradientes horizontales de densidad (~0.2 kg/m3 x km) (Graham et al., 1992; Graham, 1993; Letelier et al., 2009). La extensión espacial de la sombra de surgencia está asociada a la interacción del viento y corrientes con la topografía de la costa y, dado que está asociado a la surgencia, el debilitamiento de vientos favorables a surgencia resulta en variaciones en la extensión de la sombra de surgencia (Graham y Largier, 1997).

Las sombras de surgencia son de interés debido a que sus características físicas particulares ayudan a que dichas regiones presenten un incremento en la actividad biológica (Graham et al., 1992; Graham y Largier, 1997; Marín et al., 2001). Desde este punto de vista, el golfo de Arauco es conocido por su gran productividad biológica y, al igual que otras zonas de sombra de surgencia, puede actuar como sitio de retención para el plancton (Landaeta y Castro, 2006). En general, bahías orientadas hacia el norte que enfrentan el Ecuador a lo largo de la región de surgencia chilena, como la bahía de Tongoy (cerca de 30°S) y bahía de Mejillones (~23°S), parecen jugar un rol similar (Castilla et al., 2002; Marín et al., 2003).

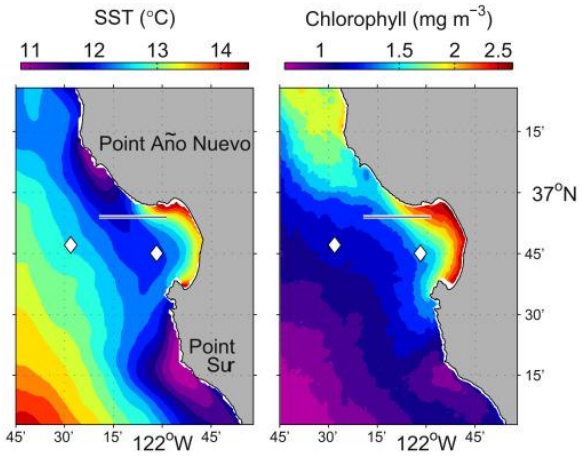

Figura 10. Temperatura superficial del mar (izquierda) y concentración de clorofila-a a nivel superficial (derecha) durante el mes de junio (promedio 2004 - 2008) en Bahía de Monterey, California EE.UU. (Zhang et al., 2015). La sombra de surgencia está representada por las altas temperaturas al interior de la bahía.

Algunos estudios han mostrado que la sombra de surgencia responde fuertemente a las variaciones en el forzamiento del viento desde la escala sinóptica a la escala estacional (Rosenfeld et al., 1994; Graham y Largier, 1997; Ramp et al., 2005; Woodson et al., 2007, 2009). La suma de factores como la presencia de gradientes de temperatura horizontales asociados a los frentes de surgencia, presencia de terrenos elevados (montañas y/o cordilleras), orientación de la línea de costa y otras características topográficas, afectan los flujos superficiales como el esfuerzo del viento y la boyantes (Strub et al., 1998). Kaplan et al. (2003) mostraron que la estratificación, provocada por el calentamiento diurno debido a la radiación solar, puede ser contrarrestada por efecto del cizalle que ejerce el estrés del viento sobre la columna de agua explicando, con ello, los cambios en la temperatura diurna observada en dos localidades costeras (Chile norte y central). En la bahía de Monterey (California), estos movimientos diurnos generados por la brisa marina coinciden con los cambios en la temperatura del agua (Rosman et al., 2007).

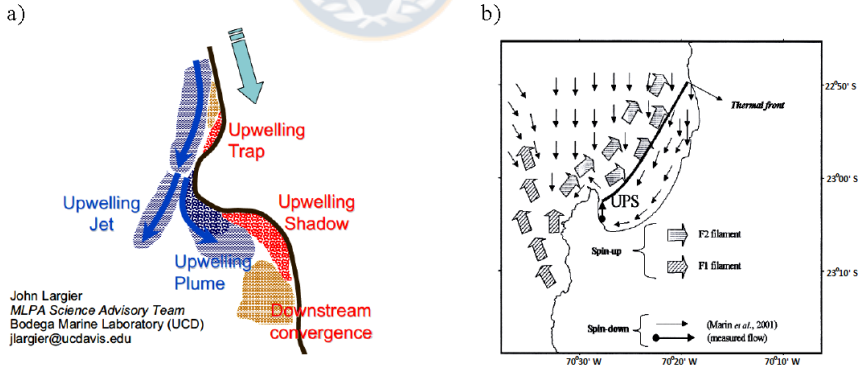

Figura 11. Esquema de la sombra de surgencia. a) Modelo de John Largier. Tomado de The Environment - Ocean Patterns: If we knew the hue of the blue (HN). b) Modelo de Marín et al. (2003) (Bahía Mejillones – HS).

1.6. Balance de Calor

La variación espacial y temporal de la temperatura del océano es la respuesta a los procesos de transferencia de calor entre el océano y la atmósfera. La dimensión y

naturaleza de estas variaciones en la temperatura dependen del flujo de calor que ingresa o sale del océano (Talley, 2011). La ecuación del balance de calor (ecuación 1.6.1) permite evaluar los procesos por los cuales el océano gana o pierde calor. Hay cuatro componentes principales que determinan el flujo de calor neto: radiación solar entrante, radiación saliente de retorno, pérdida de calor por evaporación y transferencia mecánica de calor entre el océano y la atmósfera (Tomczak y Godfrey, 2003).

$$Q_T = Qs + Qb + Qh + Qe + Qv \quad (1.6.1)$$

donde:

Q_T es la ganancia (+) o pérdida (-) neta de calor del océano, Qs es la radiación solar neta de onda corta (siempre +), Qb es la radiación neta de onda larga (casi siempre -), Qh es el flujo de calor sensible, (+) o (-) dependiendo de la diferencia entre la temperatura del aire y del agua, Qe es el flujo de calor latente (casi siempre -) y, Qv es la advección de calor entre dos flujos, uno entrante y uno saliente (Talley, 2011). La unidad de medida de estos términos es Wm^{-2}.

La variabilidad de la temperatura en el Pacífico ecuatorial oriental a escala anual e interanual es regida por los términos advectivos y por los flujos de calor, aire-mar. La radiación de onda corta (Qs) es el término que más aporta al calentamiento mientras que el flujo de calor latente (Qe) es el que domina el enfriamiento (Garcés-Vargas y Abarca-del Río, 2012). Durante los eventos de El Niño y La Niña el (Qe) es el término que presenta mayores cambios durante los primeros meses del año con tendencia al calentamiento durante La Niña y al enfriamiento durante EL Niño (Garcés-Vargas y Abarca-del Río, 2012). Debido al ángulo de incidencia de los rayos provenientes del sol, la radiación solar absorbida es mayor en los trópicos y disminuye hacia los polos (Stewart, 2008; Garcés-Vargas y Abarca-del Río, 2012) con valores promedio en torno a 160 ± 110 Wm^{-2} en 40°S (Garcés-Vargas y Abarca-del Río, 2012). La radiación neta que llega a la superficie se ve afectada por la época del año y la cobertura de nubes, presentando un ciclo estacional con

valores más altos durante el verano austral (Dic/Ene/Feb) (Garcés-Vargas y Abarca-del Río, 2012).

Por otro lado, el flujo de calor latente o evaporativo se asocia a la humedad relativa, la temperatura superficial del mar y la velocidad del viento. Vientos más intensos y aire más seco facilitan el proceso de evaporación del agua, a diferencia de vientos débiles y humedad relativa cercana al 100% (Stewart, 2008). Entre 25°S y 40°S los vientos más fuertes se presentan durante primavera y mediados de verano, mientras que la humedad relativa tiene su máximo en otoño y su mínimo en primavera, indicando que la estacionalidad del calor latente está gobernada por los vientos (Garcés-Vargas y Abarca-del Río, 2012).

El flujo de calor sensible es la transferencia directa de calor entre el océano y la atmósfera, y depende de la diferencia de temperatura entre ambos, así como de la intensidad del viento. Entre más fuerte sea la componente del viento y mayor la diferencia de temperatura, mayor será el flujo de calor (Stewart, 2008; Talley, 2011). De este modo, cuando el océano está más caliente (frío) que la atmósfera la transferencia de calor será desde el agua (aire) hacia el aire (agua); es decir, el océano perderá (ganará) calor.

2. HIPÓTESIS Y OBJETIVOS

2.1. Hipótesis

Hipótesis 1: La presencia de sombras de surgencia al interior del golfo de Arauco está relacionada con una relajación del viento desde el suroeste y/o inversión a viento desde el norte.

Hipótesis 2: A escala sinóptica, el incremento de la temperatura superficial del mar en áreas de sombras de surgencia es dominado por procesos radiativos.

2.2. Objetivos

Para contrastar las hipótesis propuestas se plantean los siguientes objetivos:

Objetivo 1. Caracterizar la variabilidad del esfuerzo del viento y del rotor del viento en las escalas interanual, estacional y sinóptica tanto al interior del golfo de Arauco como al oeste de punta Lavapié.

Objetivo 2. Definir un índice de sombra de surgencia que represente adecuadamente el proceso físico y que permita caracterizar estadísticamente su presencia/ausencia a lo largo del período de estudio.

Objetivo 3. Determinar bajo qué condiciones radiativas y de forzamiento del viento local se generan sombras de surgencia al interior del golfo de Arauco.

Objetivo 4. Determinar la respuesta de las corrientes al interior del golfo durante el desarrollo de una sombra de surgencia.

Objetivo 5. Evaluar variaciones en la intensidad de las sombras de surgencia asociadas a procesos atmosféricos de escala sinóptica.

3. DATOS Y METODOLOGÍA

3.1. Capítulo 1: Variabilidad interanual y estacional de las sombras de surgencia.

Se usaron quince años (2002-2016) de datos diarios de temperatura superficial del mar (TSM) del Geostationary Operational Environmental Satellite (GOES). A estos datos se les aplicó un análisis estadístico básico que incluyó porcentaje de datos válidos, tendencias a largo plazo, promedio y desviación estándar. Para evaluar variaciones estacionales los datos fueron agrupados en meses según la estación: verano (Ene-Mar), otoño (Abr-Jun), invierno (Jul-Sep) y primavera (Oct-Dic).

Del producto de reanálisis ERA-5 del ECMWF (European Centre for Medium-Range Weather Forecasts) se usaron datos de radiación solar, radiación termal, flujos de calor sensible y calor latente con una resolución temporal de 4-horas, y datos de viento cada 3-horas. Con los datos de viento se calculó el estrés del viento (ecuación 3.1.1) y el rotor del estrés del viento (ecuación 3.1.2) siguiendo la metodología de Bakun (1973) y Bakun (1991), respectivamente:

$$\tau_y = \rho_a C_d |\vec{V}| \vec{v} \quad , \quad \tau_x = \rho_a C_d |\vec{V}| \vec{u} \tag{3.1.1}$$

$$Curl = \frac{\tau_{y(E)} - \tau_{y(W)}}{\Delta x} - \frac{\tau_{x(N)} - \tau_{x(S)}}{\Delta y} \tag{3.1.2}$$

donde:

En la ecuación 3.1.1 τ_y and τ_x son los vectores del estrés del viento, ρ_a es la densidad del aire, Cd es el coeficiente de arrastre, |V| es la magnitud del viento y, $\vec{v}$ y $\vec{u}$ son las componentes del viento a lo largo y perpendicular a la costa, respectivamente.

En la ecuación 3.1.2 $\tau_y(E)$; $\tau_y(W)$; $\tau_x(N)$ y $\tau_x(S)$ es el estrés del viento del punto de grilla más hacia el este, oeste, norte y sur, respectivamente; Δx es la distancia entre $\tau_y(E)$ y $\tau_y(W)$ y Δy es la distancia entre $\tau_x(N)$ y $\tau_x(S)$.

La validación de los datos de viento del ERA-5 se realizó siguiendo la metodología propuesta por Devis-Morales et al. (2017) y utilizando series de tiempo de 2 pixeles cercanos a la estación meteorológica de Carriel Sur (36.7833°S; 73.0667°O). Esta validación incluyó la estadística básica (valores mínimo y máximo, promedio, desviación estándar y varianza) y una comparación de algunos parámetros estadísticos (error cuadrático medio (ECM), el coeficiente de correlación (r), índices de dispersión y de sesgo, entre otros). A los datos de dirección del viento provenientes del ERA-5 y de la estación Carriel Sur se les aplicó una corrección por declinación magnética de 5.9°. Posteriormente, se calcularon las componentes del viento perpendicular y a lo largo de la costa. Además, como información complementaria se consideraron datos diarios de velocidad de la corriente total obtenidos del sitio web de GLOBCURRENT (http:// globcurrent.ifremer.fr/).

A fin de evaluar las diferencias zonales de temperatura entre el golfo de Arauco (GA) y las aguas costeras frente a punta Lavapié (PL) y a la isla Santa María (SMI), asociadas a los eventos de sombra de surgencia, se desarrolló un Índice de Sombra de Surgencia (USI por sus siglas en inglés) definido por la siguiente ecuación:

$$USI = (T_{GA} - T_{PL}) * m_f \qquad (3.1.3)$$

donde:

T_{GA} = promedio de la temperatura superficial del mar en el golfo de Arauco.

T_{PL} = promedio de la temperatura superficial del mar al oeste de punta Lavapié/isla Santa María.

m_f = factor de ponderación adimensional (ecuación 3.1.4) que va de 0 (día más frío) a 1 (día más cálido).

$$m_{f(t)} = \frac{SST\_mean_{(t)} - Min}{r} \quad (3.1.4)$$

donde:

$SST\_mean_{(t)}$ es el promedio de la TSM del área de estudio (36°S, 75°O a 38°S, 73°O) en el tiempo *t*; *t* son los días desde enero 1 del 2002 hasta diciembre 31 del 2016; r es el rango de SST_mean: Max - Min = 10.21°C; Max es el valor máximo de SST_mean (19.44°C) y Min es el valor mínimo de SST_mean (9.23°C).

Para evaluar el incremento de la TSM en el interior del golfo debido al flujo de calor, se calculó el tiempo de residencia (R) siguiendo la metodología propuesta por Graham y Largier (1997):

$$R = \rho * c * H * \frac{\Delta T}{Q} \quad (3.1.5)$$

Donde ρ es la densidad del agua de mar (1026 kg m^{-3}); c es la capacidad calórica del agua de mar (3990 J°C^{-1} kg^{-1}); H es la profundidad de la capa superficial (para este estudio se consideraron dos escenarios: H=10 m y H=15 m); ΔT es la diferencia entre T_{GA} y T_{PL}; Q (W.m^{-2}) es el balance del flujo de calor (Q_{net} = radiación de onda corta + radiación de onda larga + flujo de calor sensible + flujo de calor latente). Las variables de radiación se obtuvieron del ERA-5.

3.2. Capítulo 2: Variabilidad sinóptica de las sombras de surgencia.

Se usaron alrededor de nueve años (Ene/2011 - Sep/2019) de datos diarios de TSM provenientes del Global 1 km Sea Surface Temperature (G1SST). Datos de presión del

nivel del mar y de vientos zonales y meridionales (10 m sobre la superficie) se obtuvieron del ERA-5. Para el análisis de compuesto a gran escala se utilizaron promedios diarios (centrados en 12 UTC), mientras que para el análisis a escala sinóptica de eventos particulares se usaron datos horarios.

Para identificar los días con y sin sombra de surgencia para este período de datos, se calculó el USI usando la ecuación 3.1.3; las áreas para el cálculo se muestran en la Figura 12. Considerando que los eventos de chorro costero y de sombra de surgencia son más frecuentes a fines de primavera y durante el verano austral (Muñoz y Garreaud, 2005; Wong et al., 2021), este estudio se enfocó entre noviembre y marzo.

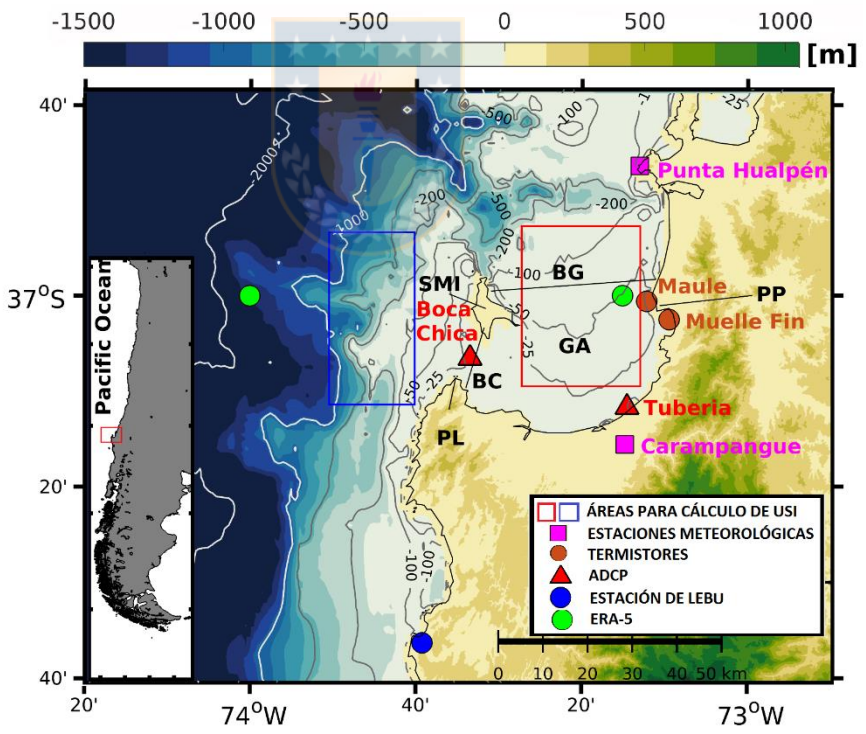

Figura 12. Ubicación de las estaciones meteorológicas, termistores costeros y ADCP de las cuales se obtuvieron los datos *in-situ*. Los cuadros azul y rojo son las áreas para realizar el cálculo del USI. Los círculos verdes son los datos de vientos del ERA-5 que fueron usados y el círculo azul corresponde a datos facilitados por el SHOA.

Para analizar la evolución de las sombras de surgencia en el golfo de Arauco (GA) y estudiarlas junto con las condiciones atmosféricas, un evento de sombra de surgencia se definió como períodos de 3 o más días consecutivos de sombra de surgencia con, al menos, dos días sin sombra de surgencia entre ellos, para evitar el traslape entre eventos. Una vez identificados los eventos, el análisis de compuestos consistió en calcular los campos promedio dos días antes (día -2), al inicio (día 1) y al tercer día (día 3) de los eventos de sombra de surgencia. Para evaluar el forzamiento atmosférico y los cambios oceánicos referentes a las condiciones sin sombra, el campo medio de los días sin sombra de surgencia fue sustraído de los compuestos mencionados.

La disponibilidad de datos *in-situ* de corrientes y temperatura en el interior del golfo, permitió seleccionar dos casos de estudio: uno en enero del 2012 (caso C1) y otro en diciembre del 2016 (caso C2). Los datos de corrientes costeras correspondieron a anclajes ubicados en el sitio denominado en este estudio como Tubería (37$^°11'41"S, 73°14'28"O) y en boca Chica (3°6'33"S, 73°33'25"O) para C1 y C2, respectivamente. A fin de poder comparar las corrientes entre ambos sectores, se usó un sistema estándar de coordenadas con el *eje-x* positivo hacia el este y *eje-y* positivo hacia el norte. Se calcularon los promedios horarios y se removió la variabilidad intramareal de las corrientes, usando análisis armónico (T_TIDE: Pawlowicz et al. (2002)). Posteriormente se aplicó un filtro coseno-Lanczos de 30 horas para remover las altas frecuencias restantes.

Los datos de temperatura correspondieron a registros de termistores desplegados en el muelle del puerto de Coronel (37°2'31"S, 73°9'21.6"O) y en el sector Maule (37°0'35.6"S, 73°12'4"O) para C1 y C2, respectivamente. Datos de temperatura superficial del mar (TSM) de la estación de Lebu (37°35'39"S, 73°39'5"O), al sur de punta Lavapié, fueron facilitados por el Servicio Hidrográfico y Oceanográfico de la Armada de Chile (SHOA). Mientras que datos locales de viento se obtuvieron de distintas localidades según la disponibilidad para cada caso de estudio. La estación de Carampangue (37°15'35.6"S, 73°14'44"O) se usó para el caso C1, mientras que para el caso C2 se usaron datos de punta

Hualpén (36°46'24"S, 73°12'54"O). Con fines comparativos se seleccionaron dos puntos meridionales de viento del ERA-5 para contrastar con los datos *in-situ*. En la *Figura 12* se muestra la ubicación de las estaciones mencionadas.

4. RESULTADOS

4.1.Capítulo 1

Estructura termal superficial y variabilidad de las sombras de surgencia en el Golfo de Arauco, Chile

Artículo publicado en Journal of Geophysical Research: Oceans.

Surface Thermal Structure and Variability of Upwelling Shadows in the Gulf of Arauco, Chile. (https://doi.org/10.1029/2020JC016194)

Zeneida Wong, Gonzalo S. Saldías, John L. Largier, P. Ted Strub, Marcus Sobarzo.

Resumen

Se estudió la sombra de surgencia en el golfo de Arauco (GA) usando 15 años de imágenes satelitales diarias de temperatura superficial del mar (TSM) del GOES (Geostationary Operational Environmental Satellites), así como datos de flujo de calor y viento del producto de reanálisis ERA5. Se desarrolló un Índice de Sombra de Surgencia (USI) sobre la base de diferencias de TSM entre el GA y la región costa afuera frente a punta Lavapié (PL), caracterizada por surgencia activa. Valores de USI >0.91°C y diferencias de TSM <1.1°C, correspondieron a un día con sombra de surgencia. Estos casos ocurrieron un 10.29% del tiempo, siendo más frecuentes en primavera/verano con vientos favorables a surgencia y un fuerte rotor del estrés de viento ciclónico, intercalado con relajaciones del viento. Correlaciones múltiples entre USI, rotor del viento y radiación solar mostraron un r^2 = 40-80% para algunos meses de verano. 53% de los eventos duraron solo un día, el 34% de ellos duraron entre 2 y 4 días y el 9% se extendieron por más de 4 días. Tiempos de residencia de más de 15 días fueron observados en el GA durante los eventos de sombra de surgencia. Durante relajaciones del viento sur (menores a 2 días), las aguas frías superficiales fluyeron hacia el norte de PL curvando hacia la costa y entrando al golfo desde el norte, debilitando el gradiente termal entre PL y GA y por ende

la sombra de surgencia. Largos periodos de relajación (una semana o más) resultaron en disipación del gradiente termal debido al calentamiento de las aguas costa afuera.

JGR Oceans

RESEARCH ARTICLE
10.1029/2020JC016194

Surface Thermal Structure and Variability of Upwelling Shadows in the Gulf of Arauco, Chile

Zeneida Wong[1,2], Gonzalo S. Saldías[3,4], John L. Largier[5,6], P. Ted Strub[7], and Marcus Sobarzo[2,8,9]

[1]Graduate Program in Oceanography, Department of Oceanography, Faculty of Natural Sciences and Oceanography, University of Concepción, Concepción, Chile, [2]Ecosystem Studies Program in the Gulf of Arauco (PREGA), University of Concepción, Concepción, Chile, [3]Departamento de Física, Facultad de Ciencias, Universidad del Bío-Bío, Concepción, Chile, [4]Centro FONDAP de Investigación en Dinámica de Ecosistemas Marinos de Altas Latitudes (IDEAL), Valdivia, Chile, [5]Coastal & Marine Sciences Institute, University of California Davis, Bodega Bay, CA, USA, [6]Department of Environmental Science & Policy, University of California Davis, Davis, CA, USA, [7]College of Earth, Ocean, and Atmospheric Sciences, Oregon State University, Corvallis, OR, USA, [8]Department of Oceanography, Faculty of Natural Sciences and Oceanography, University of Concepción, Concepción, Chile, [9]Interdisciplinary Center for Aquaculture Research (INCAR), University of Concepción, Concepción, Chile

Key Points:

- We developed an upwelling shadow index for the Gulf of Arauco in central Chile to identify its presence throughout the year
- A scheme of upwelling shadow evolution is analyzed, highlighting the role of wind stress curl and heat flux, resulting in higher residence times in the Gulf
- The upwelling shadows can develop in a cold (November–December) or warm (January–February) environment and can include interannual sea surface temperature variability

Correspondence to:
M. Sobarzo,
msobarz@udec.cl

Citation:
Wong, Z., Saldías, G. S., Largier, J. L., Strub, P. T., & Sobarzo, M. (2021). Surface thermal structure and variability of upwelling shadows in the Gulf of Arauco, Chile. *Journal of Geophysical Research: Oceans*, *126*, e2020JC016194. https://doi.org/10.1029/2020JC016194

Received 3 MAR 2020
Accepted 5 MAR 2021

Abstract The upwelling shadow in the Gulf of Arauco (GA) is studied using 15 years of daily satellite images of Sea Surface Temperature (SST) from Geostationary Operational Environmental Satellites (GOES), as well as heat flux and wind data from the ERA5 reanalysis product. An Upwelling Shadow Index (USI) is developed based on the SST differences between the GA and the region off Punta Lavapie (PL) farther offshore, characterized by active upwelling. USI values greater than 0.91°C and SST differences less than 1.1°C, correspond to an upwelling shadow event. These cases occurred 10.29% of the time and were more frequent in spring/summer during events of upwelling-favorable winds with strong cyclonic wind stress curl, interspersed with wind relaxations. Multiple correlations between USI and wind stress curl and solar radiation showed an r^2 = 40%–80% for some summer months. Most events persisted for only 1 day (53%), whereas 34% of upwelling shadow events lasted between 2 and 4 days and 9% of events were longer than 4 days. Water residence times as long as 15 days were observed in the GA during upwelling shadow events. During southerly wind relaxation (less than 2 days), cold surface waters flowing north from PL curved onshore and entered the GA from the north, weakening the thermal gradient between PL and GA and the upwelling shadow. Long periods of wind relaxation (at least 1 week) resulted in the dissipation of the thermal gradient due to the warming of offshore waters.

Plain Language Summary Coastal upwelling has been defined as the rise of subsurface cold waters in response to wind forcing. When this phenomenon occurs close to embayments facing the equator, the inner sea can remain sheltered to the alongshore winds, which induces a local surface warming. Thus, an upwelling shadow has been defined as "a localized region of an active coastal upwelling system within which upwelling is reduced, and a coherent pattern of anomalously high surface temperature is observed." Here, the upwelling shadow in the Gulf of Arauco (GA) (Chile) was studied using 15 years of daily satellite images of sea surface temperature, solar radiation, and wind data. As a result, an Upwelling Shadow Index was developed based on the temperature differences between the GA and the offshore waters off Punta Lavapie, characterized by active upwelling. This index included a daily factor from 0 to 1, based on the regional SST average, where 0 is the coldest day and 1 is the warmest day in the 15 years. According with this Index, an upwelling shadow condition occurred 10.29% of the time and was more common in spring/summer seasons during upwelling favorable winds.

1. Introduction

Enhanced coastal upwelling usually occurs near capes (e.g., Castelao & Barth, 2007), due to vorticity effects along with the acceleration of winds and currents (Largier, 2020). Moreover, the wind shadows and upwelling circulation around capes can also generate upwelling shadows on the side protected from the upwelling jet and alongshore wind. An upwelling shadow has been defined as "a localized region of an active coastal upwelling system within which upwelling is reduced, and a coherent pattern of anomalously high

surface temperature is observed" (sensu Graham & Largier, 1997). Graham et al. (1992) noticed that, during an upwelling event in northern Monterey Bay, coastal surface waters were significantly warmer (close 16°C) than offshore waters (typically <12°C), proposing that, these zonal gradients in the sea surface temperature (SST) were ubiquitous features of upwelling regions. The local warming associated with upwelling shadows due to insolation has been associated with the residence time of a bay (e.g., ~8 days for Monterey Bay, Graham and Largier (1997); ~12 days for Antofagasta Bay, Piñones et al., 2007). Upwelling may also be reduced in smaller bays where only weak temperature differences develop due to their short residence times (e.g., Cartagena Bay, Bonicelli, Moffat, et al., 2014; Bodega Bay, Roughan et al., 2005). Also, the warming of surface waters in a bay is important ecologically since a marked thermocline and thermal front influence habitat and larval dispersal (Largier, 2020).

Upwelling shadows exhibit a high cross-shore temperature gradient (~0.3°C km^{-1}), with positive spatial anomalies in sea surface temperatures (≥2°C) and sharp horizontal density gradients (~0.11 kg m^{-3} km^{-1}; Graham, 1993; Graham et al., 1992). Unlike the classical upwelling front, which has a high spatial and temporal variability in its cross-shore position, an upwelling shadow front can persist spatially and temporally during prolonged periods because of its association with fixed topography, that is, headlands (Largier, 2020). The spatial extent of the upwelling shadow is associated with the interaction of wind and currents with coastal topography. Some studies have shown that an upwelling shadow responds strongly to variations of the wind forcing, from daily to seasonal scales (Graham & Largier, 1997; Ramp et al., 2005; Rosenfeld et al., 1994; Woodson et al., 2007). Woodson et al. (2009) established that the alongshore location of the upwelling shadow front at the northern edge of the Monterey Bay was driven by regional wind forcing through an alongshore pressure gradient, buoyancy forces due to the temperature change across the front, and local wind forcing (the diurnal sea breeze). Also, they found that during relaxations events, the upwelling shadow water mass moved poleward along the coast with an observed propagation speed of about 5 km day^{-1}.

Along the Chilean coast, the understanding of the upwelling shadow process has been related to the ecological implications of these areas as retention centers, providing sheltered breeding and feeding grounds for marine animals. Upwelling shadows have been identified in Mejillones Bay (Marín et al., 2001, 2003), Valparaíso Bay (Aiken et al., 2008), Cartagena Bay (Bonicelli, Moffat, et al., 2014; Bonicelli, Tapia, & Navarrete, 2014), La Serena Bay (Garreaud et al., 2011; Lagos et al., 2016), Antofagasta Bay (Largier, 2020; Piñones et al., 2007), and in the Gulf of Arauco (Letelier et al., 2009). These studies have focused on defining upwelling shadow events, describing the thermal contrasts and effects of recirculation on the coastal ecosystem. It has been proposed that the shadow persists during the spin-up phase (onset or development of upwelling) and vanishes during the spin-down phase (relaxation) in Mejillones Bay (23°03′S; Marín et al., 2003). The oceanic areas adjacent to these bays have been recognized as strong upwelling regions, forced by equatorward wind stress during the spring-summer upwelling season. These winds vary at different time scales from daily, synoptic, seasonal, and inter-annual variability (Letelier et al., 2009; Rahn, 2012; Rahn & Garreaud, 2014; Sobarzo et al., 2007). Seasonal and inter-annual variability is related to the displacement of the South Pacific Anticyclone (SPA; Ancapichun & Garces-Vargas, 2015; Garreaud et al., 2011), which impacts the upwelling and cooling pattern of the coastal region (Schneider et al., 2017).

The seasonal variability of wind regime in this area is determined by the meridional migration of the SPA (centered at 28°–31°S), high latitude atmospheric lows, and continental atmospheric lows (Saavedra, 1980). Here, and during summer, intensified equatorward winds coincide with the most intense alongshore atmospheric pressure gradient (Rahn & Garreaud, 2014). On the adjacent continental shelf, wind-induced mixing competes with two other seasonal processes that stratify the water column: the mixed layer's heat balance dominated by the net surface heat flux (maximum in January), and the freshwater balance, dominated by river discharges and precipitation (maximum in June–July; Sobarzo et al., 2007). Surface temperature closely follows the annual cycle of the net surface heat flux, resulting in a shallow, warm mixed layer from November to April. Reduction of upwelling-favorable winds by the end of summer combined with continued solar input lead to considerable thermal stratification in the upper water column during late summer and early fall. Oppositely, surface cooling occurs from April to June due to the low solar radiation in winter. Other factors that contribute to enhanced nearshore cooling are the orientation of the coastline (Figueroa & Moffat, 2000), the presence of submarine canyons (Sobarzo et al., 2016), the input of cold continental freshwater (Saldías et al., 2012), and the advective contribution of subantarctic waters from higher latitudes

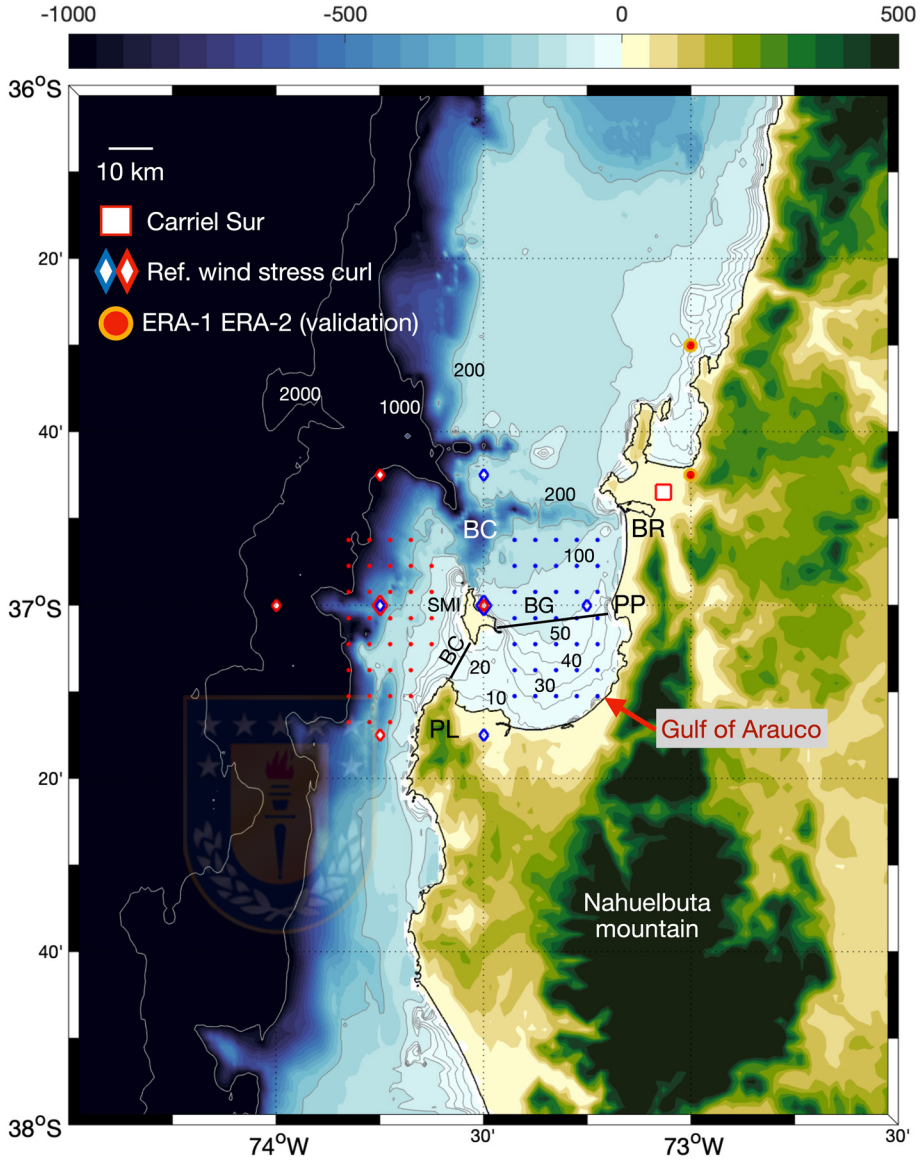

Figure 1. Gulf of Arauco and location of meteorological station of Carriel Sur, also grid points of ERA5-Winds data used to validate and reference of how wind stress curl was estimated with adjacent grid points. Gray lines are isobaths. Red and blue points are pixels selected to estimate the upwelling shadow index. Orange-red circles are pixels from the ERA5-wind product used to validate the data. BC: Biobio Canyon; BR: Biobio River; SMI: Santa Maria Island; BG: Boca Grande; PP: Punta Puchoco; BC: Boca Chica; PL: Punta Lavapie.

(Strub et al., 1998). Aside from the physical consequences of this surface cooling, the upwelling of cold and nutrient-rich waters promotes high biological productivity in the coastal region, which supports a rich marine ecosystem (Daneri et al., 2000; Escribano & Morales, 2012; Letelier et al., 2009).

The GA is the largest semi-enclosed embayment along the Chilean coast north of Puerto Montt (41°28′S). It has been recognized as an active upwelling shadow area and a retention site for plankton (Castro et al., 2007; Landaeta & Castro, 2006; Letelier et al., 2009). Most of the gulf is shallower than 100 m and is bounded, on its west side, by the Santa Maria Island (SMI), which splits the mouth into a small western channel ("Boca Chica"), and a wider northward channel ("Boca Grande"; Figure 1). Considering the Boca Grande as the section located between Punta Puchoco (PP) and SMI (with 25 km wide and a mean depth of 50 m) and the Boca Chica, as the section located between SMI and Punta Lavapie (with 8 km wide and a mean depth of 20 m), the area of the Boca Chica is around 7 times smaller than Boca Grande. Using two days of towed

ADCP, Valle-Levinson et al. (2003), described residual flows at Boca Grande and Boca Chica during late spring 2000. With northward wind conditions (upwelling-favorable), they found net downwind flow over the shallow areas on the east side of Boca Grande. Also, they found a net upwind flow in the deepest part around the middle of this entrance. On the other hand, mean flows illustrate a surface outflow and a flow into the gulf near the bottom. According to these available measurements, the gulf exports waters through the surface layers and receives cold and suboxic waters through the middle and deep layers and (preferentially through Boca Grande) during upwelling-favorable wind conditions. The main freshwater discharge from the Biobio River is located on the northeast side of the Gulf, with weak discharges in spring-summer and peak outflows ~2,000 m^3 s^{-1} in winter (Saldías et al., 2012; Sobarzo et al., 2007).

Compared with other coastal areas where upwelling shadows have been described, the GA has unique geomorphological features that need to be highlighted (Figure 1): (a) PL extends zonally to the west in an extension close to 40 km constituting the head of the GA. Other prominent capes on the coast of Chile, such as Curaumilla (33°05′S), Lengua de Vaca (36°15′S), or Mejillones (23°02′S), do not exceed 25 km in an East-West direction. The northern part of Monterey Bay (36°58′N; Santa Cruz, USA), where the upwelling shadow phenomenon was first described, reaches a zonal extension less than 25 km. (b) This zonal extension means that PL is the place on the Chilean coast where the coastline changes its orientation most dramatically (30°). South of PL, the orientation of the coastline is toward 350° (relative to the geographical North). North of PL, the coastline is oriented toward 20°, with respect to the geographical North (Valle-Levinson et al., 2003). (c) South of GA, the western border of the Nahuelbuta Mountain is located. The typical heights between the Nahuelbuta Mountains and PL fluctuate around 200–300 m with values that, in PL, can reach 350 m high. This orography constitutes a natural barrier that protects the GA from most of the influence of the southerly winds. As will be demonstrated in this work, this orography will strongly affect the distribution of the southerly winds inside and outside the Gulf (west of PL). Finally, (d) the width of the continental shelf is of the order of 12 km south of PL. This condition changes sharply north of the Biobio Canyon, reaching ~60 km off Concepcion (Sobarzo & Djurfeldt, 2004). This bathymetry, including the Biobio submarine canyon on the northern side and SMI on its western edge (just 9 km north of PL) makes the GA a unique, semi-enclosed embayment, connected with subsurface waters of the continental slope through the Biobio Canyon and its tributary located at the northern end of SMI (Sobarzo et al., 2016).

Here, we describe the spatial and temporal variability of the upwelling shadows in the GA based on a detailed analysis of 15 years of daily satellite images of SST. The methods and observations are described in Section 2, where an upwelling shadow index is defined based on the observed thermal differences. The results are presented in Section 3, highlighting (i) mean fields and seasonal variability of SST and winds, (ii) interannual variability, (iii) definition of the Upwelling Shadow Index, and (iv) validation of the Index and its relationship with winds and solar radiation. Finally, the physical mechanisms that explain the variability of the upwelling shadows are discussed in Section 4.

2. Methods and Observations

2.1. Satellite and Coastal Data

Fifteen years (2002–2016) of daily SST data from the Geostationary Operational Environmental Satellite (GOES) were used, with a spatial resolution of ~4 km (141 × 141 pixels between 33°S–40°S and between 71°W–78°W). Cloud-free good quality daily images fluctuated between 40% and 80% in the study region (Figure 2a). The decrease in this percentage coastward and, primarily, south of Punta Lavapie has been related to the increase in cloud cover in those areas (Letelier et al., 2009). The use of GOES SST images increases the probability of obtaining a high percentage of cloud-free data as compared to SST measurements from polar-orbiting satellites (e.g., AVHRR, MODIS). Consequently, they have been previously used in other eastern boundaries for the study of SST fronts (Castelao et al., 2006).

Three-hour vector wind data were obtained from the ERA5, which is the fifth generation ECMWF (European Center for Medium-Range Weather Forecasts) atmospheric reanalysis of the global climate, and available at the Copernicus Climate Change Service Information (2019) (https://cds.climate.copernicus.eu/cdsapp#!/home). This product has a spatial resolution of ~0.25° (28 × 29 pixels used between 33°S–40°S

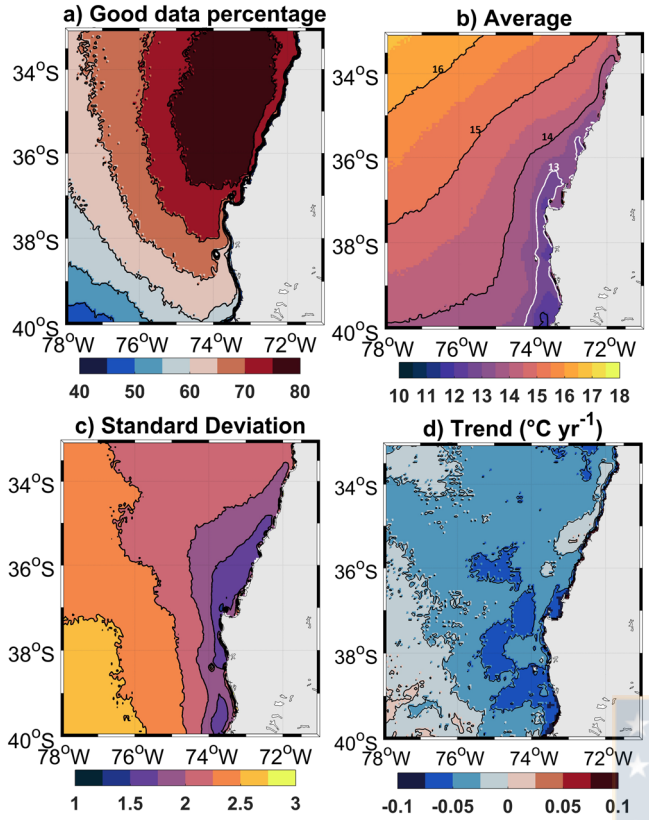

Figure 2. Statistical analysis of SST series (GOES) from 2002–2016. (a) Good data percentage, black contours every 5%. (b) Mean-field of SST. (c) The standard deviation of SST. Black contours every 0.25°C. (d) Trend, black contours every 0.025°C yr^{-1}. GOES, Geostationary Operational Environmental Satellites; SST, sea surface temperature.

Table 1
Basic Statistics of in situ Carriel Sur and ERA5 Wind Datasets

		Min	Mean	SD	Max	Var
	Comp.	m s^{-1}	m s^{-1}	m s^{-1}	m s^{-1}	m^2 s^{-2}
ERA_1	U	−7,72	1,36	2,29	10,45	5,24
	V	−16,10	1,15	3,88	9,59	15,02
	W	0,01	4,33	2,16	16,95	4,67
ERA_2	U	−6,34	1,05	1,96	8,78	3,83
	V	−13,78	0,63	2,95	7,90	8,71
	W	0,04	3,30	1,77	14,06	3,14
C. SUR	U	−10,14	1,06	2,60	10,65	6,75
	V	−16,33	0,27	3,28	9,86	10,77
	W	0,03	3,61	2,38	16,98	5,67

U: zonal component. V: meridional component. W: wind speed. Parameters are minimum (Min), mean, standard deviation (SD), maximum (Max), and variance (Var).

and between 71°W–78°W). Wind stress (Equation 1) and wind stress curl (Equation 2) were calculated following the methodology of Bakun and Nelson (1991), respectively:

$$\tau_y = \rho_a C_d \mid \vec{V} \mid \vec{v} \quad \text{and} \quad \tau_x = \rho_a C_d \mid \vec{V} \mid \vec{u} \tag{1}$$

$$Curl = \frac{\tau_{y(E)} - \tau_{y(W)}}{\Delta x} - \frac{\tau_{x(N)} - \tau_{x(S)}}{\Delta y} \tag{2}$$

For comparative purposes, and considering the wind spatial resolution, two wind stress curl time series were selected. The first, called GA, used three pixels inside of the GA and one outside. The second, called PL, used three pixels west of PL and one inside of the GA (see Figure 1 for pixels distributions).

Hourly data of wind speed and direction from a meteorological station located at Carriel Sur Airport (36.7833°S; 73.0667°W, Figure 1) were also used in the analyses. A magnetic declination of 5.9° was applied to the wind direction data from reanalysis and Carriel Sur station. The alongshore and cross-shore wind components were calculated with hourly (Carriel Sur), 3h, and daily (reanalysis) time series.

Total current velocities (sum of the geostrophic and Ekman components) obtained from the GLOBCURRENT website (http://globcurrent.ifremer.fr/), which constitute a Merged Global Ocean Gridded Absolute Geostrophic Velocities from SSALTO/Duacs AVISO L4 product. These data have a spatial resolution of ∼0.25° (30 × 30 pixels between 33°– 40°S and between 71° – 78°W) and a temporal resolution of one day.

Solar radiation, thermal radiation, sensible and latent heat flux values corresponding to ERA5 product were also downloaded from Climate Data Store (https://cds.climate.copernicus.eu/cdsapp#!/home), with a resolution of ∼0.25° (5 × 5 pixels between 36.5° and 37.5°S and between 73° and 74°W), and a temporal resolution of 4 h.

2.2. ERA-5 Wind Data Validation

ERA5 is the latest atmospheric reanalysis generated by ECMWF, using 4D-Var data assimilation in CY41R2 of ECMWF's Integrated Forecast System (IFS). The IFS is combined with a soil model, with parameters that can be assigned as surface parameters, and an ocean wave model. This combination makes ERA5 better than its predecessor ERA-Interim. ERA5 product has been validated previously in several oceanic regions with excellent results. However, it is known that the validation of these data varies among regions. Here, 15 years of 3h wind data were used from the Carriel Sur Airport to validate the data from two coastal pixels (Figure 1). Table 1 compares some descriptive statistics at these three locations and, in Table 2, a statistical comparison is made based on the root mean square error (RMSE) and the correlation coefficients (r), among others (Devis-Morales et al., 2017).

The closest ERA site to Carriel Sur Airport (pixel 2) showed the best fit with the observed data. The alongshore component has a correlation coefficient of $r^2 = 75.25\%$. The lower r^2 of the east-west component is expected due to the influence of wind variability on the daily scale (sea breeze), especially in the spring-summer season. Because this high-frequency

Table 2
Comparative Analyses Between in situ Carriel Sur and ERA5 Wind Datasets

		Bias	BI	RMSE			R^2	SI
	Comp.	m s^{-1}	m s^{-1}	m s^{-1}	R	Pval	%	%
ERA_1	U	0,31	0,29	1,95	0,69	0,00	48,27	182
	V	0,88	3,25	2,20	0,85	0,00	72,88	743
	W	0,72	0,20	1,74	0,76	0,00	58,15	44
ERA_2	U	−0,01	−0,01	2,09	0,61	0,00	37,19	198
	V	0,36	1,32	1,68	0,87	0,00	75,25	602
	W	−0,31	0,09	1,50	0,79	0,00	62,06	41

U: Zonal Component. V: Meridional Component. W: Wind Speed. The Parameters Shown are: Bias, BI (Bias Index), Root Mean Square Error (RMSE), Correlation Coefficient (r), P-value, Determination Coefficient (r^2) and, Scattering Index (SI).

variability depends on the thermal contrast between the ocean and the mainland, the coastline's irregularity (bays, points, etc.) makes it difficult to fit the observed zonal wind and the reanalysis. Bias less than 0.5 m/s and a BI (difference from the means) less than 1.5 m/s indicate that ERA winds do not overestimate/underestimate extreme values. These results suggest an acceptable skill level. Scatter Index (SI) shows a significant variability of the difference concerning the mean. This high variability could be due to Carriel Sur station's location and the effect of surrounding topography. Probably, atmospheric products do not represent winds adequately near the coast. On the long-term (9-years) average, the alongshore ERA5 wind measured west of PL (considering spring and summer measurements) did not show the expected drop-off (Astudillo et al., 2017), but north of GA ERA5 wind was able to better represent the drop-off (not shown).

2.3. Definition of an Upwelling Shadow Index (USI) for the GA

In order to evaluate the zonal temperature differences associated with the upwelling shadow between the GA and coastal waters off Punta Lavapie (PL) and Santa Maria Island (SMI), 35 pixels inside the gulf and 35 pixels west of Punta Lavapie were selected (Figure 1). "Good quality days" were defined as those containing more than 40% of valid pixels in each area. Using these valid pixels, the USI was defined as:

$$USI = (T_{GA} - T_{PL}) * m_f \tag{3}$$

where:

T_{GA} = mean SST in the GA.
T_{PL} = mean SST west of Punta Lavapie/Santa Maria Island.
m_f = weighting factor, which was calculated as follow:

$$m_{f(t)} = \frac{SST\_mean_{(t)} - Min}{r} \tag{4}$$

where:

$SST\_mean_{(t)}$ = average SST of the study area (36°S, 75°W to 38°S, 73°W) at t time.
$_{(t)}$ = Days from January 1, 2002 to December 31, 2016.
Min = minimum value of SST_mean = 9.23°C.
Max = maximum value of SST_mean = 19.44°C.
r = range of SST_mean values = Max−Min = 10.21°C.

$m_{f(t)}$ results in a time series ranging from 0 to 1 (dimensionless), where 0 is the coldest day and 1 is the warmest day of the entire record.

This daily index USI (Equation 3) increases with the difference of the average temperature in the GA (T_{GA}) and the region off Punta Lavapie (T_{PL}), and with the increase of the regional average SST. Thus, a higher weight is placed on the upwelling season (spring-summer). Because T_{GA} and T_{PL} vary simultaneously, the same temperature difference can occur in colder or warmer surface conditions, depending on the season or the synoptic weather condition. The m_f factor weights spring-summer upwelling events when a cold filament develops near PL while the regional average SST is high. Notably, the spatial coefficient of variation of both areas (GA and PL) was less than 18%, indicating coherent daily spatial averages for both areas.

Basic descriptive statistics (percentage of useful data, long-term trends, mean and standard deviation) were computed with the 15-years SST data. Seasonal variability was evaluated grouping the months according to summer (January–March), fall (April–June), winter (July–September), and spring (October–December).

2.4. Residence Time

To analyze the temperature increase inside the gulf due to the heat flux, the residence time (R) was estimated following Graham and Largier (1997):

$$R = \rho * c * H * \frac{\Delta T}{Q} \quad (5)$$

where ρ is the density of seawater (1,026 kg m^{-3}); c is the heat capacity of seawater (3990 J°C^{-1} kg^{-1}); H is the surface layer (here were considered two scenarios: H = 10 m and H = 15 m); ΔT is the difference between T_{GA} (we consider as "measured" temperature, the temperature inside the gulf) and T_{PL} (we consider as "expected" temperature, the temperature of upwelling waters); Q (Wm^{-2}) is the heat flux balance (Qnet = short wave radiation + outgoing longwave radiation + sensible heat flux + latent heat flux) calculated from ERA-5 radiation variables.

3. Results

3.1. Trends, Mean, and Seasonal Variability of SST and Winds

The average SST field showed a coastal cold-water filament extending northward from Punta Lavapie, as represented by the 13°C isotherm. This filament produced a contrast between cold upwelling waters off Punta Lavapie and slightly warmer waters (around 1°C) inside the GA (Figure 2b). The annual mean SST condition, therefore, reflects a typical upwelling shadow structure within the GA. The SST of this filament showed less relative variability (<1.75°C) than the GA (~2°C) and the oceanic waters (>2°C) (Figure 2c). Probably, this is because the coastal SST is kept fairly cold by coastal upwelling during spring-summer, or by winter surface cooling. The entire region showed a linear cooling trend with values less than −0.025°C yr^{-1} (Figure 2d), and with an average p-value of 0.0032.

Seasonally, the highest percentages of good-quality data were observed during summer (>80%) and spring (70%–85%). During fall and winter, the availability of data varied between 50%–70% (Figure 3a). On average, a clear upwelling shadow was displayed in summer and spring. This surface thermal difference was induced by the arrival of colder upwelling waters off Punta Lavapie and warmer waters within the GA, which are the result of the gulf's re-circulation and solar radiation. During fall this average thermal contrast was not evident, and in winter the average SST structure was more horizontally homogeneous with temperatures below 12°C (Figure 3b). The highest variability was observed in spring-summer (SD >1.4°C) and associated with the areas of coastal upwelling. The smallest standard deviations of SST were found in winter (SD <1°C; Figure 3c). On the other hand, a linear trend of surface cooling was evident for winter, spring, and summer, being stronger in spring-summer, with values lower than −0.04°C yr^{-1}; in winter this cooling was less intense and observed closer to the coast with values lower than −0.02°C yr^{-1}. Positive trends were mostly restricted to fall, with maximum values close to 0.05°C yr^{-1} (Figure 3a), but keeping a slight cooling trend in the GA.

The average cold filament of 13°C (spring) and 14°C (summer), off Punta Lavapie, was consistent with average winds with magnitude greater than 5 m s^{-1}, and with a negative wind stress curl (clockwise), both favorable for coastal upwelling in spring-summer (Figures 4b and 4d). In fall-winter, the mean alongshore wind decreased to values <5 m s^{-1}, especially near the coast and, although the average wind stress curl remained negative, its intensity declined from $-20 \times 10^{-7}\ N\ m^{-3}$ (in summer) to $-8 \times 10^{-7}\ N\ m^{-3}$ (in fall-winter). This condition, combined with the decrease of the SST in the entire area, made the cold filament at Punta Lavapie not clearly distinguishable. The wind showed less variability close to the coast, especially in spring-summer (Figure 4c). The wind stress curl variability was higher near the coast, with a similar structure throughout the year (Figure 4e).

A comparison of annual cycles of SST, radiation, and winds within the GA and off Punta Lavapie confirmed a higher average SST in the GA during spring-summer, which favored the development of upwelling shadows (Figure 5a). Since the average incoming solar radiation is the same in both sectors (Figure 5b), the difference in the SST is related to the depth of warming and/or residence time of the water near-surface, which depends, among others, on wind forcing and incoming solar radiation (e.g., Figures 11 and 13b). The

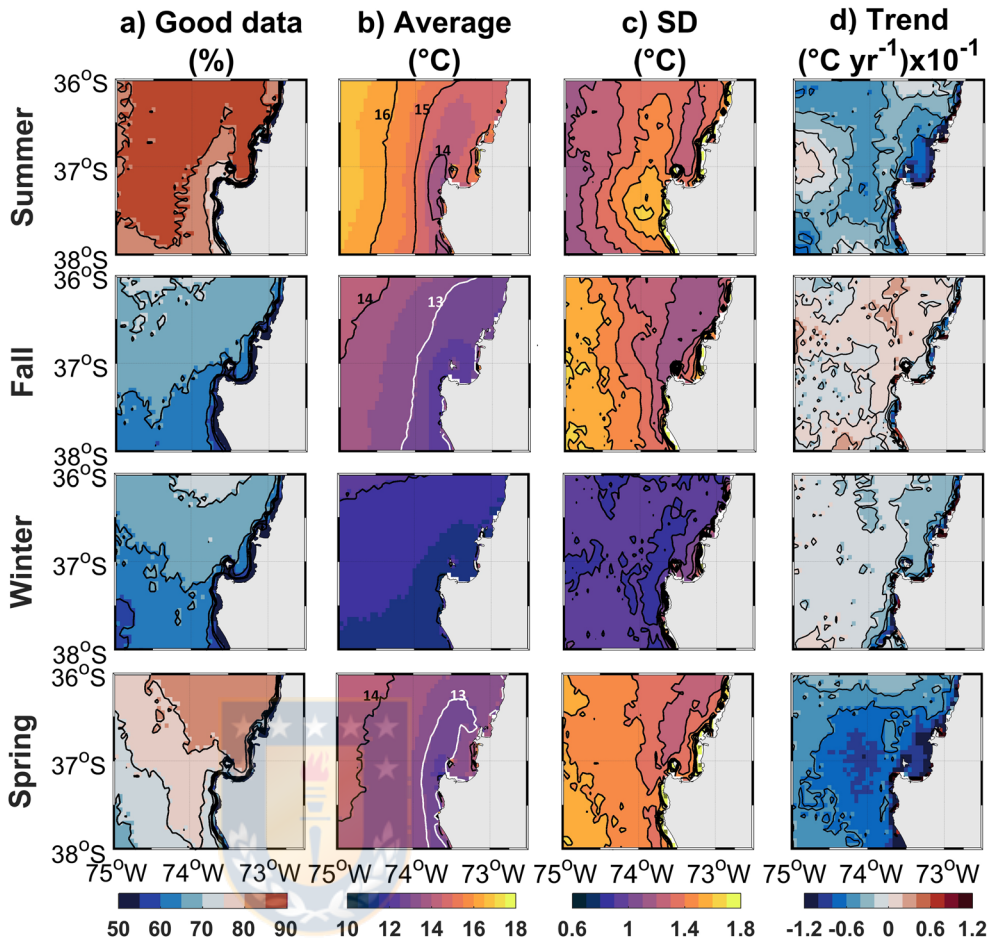

Figure 3. Seasonal statistics analysis of SST. (a) Good data percentage of the SST, black lines are percentage every 5%. (b) Mean fields of SST by season. (c) The standard deviation of SST, black lines are SD every 0.1°C. (d) Trends, black lines every 0.02°C yr^{-1}. SST, sea surface temperature.

magnitude of the mean alongshore wind stress in PL was >3 N $m^{-2} \times 10^{-2}$ greater than inside the GA from November to March (Figure 5c), which is consistent with the lowest surface temperatures off PL during spring-summer when the upwelling of cold water is commonly found. The wind stress curl was highly cyclonic in the GA from September to April (spring-summer; Figure 5d). From May to August, the mean winds in the gulf changed direction, being weakly favorable to downwelling conditions, whereas weak upwelling-favorable winds (~0.02 N m^{-2}) characterized the region off PL.

3.2. Interannual Variability of SST and Winds

Surface thermal gradients between GA and PL depend on the coastal thermal fluctuations at different time scale, from interannual to synoptic and daily scales. In this section, we begin by describing the influence of interannual variability on the USI. SST changes on this scale are associated with the latitudinal displacement of the South Pacific High (Schneider et al., 2017). When these variations were evaluated, by subtracting the SST annual cycles of the GA and PL time series, an inter-annual signal was evident in both sectors showing a warm phase that lasted until December 2006 (Figure 6a). From December 2006 to March 2014, both areas were dominated by a cold phase returning to a warm phase at the end of our period of study. The interannual fluctuations reached 1°C in both locations. These values were smaller than the seasonal amplitude of 4°C and 3.5°C for the GA and PL, respectively (Figure 5a). Linear correlation between wind stress anomalies and SST resulted in low correlation coefficients (r = 0.25 for GA; r = 0.35 for PL; p-values of ≈0). These warm and cold phases presented some similarities with the interannual variability of

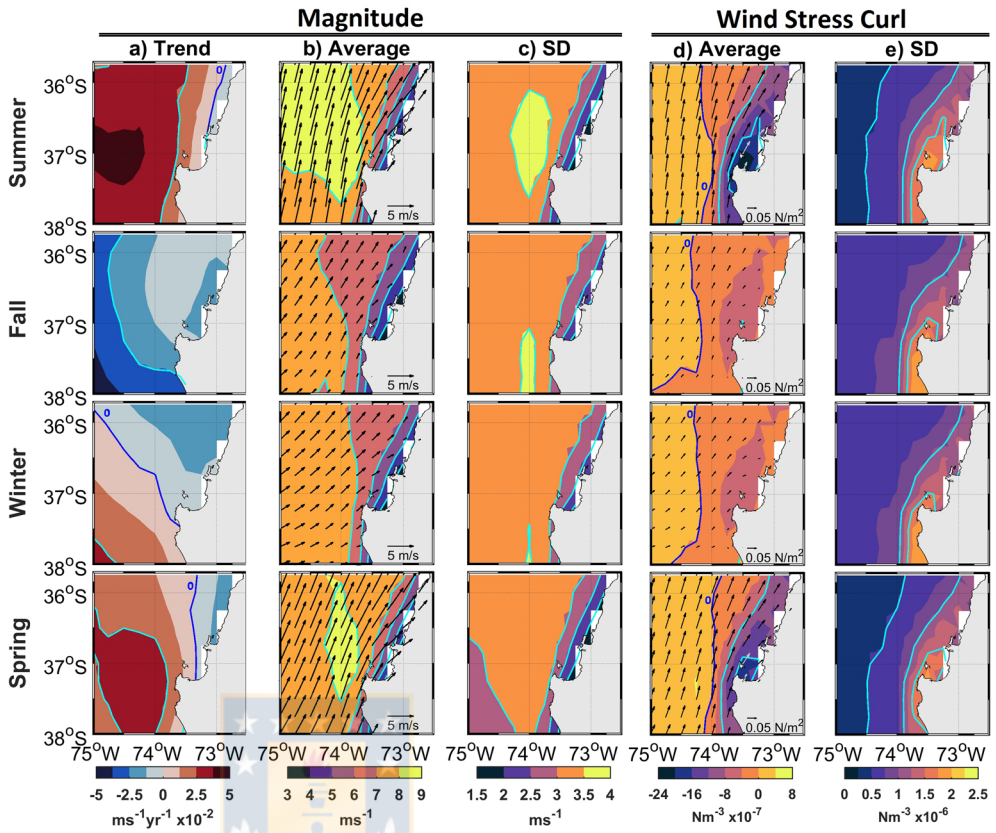

Figure 4. Seasonal statistical analysis of ERA5-Wind products from 2002 to 2016. For magnitude: (a) trend, (b) mean fields by season with their respective vectors (black arrows), and (c) standard deviation. For wind stress curl: (d) mean fields with their respective vectors of wind stress (black arrows) and (e) standard deviation.

alongshore wind stress (and wind stress curl) in GA and PL. The warm phase (2002–2006) was accompanied by downwelling-favorable coastal winds (τ_y negative, warm phase average = −0.0025 and −0.0067 N m^{-2} for GA and PL, respectively), and the cold Phase 2007–2014, was related with upwelling-favorable winds (GA cold phase average = 0.0017 N m^{-2}), especially off PL (cold phase average = 0.0047 N m^{-2}; Figure 6b). The downwelling-favorable wind stress curl (centered in SMI) was predominantly positive during the warm phase (before 2007). The subsequent cold phase was generated by upwelling-favorable wind and a negative wind stress curl (Figure 6c).

3.3. Upwelling Shadow Index and Associated Statistic

The average daily distributions of SST within the GA and west of PL (calculated on the basis of the pixels indicated in Figure 1) showed that the GA (with a mean T_{GA} = 13.31°C) was slightly warmer than PL (mean T_{PL} = 12.60°C; Figures 7a and 7b). These histograms were built using days of good quality (cloudless days) which constituted 73.90% and 73.12% of the 5,479 days of study (15 years), for the GA and PL, respectively. Based on these percentages, the T_{GA} was 0.71°C warmer than the T_{PL}. This difference increased to 1.1°C, considering only the spring-summer period of each year (not shown). The daily upwelling shadow index (*USI*) was calculated using Equation 3, and its histogram showed 17.50% negative values, which correspond to cases with a colder GA than PL (Figure 7c). On the other hand, positive values occurred on 50.90% of the days analyzed. Positive values of *USI* fluctuated between 0 and 4.

From the time series calculated with Equation 3, an upwelling shadow event was defined as the day that met the following two criteria: (i) $T_{GA}-T_{PL}$ >1.1°C and (ii) USI >0.91°C. The value of 0.91°C is the maximum USI value for SST differences less than 1.1°C between the GA and PL, which occurred on February 15, 2005, where the difference in SST between GA and PL was 1.08°C. For this day, m_f was equal to 0.84,

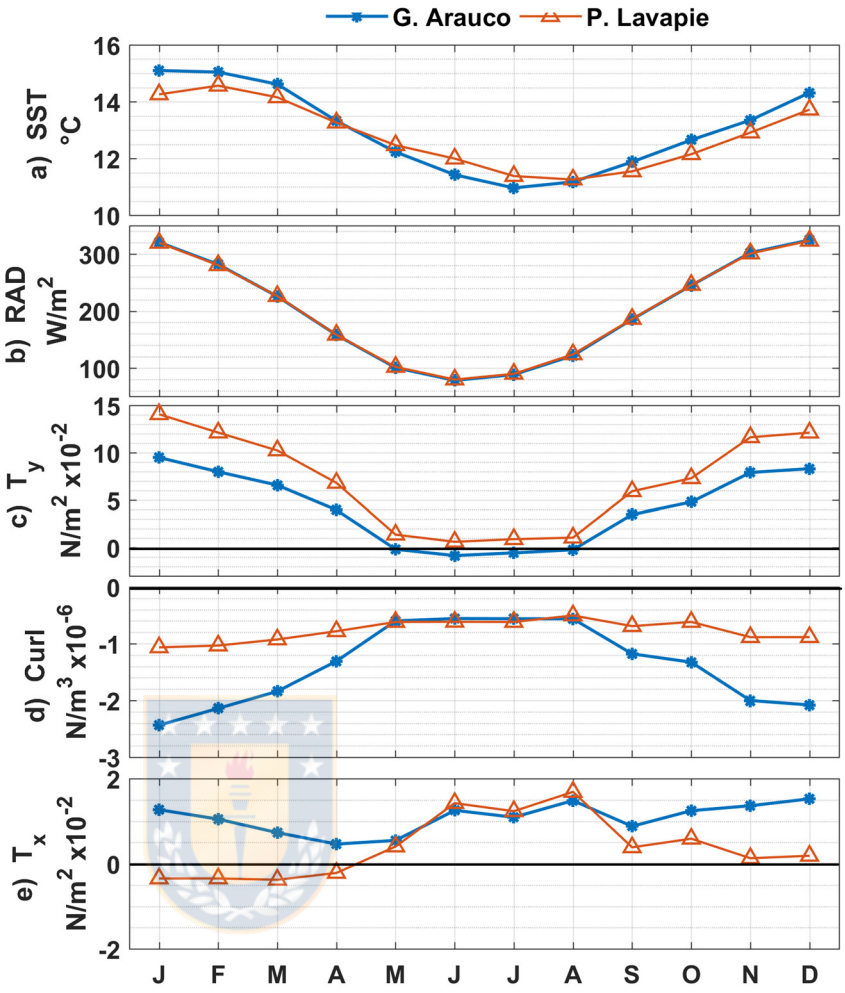

Figure 5. Annual cycles in GA (blue) and PL (orange) using data from 2002 to 2016. (a) SST-GOES. (b) Solar radiation input. (c) Alongshore wind stress. (d) Wind stress curl. (e) Cross-shore wind stress. Winds and radiation are from ERA5 product. GA, Gulf of Arauco; GOES, Geostationary Operational Environmental Satellites; PL, Punta Lavapie; SST, sea surface temperature.

giving a USI value of 0.91. USI values greater than 0.91 come from differences in SST between GA and PL greater than 1.1°C and at high values of m_f. Therefore, USI values greater than 0.91°C meet the two criteria to be considered upwelling shadow events. These events represented the 10.29% (564 days) of the entire series, occurring mainly in the spring and summer seasons. Therefore, considering only the summer days of the 15 years under study (Table 3 January to March), 71.8% of the upwelling shadow days occurred in these months. Most of the events lasted just one day (53%, 132 occurrences). Events that lasted between 2 and 4 days added up to 38% (94 occurrences), and the most extensive events were 9% (24 occurrences; Figure 7d), with only one event of 30 days. Note that some longer upwelling shadow events may have been broken up due to cloudiness or lack of data in the SST time series.

Time series of USI indicated that the upwelling shadows had a higher prevalence during spring-summer and with upwelling-favorable winds in PL and GA (Figures 8a and 8b and Table 3). Also, time series of USI showed more significant occurrences between 2002 and 2006 (warm phase; Figure 8a). Since equatorward winds are stronger in PL than in GA, in spring-summer, a negative wind stress curl was observed in both places, which could facilitate a circulation associated with retention processes, specially within the GA (Figure 8c). The wind stress curl for GA was three times more negative than in PL.

Figure 8a allowed defining a transition zone in the USI values limited by 0.19°C (minimum USI value for SST differences >1.1°C) and 0.91°C (maximum USI value for SST differences <1.1°C) (yellow horizontal

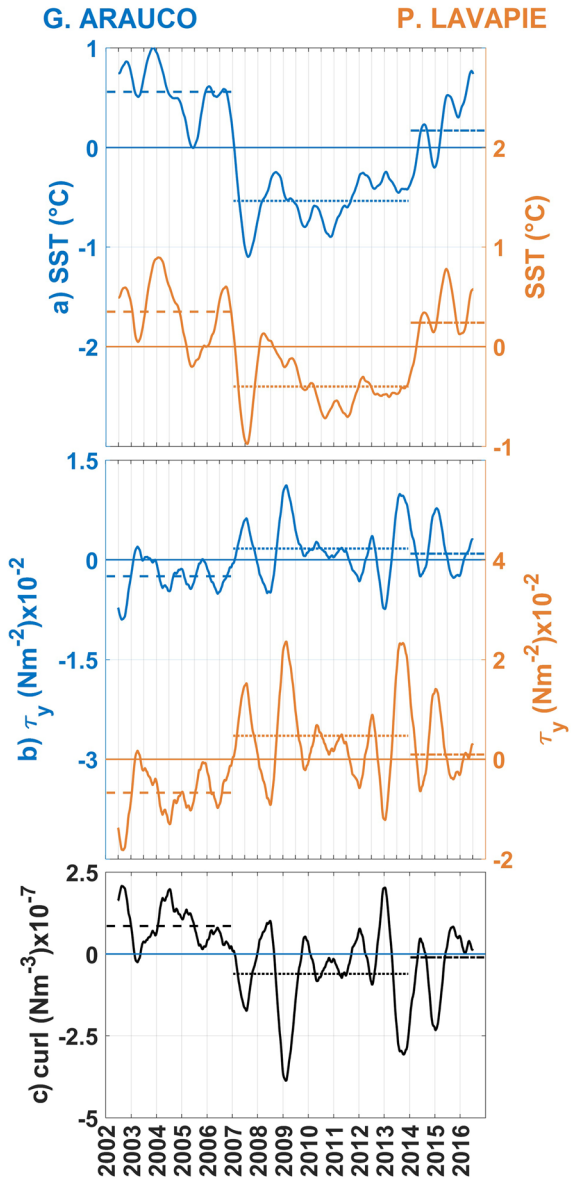

Figure 6. Interannual variability in GA (blue) and PL (orange) from 2002 to 2016. (a) SST anomalies. (b) Alongshore wind stress anomalies. (c) Wind stress curl anomalies (centered in SMI). Winds are from ERA5 product. Dashed lines, dotted lines and dashed/dotted lines in the three panels indicate the mean value of the warm/cold/warm phases. GA, Gulf of Arauco; PL, Punta Lavapie; SMI, Santa Maria Island.

lines). This transition was characterized by a mix of SST differences between GA and PL >1.1°C but with low m_f values due to low average SST in the region, and SST differences <1.1°C with high m_f (warmer regional SST averages, Figure 8a). These events occurred mainly in spring and late summer.

3.4. USI Validation for Particular Case Studies

Considering that upwelling shadows were found to be more frequent from December to March (Table 3), here two cases are analyzed to clarify the behavior of the USI and its relationship with the wind forcing and incoming solar radiation. The first period spanned from January 29 to March 3, 2013. Although these events occur during a cold year in the interannual analysis, these months showed surface temperatures higher than the seasonal average within the GA (Figure 5a). Three periods of intensification of the upwelling-favorable wind stress in GA and PL, accompanied by the corresponding increase in the residence times and in the cyclonic wind stress curl, were observed (Figures 9b and 9c). During the evolution of the first event of upwelling shadow (USI values between 0.5°C and 2.5°C, January 30 to February 6), the SST north of the GA showed warm temperatures (15°C–19°C). Currents were strongly northward, especially off PL. The average daily T_{GA} was greater than 16°C, while T_{PL} was around 14°C indicating in residence times >5 days (Figure 9b). Net heat flux between 200 and 300 W m^{-2} tends to decrease during upwelling favorable winds (Figure 9d). Strong upwelling favorable winds in PL and weak winds in GA lead to a cyclonic wind curl within the GA (Figures 9a–9d). The water in the GA warms in association with the cyclonic wind stress curl and long residence time. This upwelling event ended with an extended period of wind relaxation from February 7 to 16 (almost 10 days of wind relaxation with southward wind events in PL and GA on February 10). During this relaxation, residence times were <5 days and the USI values were less than 1.2°C with negative USI values on February 7 and 15. Heat flux values over 250 W m^{-2} dropped to 150 W m^{-2} on February 11. The change in the wind pattern generated onshore and southward currents, which weakened the upwelling shadow due to the onshore transport of cold ocean waters (see Figure 9a, February 8 and 11). This coincides with a decrease in the residence time. As the wind relaxation persisted, the GA and PL continued to warm up, and the upwelling shadow disappeared with widespread warm surface water in the region (February 14, 15, and 16). The T_{GA} remained at around 16°C, while the T_{PL} increased to almost 16°C.

From February 17 to 21 (5 days), a second intensification of upwelling-favorable winds occurred. Wind stress in PL was four times stronger than in GA, increasing the cyclonic wind stress curl and generating coastal upwelling off PL. In addition to decreasing T_{PL} below 13°C, the upwelling event cooled the surface layer throughout the study area advecting the warm front northward to 36°S (about 90 km north of PL) and causing upwelling along the coast up to Punta Nugurne (155 km north of PL, see February 18 in Figure 9e). USI values were around 1°C with residence times greater than 5 days. This second upwelling event ended during a short period of relaxation on February 22–23.

Finally, a third upwelling event lasted from February 24 to 27 (4 days), extending the surface cooling zone (SST <13°C) northward and westward (Figure 9e), with values of wind stress and residence time similar to the second upwelling event. The cumulative wind stress favorable to coastal upwelling during each particular event was not proportional to the extension of the cold upwelling water at surface. Although

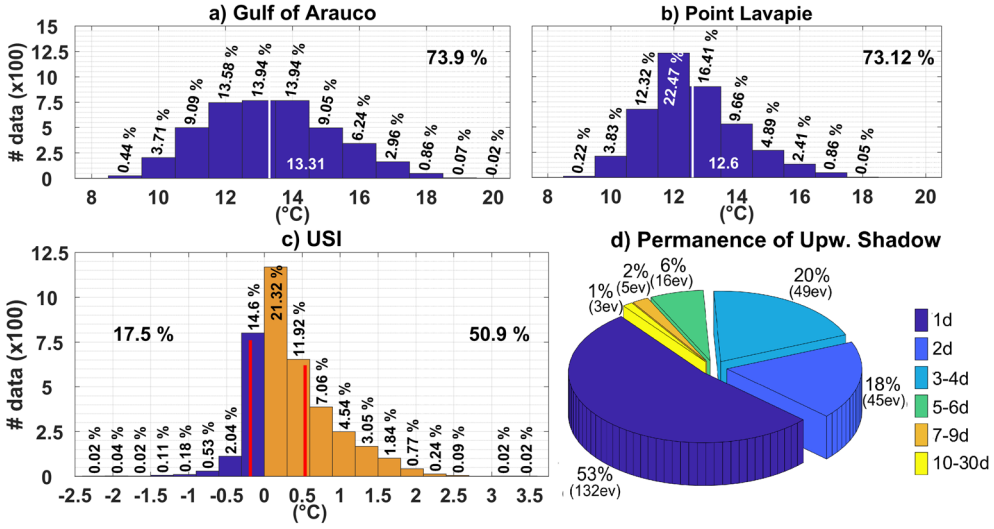

Figure 7. Histograms: (a) Mean daily temperature of the Gulf of Arauco. (b) Mean daily temperature west of Point Lavapie. (c) Upwelling Shadow Index, negative values in blue and positive values in orange. White and red lines represent the mean value of the time series. (d) Pie chart of the Upwelling Shadow events. Colors represent duration in days, each segment is labeled in percentage and number of events (ev).

the cumulative wind stress over a period of 4 days was similar during the three upwelling events (Figure 9d), the extension of the cold water (temperatures <13.5°C) varied considerably. During the third event, cold-water extension (10,000 km^2) was twice that in the previous two events (Figure 9e). This means that the third upwelling event did not start from rest (deep and flat isopycnals) but from a quasi-upwelling state. On the other hand, at the end of the first relaxation event, the area covered by the isotherm of 17°C (or greater) reached 13,000 km^2. Therefore, the surface area of cold or warm water depends not only on the cumulative wind stress during each particular upwelling event but on the previous thermal history of the surface layer. In this thermal history, the frequency, duration, and intensity of relaxation periods are fundamental in establishing the initial conditions for the next upwelling event. Also, rather than occurring during wind relaxations, the most intense upwelling shadows were related to the coastal upwelling intensification, where the thermal differences between PL and GA were more considerable (Figure 9d).

Another case study extended from November 30, 2012, until January 2, 2013. On average, T_{GA} and T_{PL} were 1°C colder than the previous case and the average isotherms of 15°C and 16°C were not observed in the study area (Figure 3b, summer vs. spring seasons). Time series started with downwelling-favorable winds (positive wind stress curl) from November 30 to December 6 and showed similar temperatures inside and outside of GA (about 14°C; Figure 10b). The USI values were negative (Figure 10d). The first upwelling event was recorded from December 7 to 10, generating intense northwards currents and a thermal gradient between T_{PL} and T_{GA} with USI values between 1°C and 1.5°C; although this upwelling event was short, and the cumulative wind stress did not increase greatly, the extension of the cold upwelling water reached around 10,000 km^2 on December 10. From December 11 to 25, there was a long wind relaxation with two wind events favorable to downwelling conditions. On average, the USI values decreased to 0.2°C, there were three cloudy days, and the currents were mostly toward the coast (Figure 10a and 10e). A second intense upwelling event was observed from December 26, 2012, to January 2, 2013, with USI values around of 1°C

Table 3
Monthly Information of Upwellling Shadow Events in the Gulf of Arauco

	January	February	March	April	May	June	July	August	September	October	November	December
#days	185	126	94	13	2	0	0	0	0	5	39	100
%	32.8	22.3	16.7	2.3	0.4	0	0	0	0	0.9	6.9	17.7
USImean	1.39	1.45	1.2	1.06	0.98	–	–	–	–	1.12	1.17	1.4

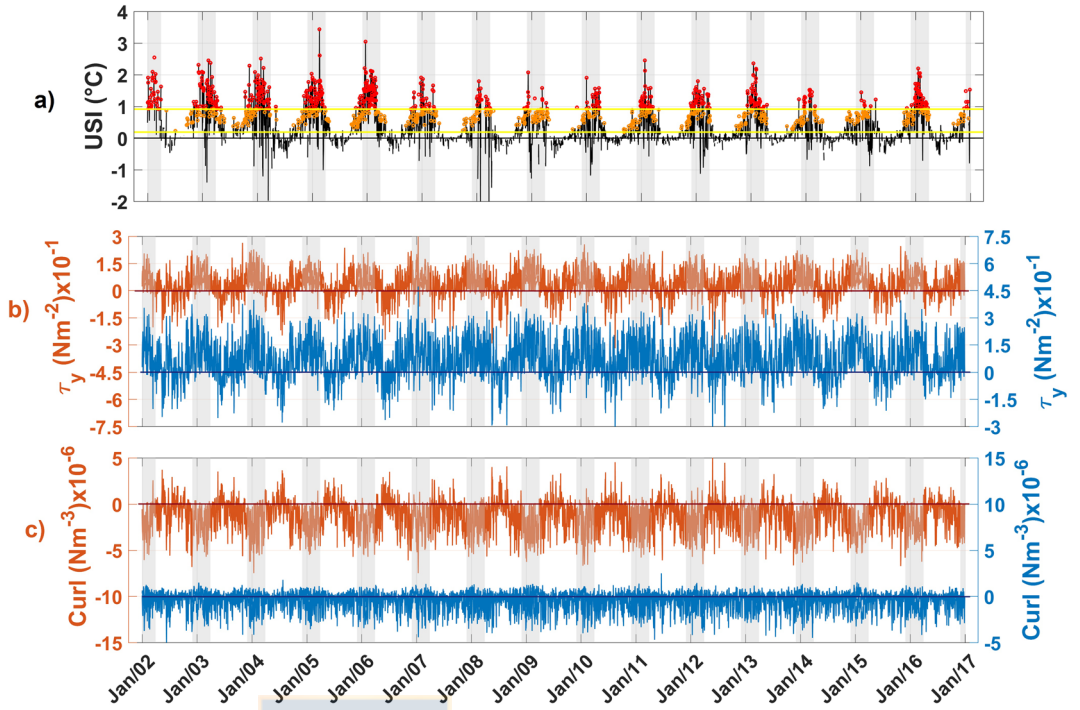

Figure 8. (a) Time series of the Upwelling shadow index; red markers are the upwelling shadow days; orange markers are days with GA-PL >1.1°C but with low USI values due to a cold environment; yellow lines are the limits of the transition zone (0.19: minimum USI value for SST differences >1.1°C and 0.91: maximum USI value for SST differences <1.1°C). (b) Alongshore wind stress in GA (orange) and PL (blue). (c) Wind stress curl in GA (orange) and PL (blue). Gray bars indicate months from December to March. GA, Gulf of Arauco; PL, Punta Lavapie; SST, sea surface temperature.

generating northward surface flows. It is clear, therefore, that during wind relaxation the temperatures of GA and PL tend to be similar. As in the previous case, greater residence times matches well with upwelling shadow events. During upwelling, on the other hand, T_{GA} and T_{PL} showed differences higher than 2°C, with USI values >1°C, and with an area covered by cold water (lower than 13.5°C, close to 10,000 km^2). The presence of cold waters during the second upwelling event was consistent with upwelling winds more persistent over time (Figure 10c and 10e). There were two coastal cooling events (close to 6,000 km^2) that were not related to upwelling favorable winds (December 6 and 19–20). Both occurred with northerly winds that generated coastal convergence, and, unlike the typical upwelling, these winds did not cause thermal gradients between GA and PL (Figure 10a and 10e). The atmosphere was likely too cold at this time, and thus producing loss of sensible heat from the ocean and surface cooling.

In these two cases, the relationship between wind stress curl and USI was evident, as demonstrated in the linear regressions between these variables (Figures 11a and 11b). In the case of December 2012, $r = -0.807$ ($r^2 = 65.18\%$; pval = 0); and, in the case of February 2013, $r = -0.74$ ($r^2 = 54.82\%$. pval $= 1 \times 10^{-5}$). Therefore, the intensification of cyclonic wind stress curl was statistically related to an increase of USI for these two cases. It was also not possible to improve the regressions using lags between the series. Applying the same methodology for December, January, February, and March from 2002 to 2016, the simple linear regression between wind stress curl and USI was calculated (Figures 12a–12d). Only two December, seven February and seven March months registered r^2 over 40%. When calculating a multiple regression between the USI and the wind stress curl and the incoming solar radiation, the regression coefficients improved slightly, with 5 December, 4 January, 7 February, and 11 March months with r^2 higher than 40%. This implies that these variables can explain, up to 40% of the variance of the USI. In general, the lack of a major correlation between the wind stress curl and USI in the rest of the summer months was due to the absence of a regular alternation between upwelling and downwelling favorable coastal winds.

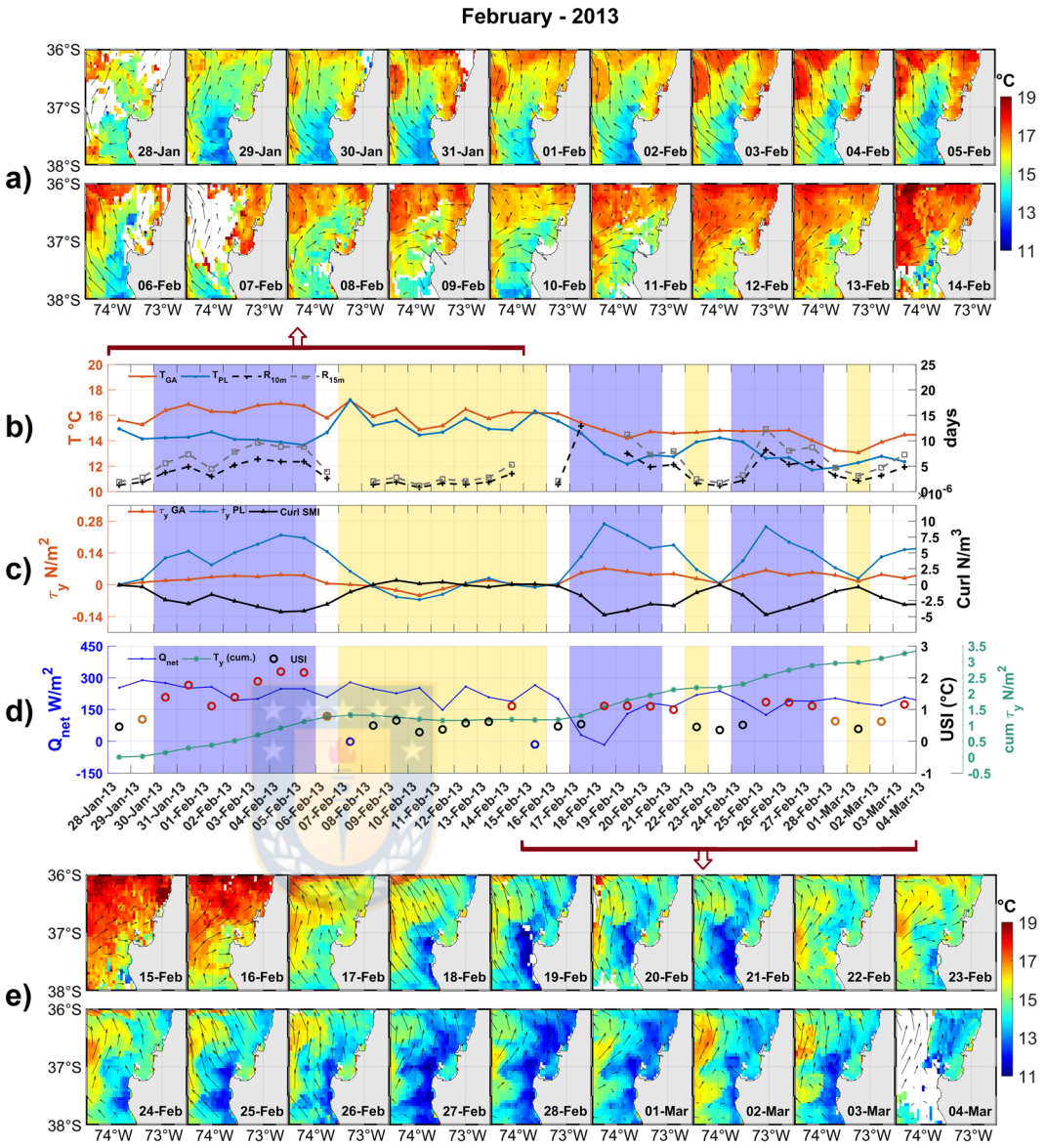

Figure 9. First case study: January 29 to March 3, 2013. (a) and (e) daily SST distribution (colors) and surface currents (arrows). (b) Left vertical axis, SST in GA (orange) and PL (blue); right vertical axis, residence times for a surface layer of 10 m (black line) and 15 m (gray line). (c) Left vertical axis, alongshore wind stress in GA and PL; right vertical axis, wind stress curl centered in SMI (black line). (d) Heat balance flux (left vertical axis); USI (right black vertical axis) red circles are upwelling shadow days, orange circles are days with GA-PL >1.1°C but with low USI values due to a cold environment, blue circle are negative values; and cumulative wind stress (right green vertical axes). GA, Gulf of Arauco; PL, Punta Lavapie; SST, sea surface temperature.

Using an average of four events lasting seven days, and adding two days before and after the evolution of a mean upwelling shadow event, a composite analysis of USI is shown in Figure 13. Cold upwelling waters west of PL and SMI expand during upwelling shadows forced by the intensification of upwelling-favorable winds in PL (Figure 13a). The temperature of this cold tongue also decreases until the southwesterly wind begins to relax (day 7). Because the southwest wind is weaker within GA than in PL, the upwelling shadow is accompanied by an increase of the cyclonic wind stress curl (Figures 13d and 13e). High variability in SST appeared in the initial days and south of PL. Finally, when the wind relaxes, high variability increases in GA due to the presence of warm surface waters from the north (Figure 13b). The mean heat flux balance does

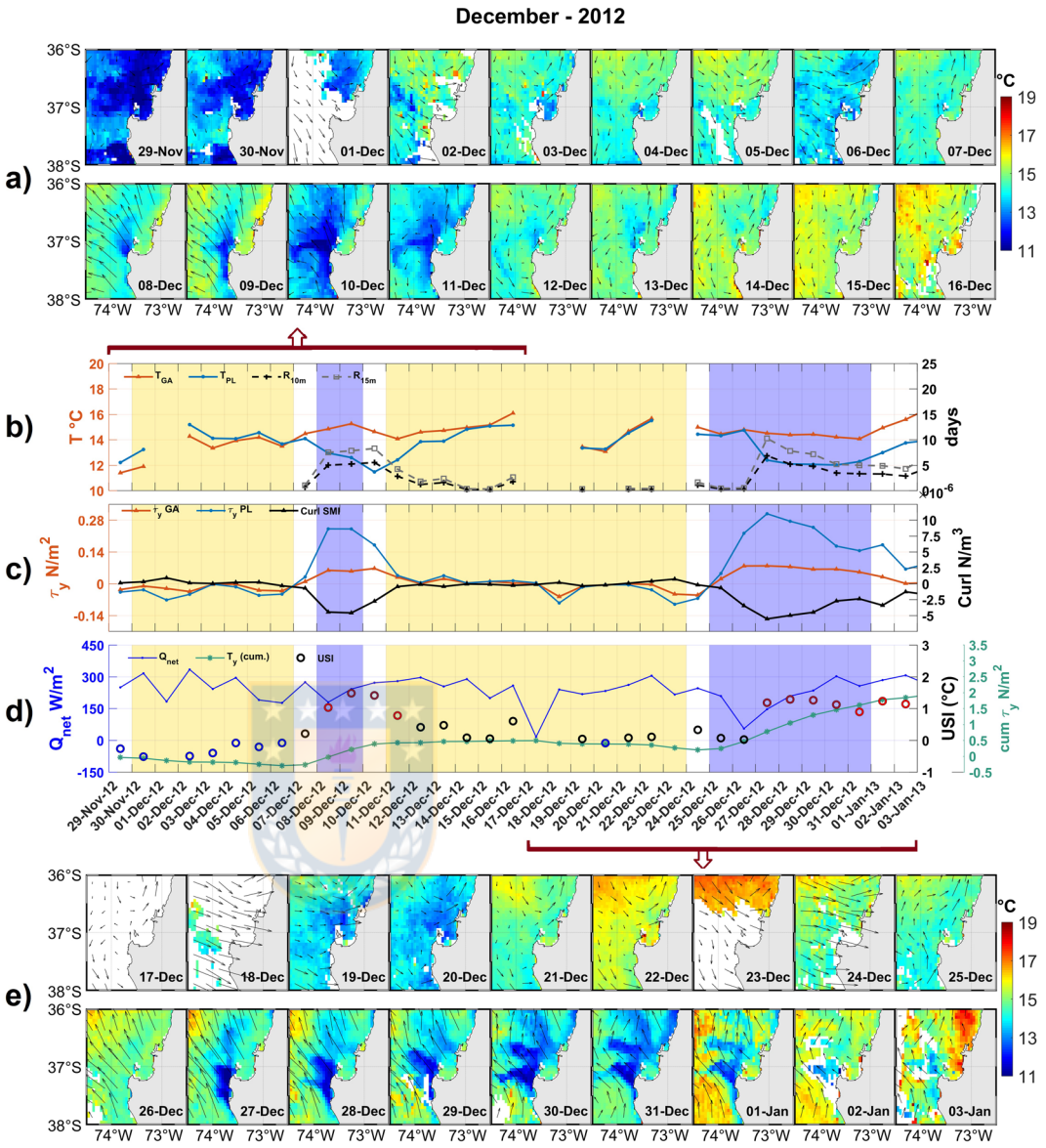

Figure 10. Second case study: November 30, 2012, to January 2, 2013. (a) Daily SST distribution (colors) and surface currents (arrows). (b) Left vertical axis, SST in GA (orange) and PL (blue); right vertical axis, residence times for a surface layer of 10 m (black line) and 15 m (gray line). (c) Left vertical axis, alongshore wind stress in GA and PL; right vertical axis, wind stress curl centered in SMI (black line). (d)Heat balance flux (left vertical axis); USI (right black vertical axis) red circles are upwelling shadow days, orange circles are "moderate" upwelling shadow in the transition zone, blue circle are negative values; and cumulative wind stress (right green vertical axes). GA, Gulf of Arauco; PL, Punta Lavapie; SMI, Santa Maria Island; SST, sea surface temperature; USI, upwelling shadow index.

not show much variability (Figure 13f). The composite analysis was applied to shorter events (lasting 3 and 5 days, not shown), resulting in a similar evolution structure.

4. Discussion

Although there is a clear definition for upwelling shadows (Graham & Largier, 1997), only a few quantitative studies demonstrate the role of the physical drivers on their evolution (Penven et al., 2000). The main physical mechanisms explaining the coastal surface warming during a relaxation event are the incoming solar radiation, and the alongshore advection (Brink et al., 1981; Dever & Lentz, 1994; Hamilton &

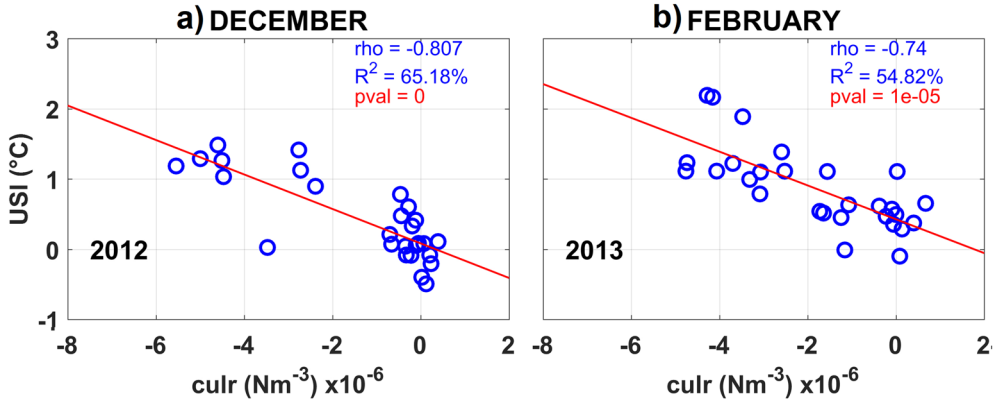

Figure 11. Correlation between USI and Wind stress curl (SMI) for (a) December 2012. (b) February 2013. SMI, Santa Maria Island; USI, upwelling shadow index.

Rattray, 1978; Lentz, 1987; Szoeke & Richman, 1981). Send et al. (1987) evaluated the topographic effect of Point Reyes (38°00′N) and the spatial variations in the upwelling-favorable wind field on coastal warming. Wang (1997) showed a positive wind stress curl sets up a strong poleward alongshore pressure gradient. This pressure gradient force drives a poleward current close to the coast into the upwelling region during active wind forcing, and it causes a surge of warm water into the upwelling zone during wind relaxation, as observed by Send et al. (1987) and Largier et al. (1993). Other studies of upwelling shadows have focused on biological aspects, given the association of this process with high coastal biological activity, including the dynamics of harmful algal blooms (HABs; Graham et al., 1992; Graham & Largier, 1997; Marín et al., 2001; Pitcher et al., 2010; Torreblanca et al., 2016; Schulien et al., 2017).

Here, the definition of an upwelling shadow index (USI) has allowed us to quantify the temporal occurrence, persistence, and intensity of the upwelling shadow events. Also, the analysis of the SST conditions (mean fields, seasonal and interannual variability) provided a better understanding of the importance of the coastal ocean's initial conditions linked to the development of upwelling shadows. This process had not been carefully studied before in the GA. The study by Letelier et al. (2009) reported upwelling shadows in the GA in association with high chlorophyll-a concentrations, nonetheless no major insights were described.

4.1. Initial Surface Thermal Conditions.

This study demonstrates that upwelling shadows occur only when northward flow separates at PL with weak circulation and longer residence times in GA, which results in GA warming due to significant incoming radiation and a marked thermal contrast between GA and PL. Considering the definition of USI in Section 3.3, there were 39 days with upwelling shadows in November and less than 14 days from April to October. Most upwelling shadow days (89.5%) occurred from December to March (Table 3). Upwelling shadows occurred when the mean SST of GA was 1.1°C higher than PL, and USI values were 0.91°C, which is the maximum USI value for SST differences <1.1°C. A two-year study carried out in Monterey Bay, Graham (1993) similarly identified upwelling shadows during spring-summer, showing that upwelling shadows are most common during the upwelling season here and in upwelling environments at similar mid-latitudes (Graham & Largier, 1997).

The initial surface thermal conditions determine two different scenarios for the development of upwelling shadows: (i) Upwelling shadows in a relatively cool surface environment (November and December) with typical SST values around 14°C, 15°C, and 16°C. Temperatures higher than 16°C were found north of 36.5°S (Figures 10a and 10e) intermittently. The area covered by warm waters could be associated with surface warming due to the solar radiation input or the influence of warm discharges from the Biobio River. During these months, colder upwelling waters reach the coast north of 36.75°S enclosing the warm water within the gulf, which results in the upwelling shadow (December 28 to 31, 2012). (ii) Upwelling shadows in a warm surface environment (January and February). During February, the isotherm of 14°C was restricted

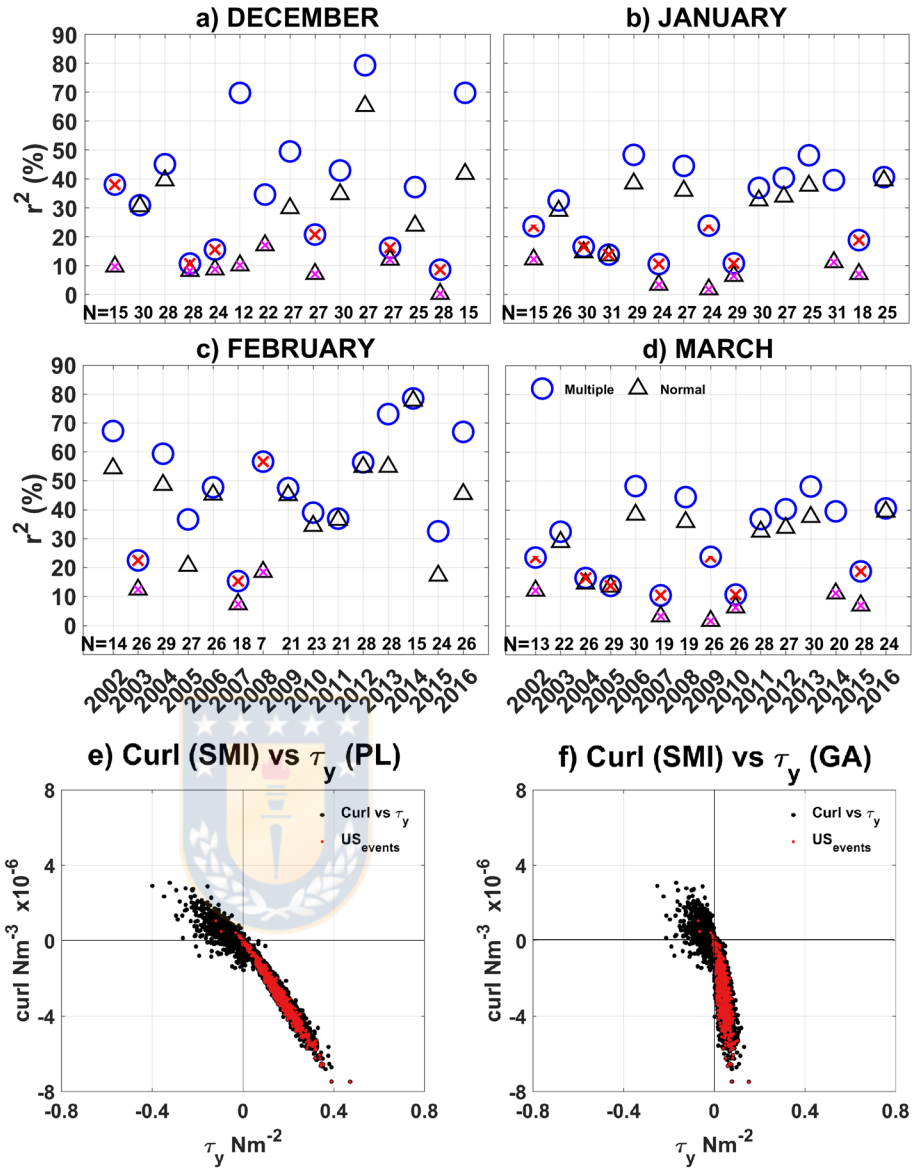

Figure 12. (a), (b), (c) and (d) Simple (USI-wind stress curl) and multiple (USI-wind stress curl-radiation) linear regression for December, January, February, and March. N: Valid days in each month. Crosses (red and magenta): means without statistical significance. (e) Dispersion diagram of wind stress curl versus. alongshore wind stress in PL. (f) Dispersion diagram of wind stress curl versus. alongshore wind stress in GA. Red points in (e) and (f) are upwelling shadow days. GA, Gulf of Arauco; PL, Punta Lavapie; USI, upwelling shadow index.

to PL and, on average, the regional SST increased by 2°C, with the isotherms of 17°C and 18°C located near the coast (Figures 9a and 9e). According to Figure 9, the surface nearshore waters seem to get warmer every day, even during active upwelling (February 1 to 6, 2013). The cold upwelled waters in PL are advected to the north, moving the warm front north to about 36°S generating a warm pool or upwelling shadow within the GA that extends 100 km alongshore. The cross-shore extent of the shadow is about 30–40 km. Once the thermal front is established, the daily wind cycle near the coast and the established zonal pressure gradient favors a southward surface flow transporting warm waters from the north to the GA. Similar to Monterey Bay, the offshore extent of the warm layer is on the order of the internal Rossby radius of deformation and, probably, these low-density lenses behave like an arrested coastal gravity current (Graham & Largier, 1997). Therefore, the nature of the upwelling shadow changes from December to February, resulting in average USI values of 1.4°C in December and 1.45°C in February (Table 3).

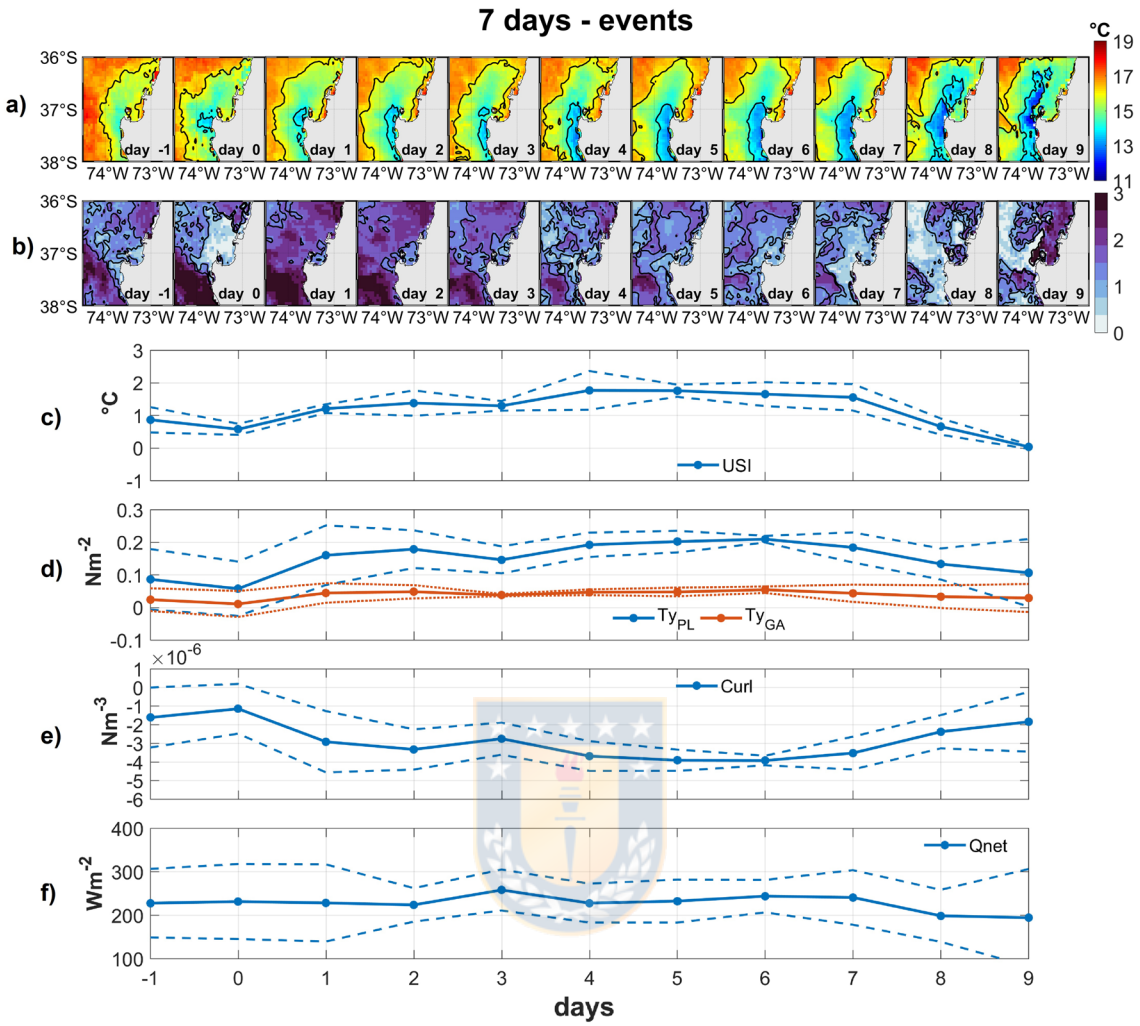

Figure 13. Composite analysis of USI (using events lasting 7 days). (a) SST average, black contours are 14°C and 16°C. (b) SST Standard Deviation, black contours are 1°C and 1.5°C. (c) USI. (d) Along shore wind stress for PL (blue) ang GA (red). (e) Wind stress curl centered in SMI. (f) Qnet (average of 36.5°S, 74°W to 37.5°S, 73°W). Dashed lines from (c) to (f) are standard deviation of the time series. SMI, Santa Maria Island; SST, sea surface temperature; USI, upwelling shadow index.

The interannual SST variability also impacts the relative differences between the GA and PL. During the first warm phase (2002–2006, Figure 6a) a positive anomaly around 1°C facilitated the occurrence of upwelling shadow events (Figure 8a) due to the predominance of warm waters that increased the contrast between cold waters off PL with warm waters in the GA. Saldías et al. (2016) and Schneider et al. (2017), attributed this change from a warm phase (2002–2006) to a cold phase (starting in 2007) to the southward shift of the South Pacific High during winter months and the influence of the ENSO interannual dynamics. The warmer period (2002–2006) was dominated by a mean positive value of the Oceanic Niño Index (0.32), whereas during the colder period (2007–2013), the mean value of the index was negative (−0.32). The influence of El Niño on the water column's temperature was also described by Graham and Largier (1997) in Monterey Bay but with more horizontally homogeneous temperatures during the warm ENSO event of 1992, opposite to the case of the GA in central-southern Chile.

4.2. Role of Wind Stress

A common characteristic of the events, which occurred on 10.29% of days over the 15 years, is that they occurred during upwelling-favorable wind conditions (in PL and the GA) and under the influence of cyclonic wind stress curl (winds more intense in PL than in the GA; Figures 12e, 12f, 13a, and 13e). Although some

events occurred during wind relaxation (about seven events), most of them occurred with a cyclonic wind stress curl (negative) and northward daily wind stress in PL, ranging between 0 and 0.4 N m^{-2} (Figure 12e). Because the upwelling shadow corresponds to a difference in the SST between PL and GA, its development evolves in two stages. The first phase occurs when the equatorward alongshore wind stress intensification increases Ekman transport with coastal cooling off PL. The wind on the GA is also equatorward but weaker because this sector is protected from southwesterly winds by the extension of the Nahuelbuta mountain toward PL (see Figure 1 and Introduction). This orography facilitates the generation of a cyclonic wind stress curl, which shifts active upwelling offshore and contributes to the surface thermal difference between PL and GA. The variability of the thermal gradient between PL and GA depends on initial thermal conditions in the GA and the persistence of equatorward winds.

The acute geometry of the coastline at PL facilitates the formation of an upwelling flow west of PL, which separates from the shoreline and drives a weak cyclonic circulation within the GA (Largier, 2020; Penven et al., 2000; Pitcher et al., 2010), consistent with warm surface water and stratification of the water column within the GA. Under this scenario, the role of SMI is unclear from our observations. The island could represent a geographic extension of PL since Boca Chica is a narrow and shallow mouth, potentially increasing the impact of the cape and cyclonic circulation within the GA. Another option is that the SMI could enhance or weaken the cyclonic circulation within the GA. Future studies, including process-oriented numerical simulation, would clarify the role of SMI on the development of upwelling shadow events.

The second phase of upwelling shadows occurs during the relaxation of the upwelling-favorable winds. The duration of relaxations is critical on the zonal thermal gradient, leading to the weakening or destruction of the upwelling shadow. During brief relaxations (a couple of days or less), the surface cold waters upwelled near PL and advected to the north of ISM end up entering into the GA from the north, causing a surface cooling and weakening of the thermal gradient between PL and GA (see, for example, on February 25 to March 1, 2013, in Figure 9e). This input of cold surface waters toward a semi-enclosed system has also been reported for Monterey Bay (Graham et al., 1992; Rosenfeld et al., 1994). During longer wind relaxations (at least 1 week), as there is no source of cold surface water in PL, the thermal gradient between PL and GA tends to disappear. An aspect associated with wind relaxation is the increase in the residence time of the GA and subsequent surface heating due to the solar radiation input, and, consequently, an increase in the USI. In Monterey Bay, wind relaxations were considered an essential source of variability in the upwelling shadow (Graham & Largier, 1997). Another factor that could influence the intensity of warming within the GA is a reversal of the wind within the GA (i.e., southward wind), facilitating the advection of warm surface water from the north.

Our results suggest that most upwelling shadows in the GA occur during upwelling-favorable winds, with an intense cyclonic wind stress curl (Figures 13a, 13d, and 13e) and with regularly interspersed periods of wind relaxation. Short upwelling relaxations end up dissipating the upwelling shadow due to the entry, from the north, of upwelled waters to the Gulf. On the other hand, long wind relaxation periods also dissipate the thermal gradient due to the general warming under these conditions. Once the alongshore wind stress has ceased, the sloping isopycnals tend to slump back, eventually destroying the surface front and potentially re-stratifying the upper water column. The scale of the front is relevant to the local dynamics since large-scale horizontal density gradients tend to maintain a geostrophic jet that flows in the same direction as the upwelling-favorable winds (Barth et al., 2000; Saldías & Allen, 2020). Northward winds induce a southward (poleward) pressure gradient and a southward coastal current when the upwelling wind weakens. This condition is more expected from January to March than in December.

Data Availability Statement

SST data can be found in the website of the Geostationary Operational Environmental Satellite (GOES https://podaac-tools.jpl.nasa.gov/drive/files/allData/goes/L3/goes_6km_nrt/docs/goes_sst_doc.html). Winds and incoming solar radiation data from ERA5 product are available at the Copernicus Climate Change Service Information 2019 (https://cds.climate.copernicus.eu/cdsapp#!/dataset/reanalysis-era5-pressure-levels?tab=form); to get these data researcher need to register for free. Geostrophic velocity and Total current (sum of the geostrophic and Ekman components) can be found in the GlobCurrent data repository

(http://globcurrent.ifremer.fr/); for FTP access, a simple registration is required to keep track of the usage of these products. Wind speed and direction data from a meteorological station located at Carriel Sur Airport are currently in the process of being archived in a public repository.

Acknowledgments
M. Sobarzo was partially supported by the Program for Ecosystem Studies in the Gulf of Arauco (PREGA), which is funded by Celulosa Arauco y Constitución S.A., and INCAR (FONDAP-CONICYT No. 15110027). Z. Wong was supported by the Scholarship CONICYT-PCHA/Doctorado Nacional/2013–21130213 (N° Folio Beca 63140267) and by Red Doctoral en Ciencia, Tecnología y Ambiente, REDOC CTA, University of Concepcion, and partially supported by PREGA. G. Saldías is partially supported by FONDECYT grant 1190805 and the Millennium Nucleus Center for the Study of Multiple Drivers on Marine Socio-Ecological Systems funded by MINECON NC120028.

References

Aiken, C. M., Castillo, M. I., & Navarrete, S. A. (2008). A simulation of the Chilean Coastal Current and associated topographic upwelling near Valparaíso, Chile. *Continental Shelf Research*, *28*(17), 2371–2381. https://doi.org/10.1016/j.csr.2008.05.006

Ancapichun, S., & Garces-Vargas, J. (2015). Variability of the Southeast Pacific subtropical anticyclone and its impact on sea surface temperature off north-central Chile. *Ciencias Marinas*, *41*(1), 1–20. https://doi.org/10.7773/cm.v41i1.2338

Astudillo, O., Dewitte, B., Mallet, M., Frappart, F., Rutllant, J. A., Ramos, M., et al. (2017). Surface winds off peru-chile: Observing closer to the coast from radar altimetry. *Remote Sensing of Environment*, *191*, 179–196. https://doi.org/10.1016/j.rse.2017.01.010

Bakun, A., & Nelson, C. S. (1991). The seasonal cycle of wind-stress curl in subtropical eastern boundary current regions. *Journal of Physical Oceanography*, *21*(12), 1815–1834. https://doi.org/10.1175/1520-0485(1991)021<1815:tscows>2.0.co;2

Barth, J. A., Pierce, S. D., & Smith, R. L. (2000). A separating coastal upwelling jet at Cape Blanco, Oregon and its connection to the California Current System. *Deep-Sea Research Part II*, *47*(5–6), 783–810. https://doi.org/10.1016/s0967-0645(99)00127-7

Bonicelli, J., Moffat, C., Navarrete, S. A., Largier, J. L., & Tapia, F. J. (2014). Spatial differences in thermal structure and variability within a small bay: Interplay of diurnal winds and tides. *Continental Shelf Research*, *88*, 72–80. https://doi.org/10.1016/j.csr.2014.07.009

Bonicelli, J., Tapia, F. J., & Navarrete, S. A. (2014). Wind-driven diurnal temperature variability across a small bay and the spatial pattern of intertidal barnacle settlement. *Journal of Experimental Marine Biology and Ecology*, *461*, 350–356. https://doi.org/10.1016/j.jembe.2014.09.003

Brink, K. H., Jones, B. H., Van Leer, J. C., Mooers, C. N. K., Stuart, D. W., Stevenson, M. R., et al. (1981). Physical and biological structure and variability in an upwelling center off Peru near 15°C during March, 1977. *Coastal Upwelling*, *1*, 473–495. https://doi.org/10.1029/CO001p0473

Castelao, R. M., & Barth, J. A. (2007). The role of wind stress curl in jet separation at a cape. *Journal of Physical Oceanography*, *37*(11), 2652–2671. https://doi.org/10.1175/2007JPO3679.1

Castelao, R. M., Mavor, T. P., Barth, J. A., & Breaker, L. C. (2006). Sea surface temperature fronts in the California Current System from geostationary satellite observations. *Journal of Geophysical Research*, *111*(C9), 1–13. https://doi.org/10.1029/2006JC003541

Castro, L. R., Troncoso, V. A., & Figueroa, D. R. (2007). Fine-scale vertical distribution of coastal and offshore copepods in the Golfo de Arauco, central Chile, during the upwelling season. *Progress in Oceanography*, *75*(3), 486–500. https://doi.org/10.1016/j.pocean.2007.08.012

Daneri, G., Dellarossa, V., Quiñones, R., Jacob, B., Montero, P., & Ulloa, O. (2000). Primary production and community respiration in the Humboldt Current System off Chile and associated oceanic areas. *Marine Ecology Progress Series*, *197*, 41–49. https://doi.org/10.3354/meps197041

Dever, E. P., & Lentz, S. J. (1994). Heat and salt balances over the northern California shelf in winter and spring. *Journal of Geophysical Research*, *99*(C8), 16001–16017. https://doi.org/10.1029/94jc01228

Devis-Morales, A., Montoya-Sánchez, R. A., Bernal, G., & Osorio, A. F. (2017). Assessment of extreme wind and waves in the Colombian Caribbean Sea for offshore applications. *Applied Ocean Research*, *69*, 10–26. https://doi.org/10.1016/j.apor.2017.09.012

Escribano, R., & Morales, C. E. (2012). Spatial and temporal scales of variability in the coastal upwelling and coastal transition zones off central-southern Chile (35-40°S). *Progress in Oceanography*, *92–95*, 1–7. https://doi.org/10.1016/j.pocean.2011.07.019

Figueroa, D., & Moffat, C. (2000). On the influence of topography in the induction of coastal upwelling along the Chilean coast. *Geophysical Research Letters*, *27*(23), 3905–3908. https://doi.org/10.1029/1999gl011302

Garreaud, R. D., Rutllant, J. A., Muñoz, R. C., Rahn, D. A., Ramos, M., & Figueroa, D. (2011). Vocals-cupex: The chilean upwelling experiment. *Atmospheric Chemistry and Physics*, *11*, 2015–2029. https://doi.org/10.5194/acp-11-2015-2011

Graham, W. M. (1993). Spatio-temporal scale assessment of an "Upwelling Shadow" in Northern Monterey Bay, California. *Estuaries*, *16*(1), 83–91. https://doi.org/10.2307/1352766

Graham, W. M., Field, J. G., & Potts, D. C. (1992). Persistent? upwelling shadows? and their influence on zooplankton distributions. *Marine Biology*, *114*(4), 561–570. https://doi.org/10.1007/bf00357253

Graham, W. M., & Largier, J. L. (1997). Upwelling shadows as nearshore retention sites: The example of northern Monterey Bay. *Continental Shelf Research*, *17*(5), 509–532. https://doi.org/10.1016/s0278-4343(96)00045-3

Hamilton, P., & Rattray, M., Jr. (1978). A numerical model of the depth-dependent, wind-driven upwelling circulation on a continental shelf. *Journal of Physical Oceanography*, *8*(3), 437–457. https://doi.org/10.1175/1520-0485(1978)008<0437:anmotd>2.0.co;2

Lagos, N., Benítez, S., Duarte, C., Lardies, M., Broitman, B., Tapia, C., et al. (2016). Effects of temperature and ocean acidification on shell characteristics of Argopecten purpuratus: Implications for scallop aquaculture in an upwelling-influenced area. *Aquaculture Environment Interactions*, *8*, 357–370. https://doi.org/10.3354/aei00183

Landaeta, M. F., & Castro, L. R. (2006). Spawning and larval survival of the Chilean hake Merluccius gayi under later summer conditions in the Gulf of Arauco, central Chile. *Fisheries Research*, *77*(1), 115–121. https://doi.org/10.1016/j.fishres.2005.08.006

Largier, J. L. (2020). Upwelling bays: How coastal upwelling controls circulation, habitat, and productivity in bays? *Annual Reviews of Marine Sciences*, *12*. https://doi.org/10.1146/annurev-marine-010419-011020

Largier, J. L., Magnell, B. A., & Winant, C. D. (1993). Subtidal circulation over the northern California shelf. *Journal of Geophysical Research*, *98*(C10), 18147–18179. https://doi.org/10.1029/93jc01074

Lentz, S. J. (1987). A heat budget for the northern California shelf during CODE 2. *Journal of Geophysical Research*, *92*(C13), 14491–14509. https://doi.org/10.1029/jc092ic13p14491

Letelier, J., Pizarro, O., & Nuñez, S. (2009). Seasonal variability of coastal upwelling and the upwelling front of central Chile. *Journal of Geophysical Research*, *114*(C12), 1–16. https://doi.org/10.1029/2008JC005171

Marín, V. H., Delgado, L. E., & Escribano, R. (2003). Upwelling shadows at Mejillones Bay (northern Chilean coast): A remote sensing in situ analysis. *Investigaciones Marinas*, *31*(2), 47–55. https://doi.org/10.4067/s0717-71782003000200005

Marín, V. H., Escribano, R., Delgado, L. E., Olivares, G., & Hidalgo, P. (2001). Nearshore circulation in a coastal upwelling site off the northern Humboldt Current System. *Continental Shelf Research*, *21*(13), 1317–1329

Penven, P., Roy, C., de verdière, A. C., & Largier, J. (2000). Simulation of a coastal jet retention process using a barotropic model. *Oceanologica Acta*, *23*(5), 615–634. https://doi.org/10.1016/s0399-1784(00)01106-3

Piñones, A., Castilla, J., Guiñez, R., & Largier, J. (2007). Nearshore surface temperatures in Antofagasta Bay (Chile) and adjacent upwelling centres. *Ciencias Marinas*, *33*(1), 37–48. https://doi.org/10.7773/cm.v33i1.1226

Pitcher, G. C., Figueiras, F. G., Hickey, B. M., & Moita, M. T. (2010). The physical oceanography of upwelling systems and the development of harmful algal blooms. *Progress in Oceanography*, *85*(1–2), 5–32. https://doi.org/10.1016/j.pocean.2010.02.002

Rahn, D. A. (2012). Influence of large scale oscillations on upwelling-favorable coastal wind off central Chile. *Journal of Geophysical Research*, *117*, a. https://doi.org/10.1029/2012JD018016

Rahn, D. A., & Garreaud, R. D. (2014). A synoptic climatology of the near-surface wind along the west coast of South America. *International Journal of Climatology*, *34*, 780–792. https://doi.org/10.1002/joc.3724

Ramp, S. R., Paduan, J. D., Shulman, I., Kindle, J., Bahr, F. L., & Chavez, F. (2005). Observations of upwelling and relaxation events in the northern Monterey Bay during August 2000. *Journal of Geophysical Research*, *110*(C7), 1–21. https://doi.org/10.1029/2004jc002538

Rosenfeld, L. K., Schwing, F. B., Garfield, N., & Tracy, D. E. (1994). Bifurcated flow from an upwelling center: A cold water source for Monterey Bay. *Continental Shelf Research*, *14*(9), 931–964. https://doi.org/10.1016/0278-4343(94)90058-2

Roughan, M., Mace, A. J., Largier, J. L., Morgan, S. G., Fisher, J. L., & Carter, M. L. (2005). Subsurface recirculation and larval retention in the lee of a small headland: A variation on the upwelling shadow theme. *Journal of Geophysical Research*, *110*(C10), 1–18. https://doi.org/10.1029/2005JC002898

Saavedra, N. (1980). La presión y la dirección del viento en concepción. *Tralka*, *1*(2), 153–162.

Saldías, G. S., & Allen, S. E. (2020). The influence of a submarine canyon on the circulation and cross-shore exchanges around an upwelling front. *Journal of Physical Oceanography*, *50*(6), 1677–1698. https://doi.org/10.1175/jpo-d-19-0130.1

Saldías, G. S., Largier, J. L., Mendes, R., Pérez-Santos, I., Vargas, C. A., & Sobarzo, M. (2016). Satellite-measured interannual variability of turbid river plumes off central-southern Chile: Spatial patterns and the influence of climate variability. *Progress in Oceanography*, *146*, 212–222. https://doi.org/10.1016/j.pocean.2016.07.007

Saldías, G. S., Sobarzo, M., Largier, J., Moffat, C., & Letelier, R. (2012). Seasonal variability of turbid river plumes off central Chile based on high-resolution MODIS imagery. *Remote Sensing of Environment*, *123*, 220–233. https://doi.org/10.1016/j.rse.2012.03.010

Schneider, W., Donoso, D., Garcés-Vargas, J., & Escribano, R. (2017). Water-column cooling and sea surface salinity increase in the upwelling region off central-south Chile driven by a poleward displacement of the South Pacific high. *Progress in Oceanography*, *151*, 38–48. https://doi.org/10.1016/j.pocean.2016.11.004

Schulien, J., Peacock, M., Hayashi, K., Raimondi, P., & Kudela, R. (2017). Phytoplankton and microbial abundance and bloom dynamics in the upwelling shadow of Monterey Bay, California, from 2006 to 2013. *Marine Ecology Progress Series*, *572*, 43–56. https://doi.org/10.3354/meps12142

Send, U., Beardsley, R. C., & Winant, C. D. (1987). Relaxation from upwelling in the coastal ocean dynamics experiment. *Journal of Geophysical Research*, *92*(C2), 1683–1698. https://doi.org/10.1029/jc092ic02p01683

Sobarzo, M., Bravo, L., Donoso, D., Garcés-Vargas, J., & Schneider, W. (2007). Coastal upwelling and seasonal cycles that influence the water column over the continental shelf off central Chile. *Progress in Oceanography*, *75*, 363–382. https://doi.org/10.1016/j.pocean.2007.08.022

Sobarzo, M., & Djurfeldt, L. (2004). Coastal upwelling process on a continental shelf limited by submarine canyons, Concepción, central Chile. *Journal of Geophysical Research*, *109*(C12), 1–20. https://doi.org/10.1029/2004JC002350

Sobarzo, M., Saldías, G. S., Tapia, F. J., Bravo, L., Moffat, C., & Largier, J. L. (2016). On subsurface cooling associated with the Biobio River canyon (Chile). *Journal of Geophysical Research: Oceans*, *121*, 4568–4584. https://doi.org/10.1002/2016JC011796

Strub, P. T., Mesïas, J., Montecino, V., Rutlland, J., & Salinas, S. (1998). Coastal ocean circulation off western south America. In A. R. Robinson, & K. H. Brink, (Eds.), *The sea: The global coastal ocean, regional studies and synthesis* (pp. 273–313). New York: John Wiley

Szoeke, R. A. D., & Richman, J. G. (1981). The role of wind-generated mixing in coastal upwelling. *Journal of Physical Oceanography*, *11*(11), 1534–1547. https://doi.org/10.1175/1520-0485(1981)011<1534:trowgm>2.0.co;2

Torreblanca, M. L., Pérez-Santos, I., San Martín, B., Varas, E., Zilleruelo, R., Riquelme-Bugueño, R., & Palma, Á. T. (2016). Seasonal dynamics of zooplankton in a northern Chile bay exposed to upwelling conditions. *Revista de Biología Marina y Oceanografía*, *51*(2), 273–291. https://doi.org/10.4067/s0718-19572016000200006

Valle-Levinson, A., Atkinson, L. P., Figueroa, D., & Castro, L. (2003). Flow induced by upwelling winds in an equatorward facing bay: Gulf of Arauco, Chile. *Journal of Geophysical Research*, *108*(C2). https://doi.org/10.1029/2001JC001272

Wang, D.-P. (1997). Effects of small-scale wind on coastal upwelling with application to point conception. *Journal of Geophysical Research*, *102*(C7), 15555–15566. https://doi.org/10.1029/97JC00635

Woodson, C. B., Eerkes-Medrano, D. I., Flores-Morales, A., Foley, M. M., Henkel, S. K., Hessing-Lewis, M., et al. (2007). Local diurnal upwelling driven by sea breezes in northern Monterey Bay. *Continental Shelf Research*, *27*(18), 2289–2302. https://doi.org/10.1016/j.csr.2007.05.014

Woodson, C. B., Washburn, L., Barth, J. A., Hoover, D. J., Kirincich, A. R., McManus, M. A., et al. (2009). Northern Monterey Bay upwelling shadow front: Observations of a coastally and surface-trapped buoyant plume. *Journal of Geophysical Research*, *114*(C12), 1–15. https://doi.org/10.1029/2009JC005623

4.2. Capítulo 2

Sombras de surgencia generadas por el chorro costero a lo largo de la costa oeste subtropical de América del Sur: Golfo de Arauco, Chile}

Artículo enviado en Septiembre del 2021 al Journal of Geophysical Research: Oceans. Actualmente en proceso de segunda revision (enviado en Enero 2022).

Upwelling Shadows driven by the Low-Level Jet along the Subtropical West Coast of South America: Gulf of Arauco, Chile.

Piero Mardones, Zeneida Wong, Josse Contreras-Rojas, Richard Muñoz, Eduardo Hernández and Marcus Sobarzo.

Resumen

La Sombra de surgencia (US) ha sido observada en algunas bahías de la costa oeste subtropical de América del Sur, usualmente aquellas protegidas de los vientos. Diferentes argumentos han tratado de explicarlo. Usando datos observacionales derivados de satélite y datos de reanálisis, se estudia la relación entre fenómenos atmosféricos a escala sinóptica y las sombras de surgencia en una de estas áreas, el golfo de Arauco (GA), en Chile (37ºS), una bahía semicerrada y altamente productiva. Con base en 9 años (2011 - 2019) de datos diarios de temperatura superficial del mar con resolución de 1 km (G1SST), se aplicó un índice de sombra de surgencia que permitió identificar 40 eventos de sombra de surgencia (periodos con al menos 3 días consecutivos de una condición considerada como sombra). A partir de un análisis de compuestos se propone que los anticiclones migratorios que se mueven hacia el este en la zona sur de Chile inducen la intensificación de los vientos costeros debido a la formación del chorro costero de baja altura (CLLJ), lo cual gatilla las sombras de surgencia a través de la surgencia costera afuera del golfo de Arauco. El mismo anticiclón induce un área cálida de baja presión, incrementando la temperatura superficial del mar (TSM) dentro del golfo. Cuando la baja costera está completamente desarrollada, la intensidad del viento se reduce, y se observa un débil viento norte en la

costa. El debilitamiento de los flujos convectivos netos, posiblemente debido a la relajación de este chorro costero, también incrementa la TSM y magnifica la sombra de surgencia. Otro proceso que podría incrementar la TSM dentro del golfo es la advección meridional de agua cálida desde el norte. Sin embargo, las tasas de calentamiento observadas (> 1°C/día) sugieren que esto solo podría explicar parcialmente el calentamiento dentro del golfo de Arauco.

Upwelling Shadows driven by the Low-Level Jet along the Subtropical West Coast of South America: Gulf of Arauco, Chile

Piero Mardones[2,5], Zeneida Wong[2,3,4], Josse Contreras-Rojas[2,3], Richard Muñoz[2,3,6,7], Eduardo Hernández-Miranda[2,4,6], and Marcus Sobarzo[1,2,4]

[1]Department of Oceanography, Faculty of Natural Sciences and Oceanography, University of Concepción, Concepción, Chile.

[2]Ecosystem Studies in the Gulf of Arauco (PREGA), University of Concepción, Concepción, Chile.

[3]Graduate Program in Oceanography, Department of Oceanography, Faculty of Natural Sciences and Oceanography, University of Concepción, Concepción, Chile.

[4]Interdisciplinary Center for Aquaculture Research (INCAR). University of Concepción, Concepción, Chile.

[5]Centro de Investigación en Ecosistemas de la Patagonia (CIEP).

[6]Departamento de Ecología, Facultad de Ciencias, Universidad Católica de la Santísima Concepción, Concepción, Chile.

[7]Departamento de Física, Facultad de Ciencias, Universidad del Bío-Bío, Concepción, Chile.

Key Points:

- The coastal low-level jet (CLLJ) triggers upwelling shadows through coastal upwelling outside the Gulf of Arauco (GA).
- The anticyclonic winds induce a warm low-pressure area increasing the sea surface temperature inside the Gulf.
- The northerly meridional advection of warm water could only partially explain the warming within the GA.

Corresponding author: Marcus Sobarzo, msobarz@udec.cl

Abstract

Some bays of the west coast of South America, usually protected from the winds, have been classified as upwelling shadows (US), with anomalous high sea surface temperatures (SST). Different arguments have tried to explain it. Using observational, satellite-derived, and reanalysis data, we studied the relationship between synoptic-scale atmospheric phenomena and the US in one of these areas, the Gulf of Arauco (GA), in Chile (37^{o}S), a highly productive semi-enclosed bay. We used a daily global 1 km sea surface temperature data set (G1SST) to identify 324 US days between 2011 and 2019. Then, 40 upwelling shadow events, periods with at least three consecutive US days, were found. The composite analysis proposes that the migratory anticyclones moving eastward at southern Chile induce coastal southerly wind intensification due to the coastal low-level jet (CLLJ) formation, which triggers upwelling shadows through coastal upwelling off GA. The same anticyclone induces a warm low-pressure area (coastal low) accompanied by clear skies, increasing the SST inside the Gulf. When the coastal low reaches its mature stage, wind magnitude is reduced, and weak northerly winds are observed at the coast. The weakening of the net convective fluxes, possibly due to this CLLJ relaxation, also increases the SST and exacerbates the upwelling shadow. Another process that could increase SST within the GA is the northerly meridional advection of warm water. However, the observed warming rates (>1°C/day) suggest that it could only partially explain the surface warming within the GA.

Plain Language Summary

On the South Pacific Ocean, there is a high-pressure system known as the Southeast Pacific Anticyclone (SPA), which influences the wind variability, especially along the coast of South America. In austral summer (December to March), the SPA is a little more south and closer to the coast, generating stronger southwesterly winds, contributing to the rise of cold subsurface waters (coastal upwelling). When this process occurs near a semi-enclosed embayment protected from these winds, surface waters inside these bays increase their temperature. This anomalous surface warming inside the protected bays has been defined as an upwelling shadow. Here the upwelling shadow in the Gulf of Arauco (Chile) is studied with nine years of satellite data (SST, SLP, radiation, and winds) and in-situ data (currents and temperatures) from two specific events. This analysis allows suggesting a mechanism for forming the upwelling shadows based on a synoptic-scale weather pattern.

1 Introduction

The subtropical west coast of South America is one of the world's essential eastern boundary upwelling systems (Strub et al., 1998; Sherman & Hempel, 2008). In this area, the mean low-level wind during austral summer (DJF) is northward, driven by the Southeast Pacific Anticyclone (SPA), generating a sizeable coastal upwelling zone approximately from 40°S towards the equator (Hill et al., 1998; Aguirre et al., 2012). In addition,the existence of a quasi-weekly southerly coastal low-level wind jet (CLLJ) in this region has been well documented in terms of its structure, dynamics, and variability with observations, scatterometer data, and atmospheric reanalysis (Rutllant, 1993; R. Garreaud & Muñoz, 2005; Muñoz & Garreaud, 2005; Rahn & Garreaud, 2014; Lima et al., 2018; Aguirre et al., 2021). These CLLJ events are characterized by an elongated surface wind maximum exceeding 10 ms^{-1}, whose axis is around 100-150 km off the coast of central Chile (30°S to 38°S), extending up to 1000 km latitudinally (R. Garreaud & Muñoz, 2005; Muñoz & Garreaud, 2005; Renault et al., 2009; Rahn & Garreaud, 2014; Aguirre et al., 2021). They occur year-round but are more frequent (about 60% of the time) during the spring-summer (R. Garreaud & Muñoz, 2005). The cross-shore scale of CLLJ is around 500 km, and its vertical core is close to the top of the marine boundary layer (R. Garreaud & Muñoz, 2005).

The CLLJ appears when synoptic conditions, specifically the passage of surface atmospheric high-pressure systems (i.e., migratory anticyclones) moving eastward at southern Chile, induce a northward alongshore pressure gradient force (Muñoz & Garreaud, 2005; Aguirre et al., 2021). However, this pressure gradient force is only semigeostrophically balanced, since the steep coastal topography does not allow a complete geostrophic balance near the surface. Thus, no geostrophic easterly flow is generated at low levels and the northward alongshore low-level flow -upwelling favorable- is accelerated only constrained by surface friction (Muñoz & Garreaud, 2005). However, at higher levels where topographic inhibition relaxes, an easterly flow appears with a series of consequences in the temperature and stability of the lower troposphere (Muñoz & Garreaud, 2005). This easterly flow that downs the western slope of subtropical Andes also has been independently documented in previous studies as "foehn-like" downslope winds, called by local communities in central Chile as Terral (near 30°S), Raco (near 33°S), or Puelche (near 36°S) (Montes et al., 2016; Rutllant & Garreaud, 2004; Montecinos et al., 2017). Subsidence enhanced by the downslope flow adiabatically warms the lower troposphere, and the surface pressure drops hydrostatically, generating the onset of a warm-core low-pressure area (i.e., coastal low) in central Chile

(Rutllant, 1994; Rutllant & Garreaud, 2004; R. Garreaud et al., 2002; R. Garreaud & Rutllant, 2003). Simultaneously, this coastal low north of the migratory anticyclone enhances the alongshore pressure gradient, producing positive feedback that deepens the low and extends their life (R. Garreaud & Rutllant, 2003).

Rahn and Garreaud (2014) characterized the near-surface wind along the west coast of South America. Their work generalized the relationship mentioned above between the alongshore pressure gradient and alongshore wind for the entire coast of South America and over annual time scales. Two local wind maximum were recognized in north-central Chile in their and previous studies: Lengua de Vaca (30°S) and Punta Lavapie (PL) (36°24'S) (R. D. Garreaud et al., 2011; Montecinos et al., 2011). Both maxima are embedded in the CLLJ previously described by (R. Garreaud & Muñoz, 2005) and (Muñoz & Garreaud, 2005). However, Punta Lavapie presents higher variability in the mean and distribution of coastal winds throughout the year than Lengua de Vaca. This higher variability is mainly because Punta Lavapie is located in a transition zone subject to the seasonal changes of SPA and storm tracks positions (Saavedra & Foppiano, 1992; R. D. Garreaud et al., 2014). In austral summer, the average wind and frequency of CLLJ events in this area are higher than any other zone on the west coast of South America (Rahn & Garreaud, 2014). Moreover, Aguirre et al. (2021) observed in this zone the highest probability (∼70% in spring-summer) having a CLLJ event together with a migratory anticyclone approaching the coast farther south (Aguirre et al., 2021). In other words, Punta Lavapie is, along the entire coast of north-central Chile, the place where the relationship between migratory anticyclone and CLLJ is best manifested.

Adjacent to PL is the Gulf of Arauco (GA) (Fig.1) one of the largest and most productive equatorward-facing bays in all of South America (Valle-Levinson et al., 2003; Yannicelli et al., 2006). The connection between bays and the coastal ocean, especially in upwelling regions, presents unique characteristics associated with the interaction of winds and currents with the local topography (Largier, 2020). Among these processes, the so-called upwelling shadow has been defined as "a localized region of an active coastal upwelling system within which upwelling is reduced, and a coherent pattern of anomalously high surface temperature is observed" (W. M. Graham & Largier, 1997). Upwelling shadows are characterized by a strong cross-shore temperature gradient (∼0.3°C km^{-1}), positive spatial SST anomalies (∼ 2°C), and sharp horizontal density gradients (∼0.11 kg m^{-3} km^{-1}) (W. Graham et al., 1992; W. M. Graham, 1993; W. M. Graham & Largier, 1997; V. H. Marín et al., 2001, 2003). The

presence and extent of upwelling shadows have been explained by surface water warming due to longer residence time and wind relaxation periods (W. M. Graham & Largier, 1997), regional and local wind forcing (Rosenfeld et al., 1994; W. M. Graham & Largier, 1997; Ramp et al., 2005; Woodson et al., 2007, 2009), and wind stress curl and coastal configuration (Wong et al., 2021). Particularly in GA, Wong et al. (2021) developed an index to identify upwelling shadow days (US days) based on temperature differences between GA and PL, showing that these events were more frequent during spring/summer months when upwelling-favorable winds with strong cyclonic wind stress curls were present.

Upwelling shadow areas are also important due to their particular physical characteristics, which increase the biological productivity and retention of planktonic organisms in adjacent zones (W. Graham et al., 1992; W. M. Graham, 1993; W. M. Graham & Largier, 1997; Largier, 2020; Harvey et al., 2021). The magnitude of the ecological, local and regional effects will depend on the intensity of the upwelling event, the residence time of the waters in the upwelling shadow area, and the subsequent relaxation period (W. M. Graham & Largier, 1997; Largier, 2020). The GA, like other upwelling shadow areas, can act as a retention zone for phyto and zooplankton (Daneri et al., 2000; Landaeta & Castro, 2006; Yannicelli et al., 2006; Castro et al., 2007; Hernández-Miranda et al., 2009; Escribano & Morales, 2012) which favors the high biological productivity. In general, equator-facing bays along the Chilean upwelling region such as Tongoy Bay (∼30°S) and Mejillones Bay (∼23°S) seem to play a similar role (V. H. Marín et al., 2001, 2003; Castilla et al., 2002) as the GA (Letelier et al., 2009).

Unlike Wong et al. (2021), where, through constructing a US index, upwelling shadows were analyzed from a statistical point of view (frequency and duration), this new study explores the relationship of this phenomenon with the synoptic variability of the local meteorology. It incorporates the wind forcing and a simple balance between the radiative and convective ocean-atmosphere fluxes. An explanation is given of the origin of the CLLJ, its role in the coastal upwelling generation, and its indirect role in the generation of a warm low-pressure area that changes the atmospheric pressure gradients and the heat balance in the surface layer of the GA, relaxing the wind and changing its direction. It is proposed that this process adds heat to the surface layer of the GA, increasing the thermal difference between the GA and the cooling that occurs at PL outside the GA due to coastal upwelling. Using a combination of observational, satellite-derived, and reanalysis data, we study the relationship between the CLLJ, coastal lows, and upwelling shadows in a semi-enclosed bay.

The paper is organized as follows: A brief context of the GA is provided in section 2. The various datasets, upwelling shadow index calculation and upwelling shadow events definition are presented in section 3. Our main results are described in sections 4.1 (large scale context of upwelling shadows in GA), 4.2 (general overview of two selected study cases), and 4.3 (in-situ observations of selected cases). Section 4.4 discussed the possible physical mechanisms that can explain the upwelling shadow in this area. Finally, section 5 summarizes the key findings of this work.

2 Study region

The Gulf of Arauco (GA) is the largest semi-enclosed embayment along the coast of central Chile (30°S - 38°S). The Gulf extends westward approximately 40 km, limited by the Santa Maria Island (SMI) (Figure 1). This island defines two connections with the open ocean: 1) Westward is Boca Chica (BC), located between SMI and Punta Lavapie (PL); it is 8 km wide and has a mean depth of 20 m. 2) Northward, Boca Grande (BG) is located between Punta Puchoco (PP) and SMI, and it is 25 km wide and has a mean depth of 50 m.

South of GA, the typical heights between the Nahuelbuta Mountains and PL fluctuate around 200-300 m with values that, in PL, can reach 350 m high. This orography constitutes a natural barrier that protects the GA from much of the influence of southerly winds (Sobarzo et al., 2016). So then, GA can be divided into two zones: i) South of 37^{o}S correspond to the head of the GA, shallower than 50 m, and characterized by an east-west coastline orientation; ii) North of 37^{o}S, the GA extends to the Biobio submarine canyon with depths between 50 and 500 m, approximately. Thus, this area is more exposed to wind and oceanic influences.

3 Data and methods

About nine years (January 2011 – September 2019) of daily global 1 km sea surface temperature (G1SST) were used from 36°S - 75°W to 38°S - 72°30'W. This product belongs to the Jet Propulsion Laboratory (JPL) OurOcean group as part of the Group for High-Resolution Sea Surface Temperature (GHRSST) Level 4 sea surface temperature analysis (JPL-OurOcean-Project, 2011). The G1SST analysis include satellite data from the following sensors: a) Advanced Very High-Resolution Radiometer (AVHRR), b) Advanced Along Track Scanning Radiometer (AATSR), c) Spinning Enhanced Visible and Infrared Imager (SEVIRI), d) Advanced Microwave Scanning Radiometer-EOS (AMSRE), e) Tropical Rain-

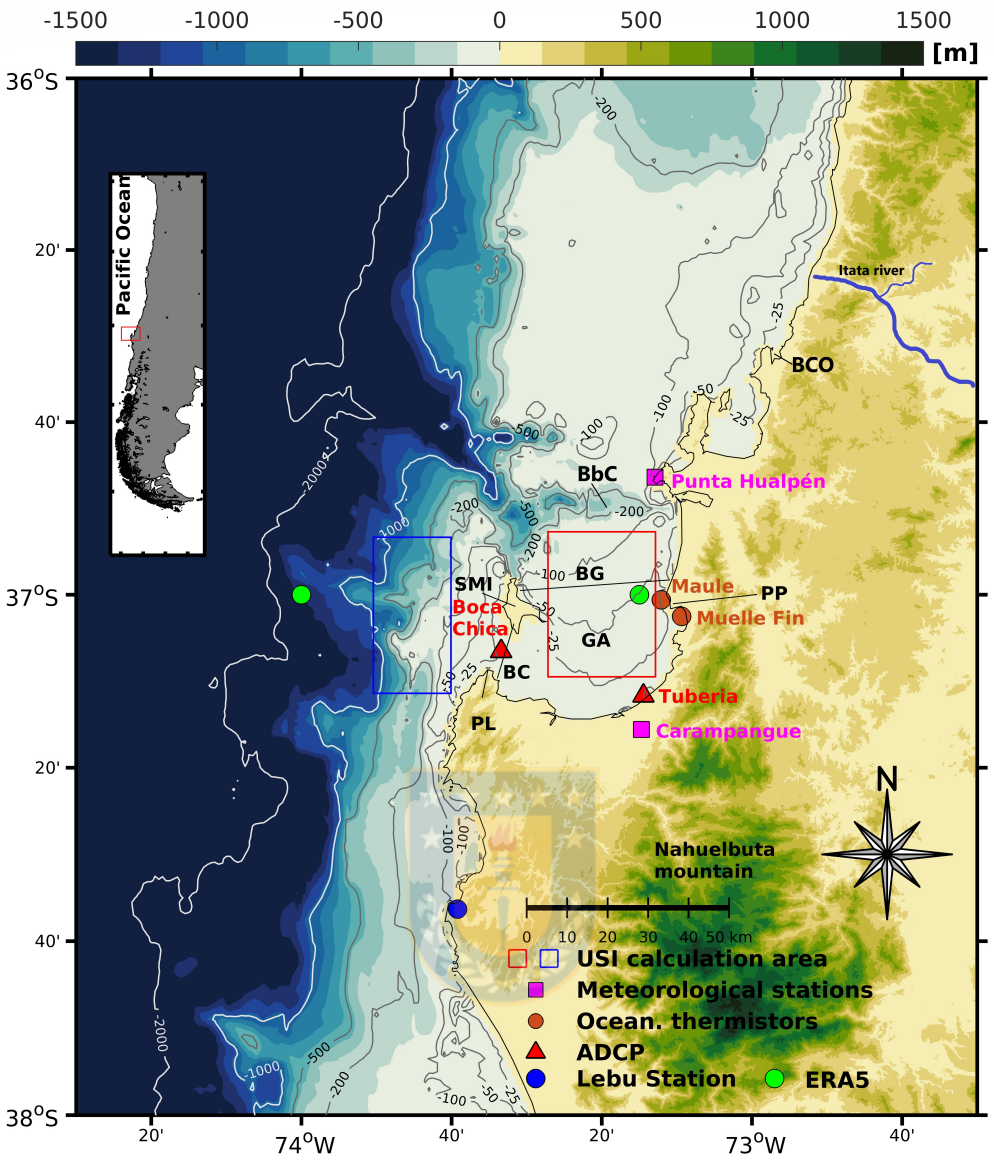

Figure 1. Study area off Central Chile showing the Gulf of Arauco and locations of meteorological stations, coastal thermistors, and acoustic doppler current profilers (ADCP). Blue and red polygons are the areas of the Upwelling Shadow Index (USI). Green circles are points where the wind was obtained from ERA5 reanalysis. Gray solid lines are isobaths, and topography/bathymetry is shown in shaded colors. BCO: Coliumo bay, BbC: Biobio Canyon, BG: Boca Grande, BC: Boca Chica, GA: Gulf of Arauco, PL: Punta Lavapie, SMI: Santa Maria Island, PP: Punta Puchoco.

fall Measuring Mission Microwave Imager (TMI), f) Moderate Resolution Imaging Spectroradiometer (MODIS), g) Geostationary Operational Environmental Satellite (GOES) Im-

ager, h) the Multi-Functional Transport Satellite 1R (MTSAT-1R) radiometer, and, i) *in situ* data from drifting and moored buoys.

For large-scale atmospheric context and composite analysis (section 4.1), we used mean sea level pressure (SLP) data and fields of zonal and meridional winds 10 m above the surface from ERA5 reanalysis (Hersbach et al., 2020). All these variables were selected in the same period of G1SST. ERA5 is the most recent atmospheric reanalysis product generated by the European Centre for Medium-Range Weather Forecasts (ECMWF). It combines historical observations, advanced modeling, and data assimilation to provide globally hourly data since 1979 for many atmospheric and ocean variables for public access. It has a spatial resolution of approximately 30 km and 137 vertical levels from the surface up to 80 km (0.01 hPa). Daily averages of the hourly selected variables from ERA5 (centered at 12 UTC) were calculated to compare with the daily data from G1SST. The hourly values were used for the synoptic analysis of the selected cases (section 4.2).

3.1 Upwelling shadow index and compositing technique

An Upwelling shadow Index (USI) was defined by Wong et al. (2021) and is calculated as follow:

$$USI = (T_{GA} - T_{PL}) * m_f \tag{1}$$

where:

T_{GA} = mean sea surface temperature in the Gulf of Arauco (red box in Figure 1).

T_{PL} = mean sea surface temperature west of Santa Maria Island (blue box in Figure 1).

m_f = weighting factor, which was calculated as follow:

$$m_{f(t)} = \frac{SST\_mean_{(t)} - Min}{r} \tag{2}$$

where:

$SST\_mean_{(t)}$ = average SST of the area: 36°S, 75°W to 38°S, 72°30'W) at t time.

$_{(t)}$ = Days from January 1, 2011 to September 15, 2019.

Min = minimum value of SST_mean = 10.74°C

Max = maximum value of SST_mean = 18.75°C

r = range of SST_mean values = Max - Min = 8.00°C.

$m_{f(t)}$ results in a time series ranging from 0 to 1 (dimensionless), where 0 is the coldest day, and 1 is the warmest day of the record.

From this index, Wong et al. (2021) considered two criteria to define an Upwelling Shadow day: (i) (T_{GA} - T_{PL}) >1.1°C (average difference between GA and PL in summer) and (ii) USI >0.91°C (maximum USI value for differences < 1.1°C). A statistical analysis of G1SST time series from GA and PL showed that these series do not have a normal distribution (in summer, GA and PL were skewed 0.29 and 0.65, respectively, not shown); therefore, the median would better represent the central value of the time series than the average to determine the criteria for USI days. Then, the median difference between GA and PL was 1.05°C and the USI value associated was 0.84°C. Those days that meet both criteria are days with upwelling shadow (US days), and the others are days without upwelling shadow (noUS days). This study ranges from November to March since low-level jet and upwelling shadow days are more frequent in late spring and austral summer (Table 1) (Muñoz & Garreaud, 2005; Wong et al., 2021). In these months, a total of 324 US days (25% of the time) and 972 noUS days were detected in GA. To analyze the evolution of upwelling shadows in the GA, we defined upwelling shadow events as periods with at least three consecutive US days and two days apart from each other to prevent overlapping between events. Thus, 40 independent upwelling shadow events in the austral summer (November-March) were selected between 2011 and 2019. These events represent roughly 63% of the total US days in the entire period. The mean fields for two days before (day -2), at onset (day 1), and the third day (day 3) of these upwelling shadows events were calculated. The mean fields for noUS days (Figure 2) were then subtracted to determine the atmospheric forcing and oceanic changes concerning non-upwelling shadow conditions.

Table 1. Monthly information of upwellling shadow days in the Gulf of Arauco from 2011 to 2019.

	Jan	Feb	Mar	Apr	May	Jun	Jul	Aug	Sep	Oct	Nov	Dec
#days	138	71	39	7	0	0	0	0	0	0	16	60
%	41.69	21.45	11.78	2.11	0	0	0	0	0	0	4.832	18.12
USI_{mean}	1.31	1.20	1.04	1.18	–	–	–	–	–	–	1.19	1.14

3.2 Observations and case selection

Two study cases were selected based on the availability of in-situ currents and temperature data inside the GA (Figure 1). The first one ranges from January 12 to 15, 2012 (C1 case), while the second ranges from November 28 to December 4, 2016 (C2 case). Currents data were recorded by upward-looking RDI Workhorse Acoustic Doppler Current Profilers (ADCP 600 kHz) deployed in Tuberia (37°11'41"S, 73°14'28"W) and Boca Chica (36°6'33"S, 73°33'25"W) for C1 and C2, respectively. The instruments were moored at 11 m (C1) and 20 m (C2) depth. Currents speed and direction were recorded at 15 minutes intervals and a size cell of 1 m. In order to compare the currents data between Tuberia and Boca Chica, a standard coordinate system with *x-axis* positive to the east and *y-axis* positive to the north was used. First, hourly averages were calculated, and intratidal variability was removed from the currents data using harmonic analysis (T_TIDE: (Pawlowicz et al., 2002)). Then, a 30-hours cosine-Lanczos filter was applied to remove the remaining high frequencies.

Temperature data were recorded by a thermistors logger chain (Onset Computer Corp., USA) deployed in the dock of the Coronel Port, within the bay of the same name (37°2'31"S, 73°9'21.6"W) and Maule (37°0'35.6"S, 73°12'4"W) for C1 and C2, respectively (Figure 1). Sea Surface Temperature (SST) from Lebu station (37°35'39"S, 73°39'51"W), outside the Gulf, was facilitated by Servicio Hidrográfico y Oceanográfico de la Armada de Chile (SHOA). Local wind from two different locations was used for each case study. Carampangue station (37°15'35.6"S, 73°14'44"S) was used to study C1, while C2 was analyzed using data from Punta Hualpén station (36°46'24"S, 73°12'54"W). Two points of meridional wind from ERA5 reanalysis were selected for each period to compare the wind forcing inside and outside of the Gulf (green circles, Fig. 1). These time series were contrasted with local wind data mentioned above.

4 Results and Discussion

4.1 Large scale context

The noUS days represented 75% of total days between November-March in the entire period. Consistently their mean fields of SLP, wind at 10 m, and SST were almost the same as those observed during the austral summer in this region (Fig 2ab). The SLP mean-field showed the SPA with its center around 35°S and with southerly/southwesterly coastal

winds -upwelling favorable- north of 40°S. Zonal winds were observed roughly between 42°S to 50°S and northwesterly winds farther south. An evident "wind dropoff" was observed, with southwesterly wind, on average, around 3 m/s more intense west of PL than inside of GA (Fig 2b). However, this difference decreases slightly northward of Boca Grande. During noUS days, SST outside the GA -west of PL- was on average about 0.5-1°C colder than the SST inside GA (Fig. 2b). The mean summer SST close and west of PL was around 13.5°C. This temperature pattern is similar to the mean SST field for austral summer observed in a previous work, where a thermal difference GA-PL of the same magnitude (around 1°C) was reported (Wong et al., 2021). Using only upwelling shadows days (defined by US index), the difference of SST between GA and PL was, on average, around 2.5-3.0°C. Also, the average wind vectors illustrated a slightly higher difference between GA-PL ($\sim$ 4m/s) for these US days, mainly due to stronger winds in PL (Figure 2c).

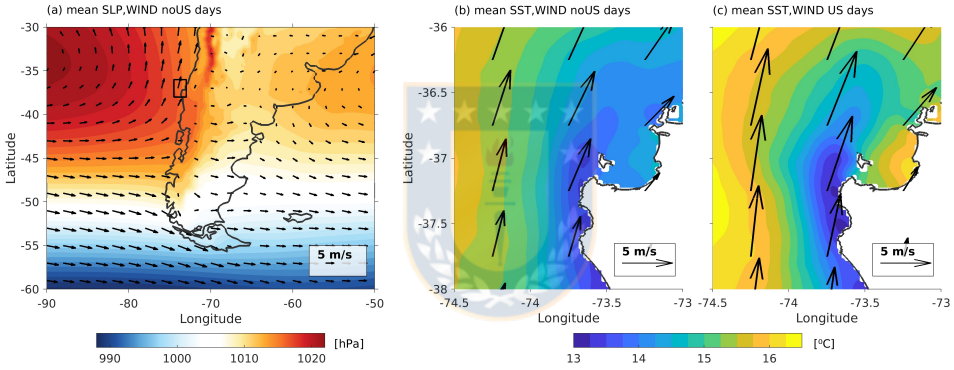

Figure 2. Mean fields for no upwelling shadow (noUS) days of (a) mean sea level pressure and wind vectors at 10 m, (b) sea surface temperature and wind vectors at 10 m. Panel (c) illustrate the same as (b), but for upwelling shadows days (US)

.

In order to analyze the evolution of US events and highlight the differences concerning noUS days, Figure 3 shows the composite anomalies (US minus noUS days) of SLP, SST, and 10 m wind at two days before (day -2), at onset (day 1), and two days after (day 3) the beginning of an US event. On day -2, negative anomalies of SLP were observed south of PL, being more intense ($\sim$ 2 hPa) between 40° and 50°S (Figure 3a). These negative anomalies can be associated with a relaxation of the South Pacific anticyclone and/or the passage of midlatitude cyclones through this area. These anomalies are consistent with the negative (northerly) 10 m wind anomalies observed in Figure 3b; however, their magnitude

was about 1.5 ms^{-1} at PL and 0.5 ms^{-1} in the GA. The SST two days before the beginning of an US event in GA was between 0.5-1° warmer than the mean of noUS days.

At the onset of an US event (day 1), strong positive anomalies of SLP ($\sim$ 4 hPa) were observed in southern Chile between 40°S and 50°S and slightly negative anomalies from PL to the north (Figure 3c). This pattern of SLP anomalies is very similar to the typical anomalies observed during the passage of a migratory anticyclone crossing the Andes through southern Chile, which ends developing a coastal low farther north. This composite pattern can be compared with previous work such as R. Garreaud et al. (2002) and R. Garreaud and Rutllant (2003), where they describe and characterize these coastal low events along the west coast of South America. These positive anomalies are also associated with cold air incursions at the east of subtropical Andes (Marengo et al., 1997; Vera & Vigliarolo, 2000; R. Garreaud, 2000). A strong contrast of SST anomalies was observed, with negative anomalies of the order of -0.4°C at PL and positive anomalies close to +1.6°C inside the GA (Figure 3d), resulting in an absolute difference between PL and GA of around 3°C and being similar to other upwelling shadow sites, such as Monterey Bay (W. M. Graham & Largier, 1997; Woodson et al., 2009). These authors found differences >2°C between inshore and offshore waters. The wind vectors in Figure 3d showed an increase (positive, southerly anomalies) in upwelling favorable winds close to 4 ms^{-1} west of PL, consistent with the cooling zone. Inside the GA, slightly positive anomalies were observed, close to 1 ms^{-1} of magnitude. This positive anomaly indicates that the difference was almost double when an upwelling shadow event begins concerning the noUS days (Figure 2a).

On day three, after the start of the upwelling shadow event, SST anomalies persist (Figure 3f), which is expected since the upwelling shadow is usually maintained for more than three consecutive days (Figure 2c). Here, SST positive anomalies >1°C are restricted within the GA, while the negative SST anomaly off PL spreads over a slightly larger area and is close to -0.7°C. In general, this pattern of SST anomalies is similar to what was found in previous work (Wong et al., 2021). Wind anomalies are smaller than at the beginning of the event, which accounts for the synoptic nature of wind forcing. Meanwhile, no positive SLP anomalies are observed south of 40°S, which may be due to the migratory anticyclone continuing to move eastward. Only negative SLP anomalies ($\sim$ 2 hPa) persist north of PL, which is consistent with the process of formation of a coastal low in this area (R. Garreaud et al., 2002).

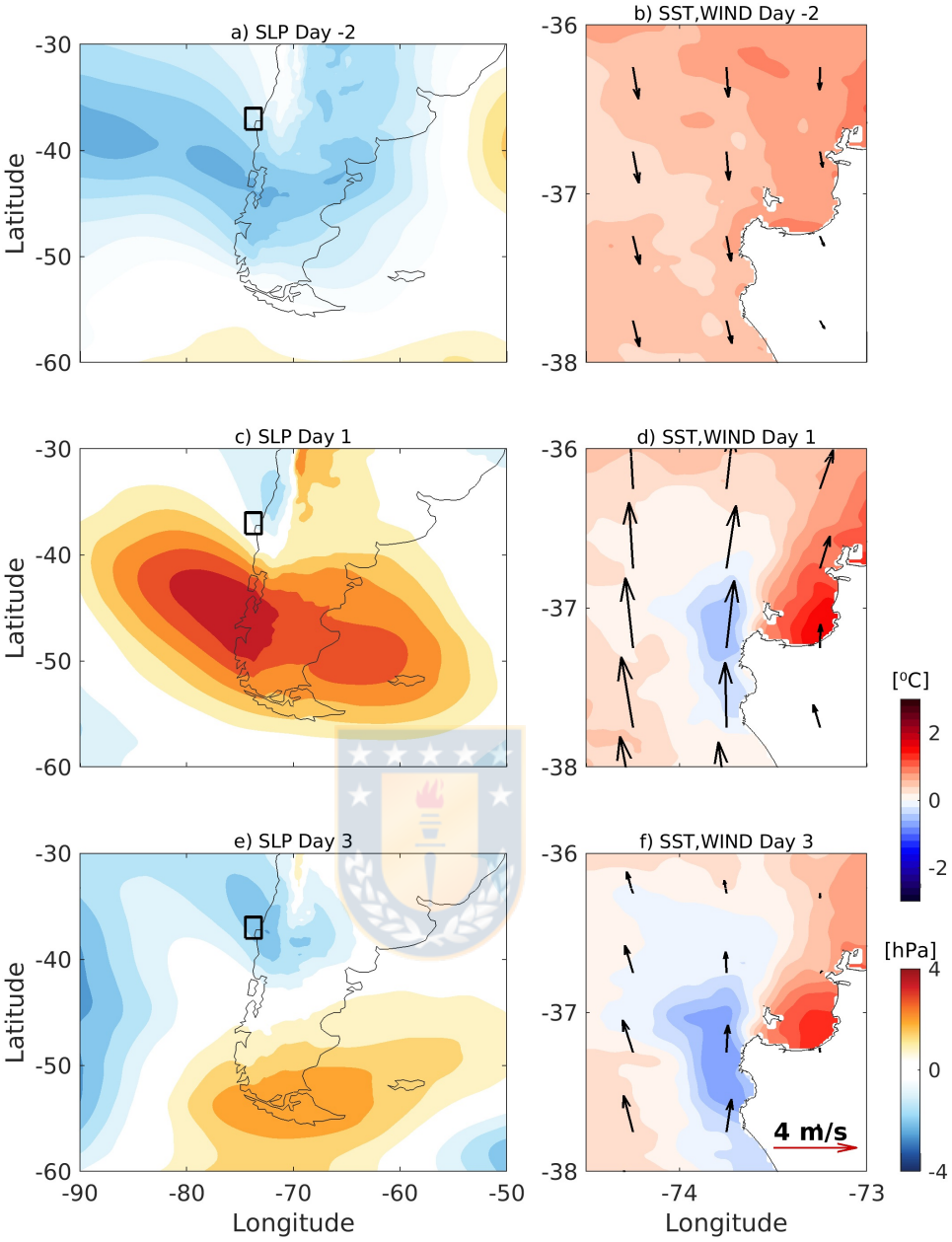

Figure 3. Composite maps of anomalies (US minus noUS days) at day -2, day 1, and day 3 of the upwelling shadow events. Composite anomalies of sea-level pressure are shown in the left panels. The right panels show sea surface temperature and 10 m wind vectors composites.

The wind intensification at day 1 mentioned above coincides with the spatial pattern of the CLLJ described in section 1 (Figure 4a). The southerly wind intensification seems

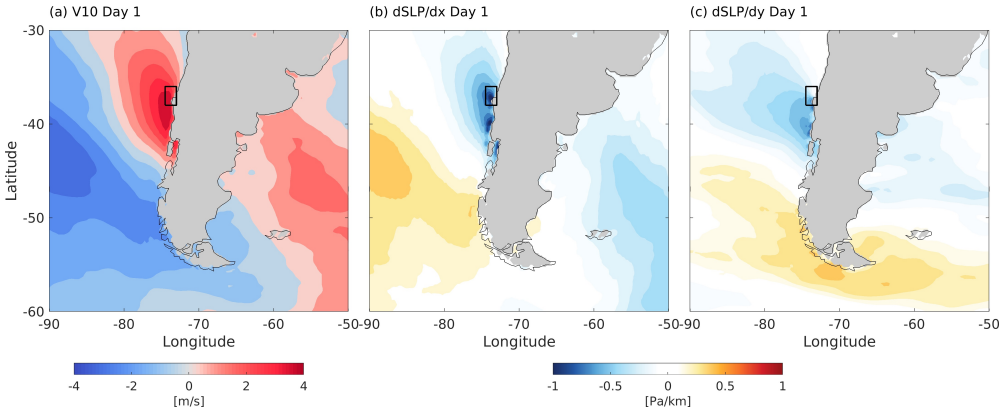

Figure 4. Composite maps of anomalies (US minus noUS days) at upwelling shadow onset (day 1) for (a) 10m meridional wind, (b) zonal gradient of sea level pressure, and (c) meridional gradient of sea level pressure.

to be forced by a negative anomaly of the zonal pressure gradient (geostrophic component, Figure 4b) but also by a negative anomaly of the meridional pressure gradient (ageostrophic component) south of PL (Figure 4c). Previous studies also report the importance of the ageostrophic component in the CLLJ formation at the subtropical west coast of South America (Muñoz & Garreaud, 2005; R. Garreaud & Muñoz, 2005; Montecinos et al., 2017). Around 50°S, the zonal pressure gradient is of the opposite sign, accounting for a northerly wind component over the ocean. A migratory anticyclone stretching towards the continent with a northwesterly inclination south of PL can explain these SLP gradient anomalies. The formation of a coastal low north of PL enhances the zonal and meridional sea level pressure gradients.

4.2 Selected upwelling shadow cases overview

This section presents a general overview of the two selected cases of synoptic upwelling shadows in the GA. Case 1 (C1) occurred during austral summer from January 12 to 15, 2012 (Figure 5) with regional SST >17°C north of 36°S and strong coastal upwelling off PL. Case 2 (C2) occurred in springtime from November 28 to December 1, 2016 (Figure 6) with a regional SST ranging from 15 to 17°C and a slightly less intense coastal upwelling off PL. Both cases presented similar characteristics, with the evident cooling close to PL due to the coastal upwelling waters and warming inside the Gulf -more evident for C2- during the upwelling shadow event. In the first two days of these events, the SLP isobars showed

a stretch towards the southeast, typical of the passage of a migratory anticyclone, with the isobar of 1020 hPa entering the continent south of PL. At the same time, a low-pressure coastal area develops north of PL, centered around 35°S (f,g panels of figures 5 and 6). The preceding pattern was consistent with the composites anomalies presented in Figure 3, giving greater robustness to the analysis of the composites by observing the average pattern in the individual events.

The main differences between both events were perceived in the previous days (day -2, Figs 5, 6), where for the C2 case, an extratropical cyclone is evident between 40°S and 50°S due to the low-pressure center and the cyclonic circulation observed. For case C1, low SLP was also featured at these latitudes at day -2, but a cyclone was observed much further south. However, the extratropical cyclone was between 40°S and 50°S at day -3 (January 9, 2012, not shown). Nevertheless, the patterns observed in both events were also consistent with that presented in the composites for day -2 of Figure 3, which showed negative anomalies of the SLP between 40°S and 50°S and negative anomalies of winds around GA at day -2, or in other words a weakening of the typical upwelling favorable winds in summer.

4.3 In-situ observations of selected cases

This section presents some local measurements that allow a more detailed view of C1 and C2 events regarding currents, temperatures (surface and bottom), and winds in coastal sectors called Boca Chica, Tubería, Maule, and Muelle Fin (Figure 1). Two ERA5 points were used to complement local wind observations in both areas (selected points marked in Figure 1). Before both events, meridional winds were northerly (around 9 ms^{-1}) and without significant differences inside and outside the GA (Figures 7 and 8). However, the meridional winds changed their direction near one day before the events, turning into southerly winds. As a result, more intense southerly winds outside the GA were evident, accounting for the wind dropoff observed in the composite from day 1 (Figure 3d). This condition increased the USI due to the cooling at PL. Based on the large-scale analyzes of previous sections, these maximum winds are associated with the coastal low-level wind jet along the subtropical west coast of South America. After the jet relaxes, a northerly wind appears again, more persistent during C1 due to the coastal low north of PL (Figs. 5 and 6).

Northerly winds favored southwestward surface currents (until 4 m depth) greater than 20 cm/s at the head of the GA (Tuberia) before and after the C1 event. However, the

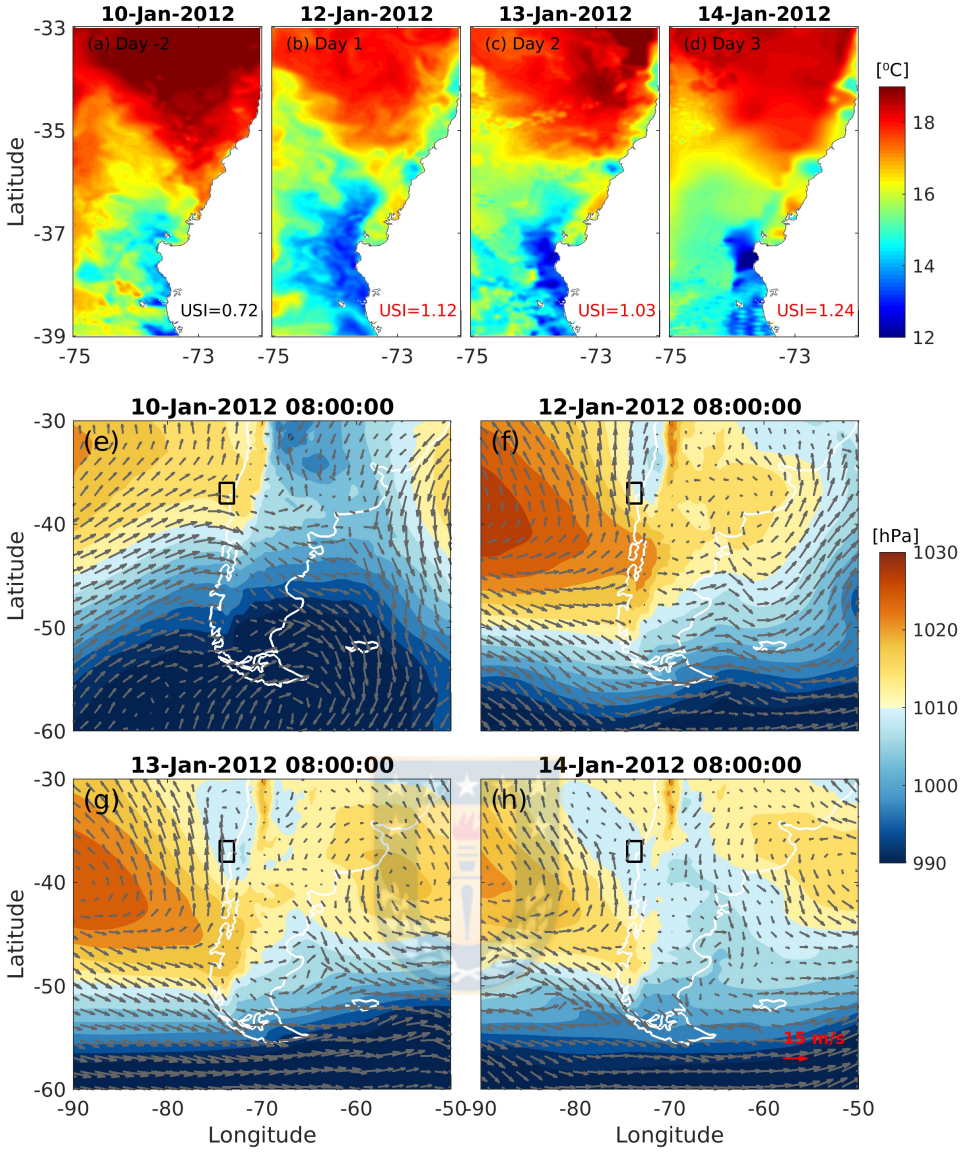

Figure 5. Evolution of the sea surface temperature (upper panels), wind vectors at 10 m (arrows), and sea level pressure in Southeast Pacific (middle and bottom panels) during the C1 upwelling shadow event. The upwelling shadow index (USI) values are indicated for each day in the upper panels. USI values in red indicate upwelling shadow days.

372 change to upwelling favorable winds during the C1 event diminished and rotated the currents
373 causing a weak northward flow, especially at the surface (less than 5 cm/s) (Fig. 7bc). In
374 Monterey Bay, W. Graham et al. (1992) found a similar slow flow during upwelling shadow
375 events. In our case, this slow flow could indicate significant water retention at the head

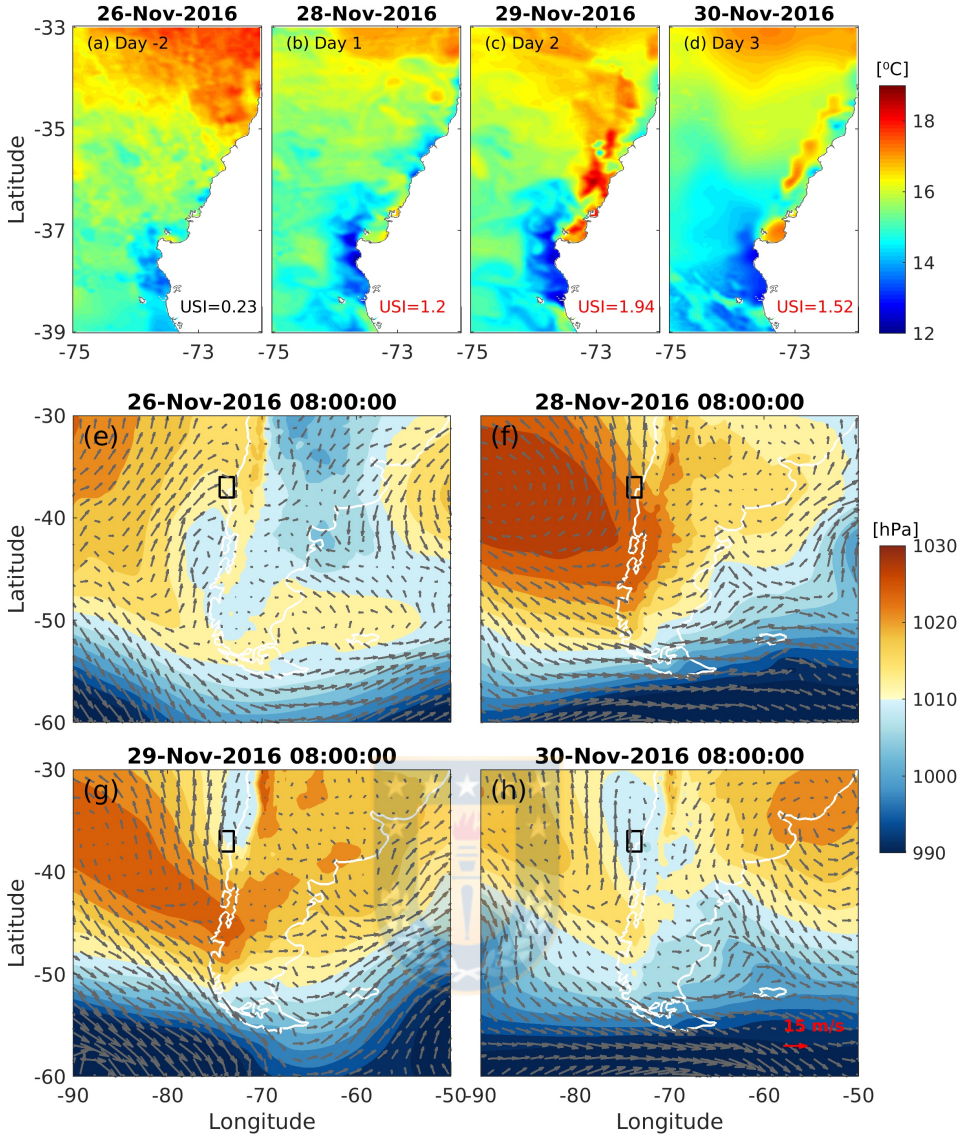

Figure 6. Evolution of the sea surface temperature (upper panels), wind vectors at 10 m (arrows), and sea level pressure in Southeast Pacific (middle and bottom panels) during the C2 upwelling shadow event. The upwelling shadow index (USI) values are indicated for each day in the upper panels. USI values in red indicate upwelling shadow days.

of the GA, where the coastal water is more sheltered from the wind influence. Thus, four days before the events, northerly winds induce southwestward and westward currents at the Tuberia and Boca Chica, respectively (Fig. 9a). When the CLLJ is present, currents are weak and with different directions in the water column (Fig. 9b). Once the CLLJ relaxes,

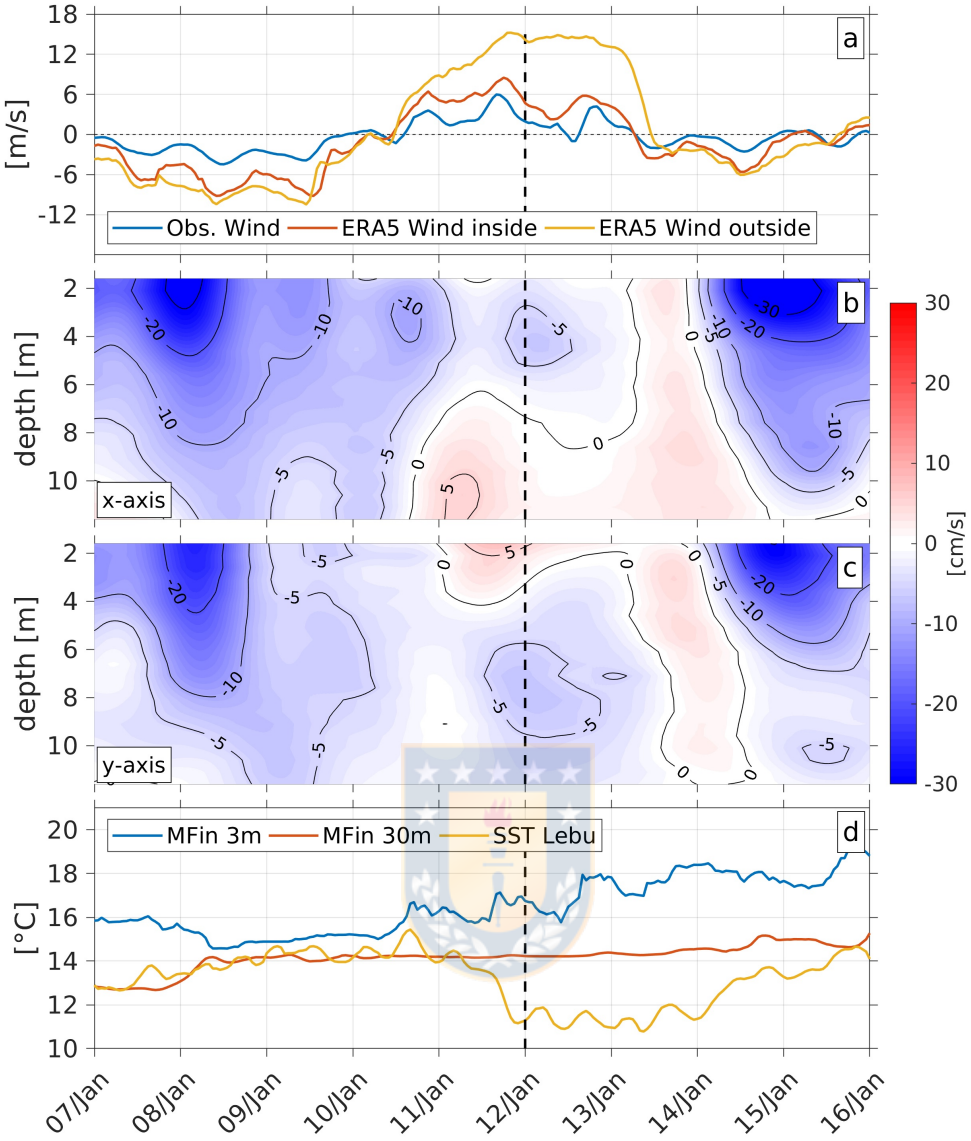

Figure 7. Time series of C1 event. (a) Meridional wind component at Carampangue Station and ERA5 selected locations. (b) Zonal and (c) Meridional current components at Tuberia's ADCP. (d) Sea temperature inside (MFin) and outside (Lebu) of GA. See Figure 1 for measurement location.

the currents return to the southwest and west at the Tuberia and Boca Chica, respectively (Fig. 9c).

Also, during the C1 event, outside of GA (Lebu Station) and in response to the upwelling favorable winds, SST decreased from near 14°C to around 11°C. However, within of GA (MFin), surface temperatures showed an increase from around 15°C on January 10th (day

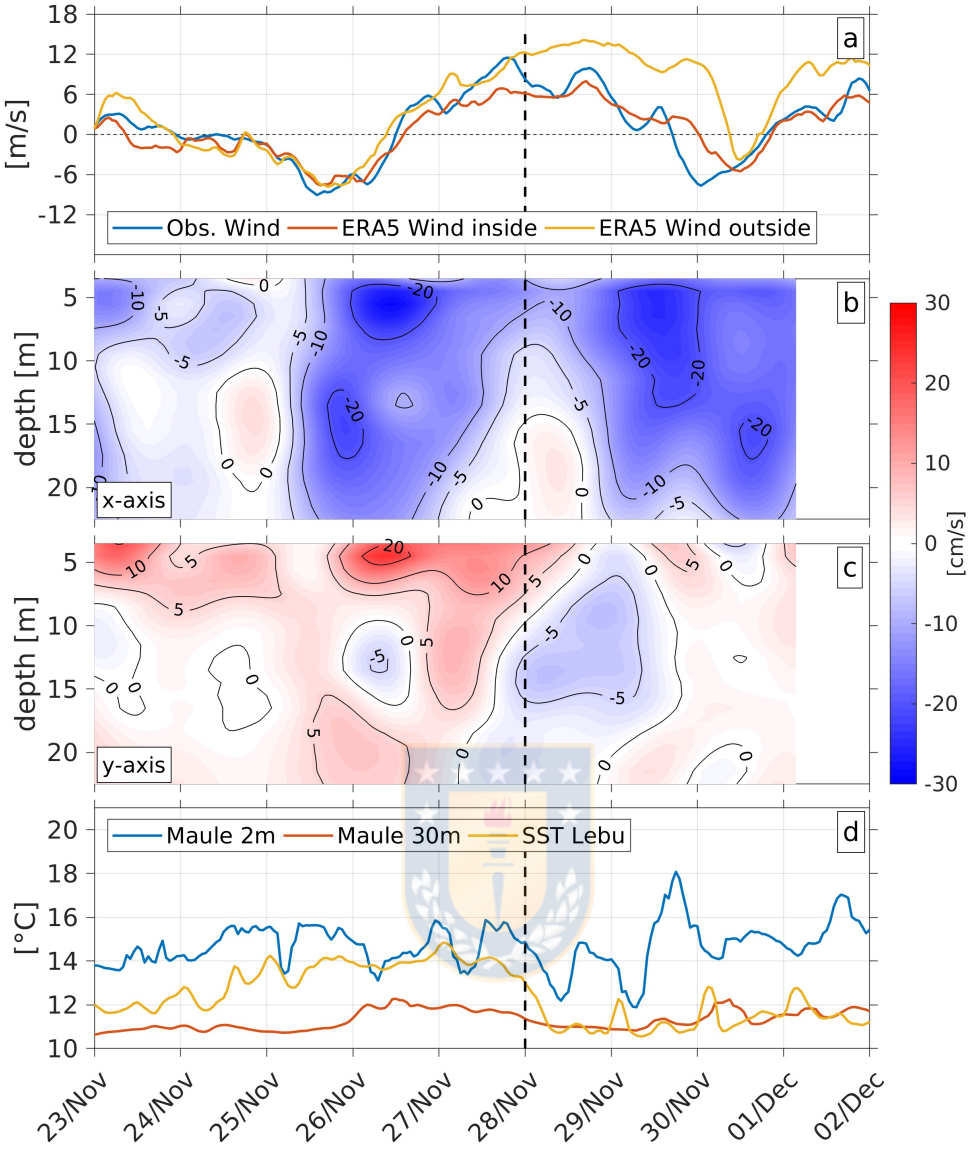

Figure 8. Time series of C2 event. (a) Meridional wind component at Hualpen Station and ERA5 selected locations. (b) Zonal and (c) Meridional current components at Boca Chica's ADCP. (d) Sea temperature inside (Maule) and outside (Lebu) of GA. Currents record only go up to December 1 in this location. See Figure 1 for measurement location.

-2) to around 18.5°C on January 14th (day 3), causing a difference close to 7°C between the SST inside and outside of GA -i.e., a strong upwelling shadow-. On the other hand, temperatures at 30 m depth remained constant around 14°C throughout the entire period (Fig. 7d). Since the water column stability around this area in summer is mainly determined

by thermal stratification (Bravo et al., 2013), it implies a very stable water column inside the GA during this upwelling shadow event. In conjunction with the observed low horizontal current velocities (Fig. 9b), the water column stability allows us to infer little exchange between surface and bottom waters -i.e., very low vertical velocities- within the GA.

During the C2 event, currents were measured at Boca Chica (Fig. 1). Similar to C1 event, negative currents at the x-axis (out GA) decreased from ∼20 cm/s two days before the event to 10 cm/s (surface) and almost 0 cm/s (bottom) at day 1 (Fig. 8b). Once more, this pattern coincides with the intensification of the southerly wind jet. These zonal currents showed a two-layer structure, with a weakened flow out of the GA near the surface and weak bottom currents entering the GA (Fig. 9b). This two-layer structure is similar to that found by Valle-Levinson et al. (2003) during the influence of upwelling winds. Temperatures outside the GA (Lebu) showed a similar pattern to C1 event, with a decrease in SST from 14°C in previous days to 11°C during the US event. Although SST inside the Gulf (in Maule) showed an increase during the US event, this time series showed a significant variability ranging from 14°C to 16°C before the event begins, increasing this range from 12°C to 18°C during the event. The temperature at 30 m depth inside the GA showed little variability (about 1°C). This relatively steady low temperature favors the water column stratification during US days (Fig. 8d).

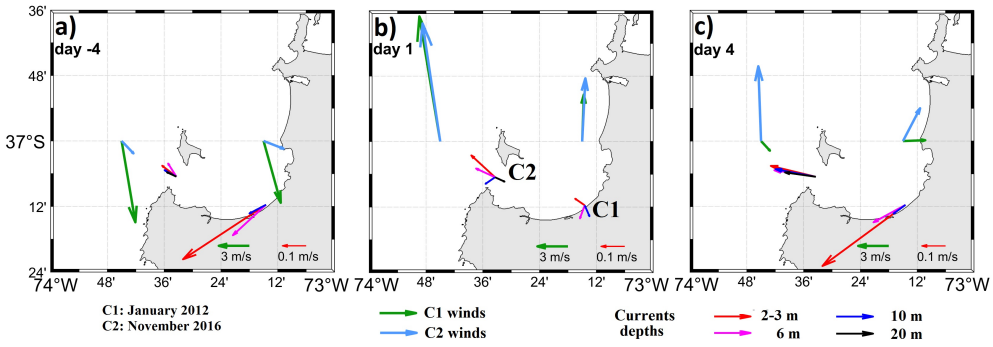

Figure 9. Scheme of the circulation in the Gulf of Arauco, based on the deployments located at Tubería (C1) and Boca Chica (C2). Panels from left to right correspond to day -4, day 1 and day 4. Red, magenta, blue and black vectors are currents at different depths. Green and light blue vectors are ERA-5 winds for each case of study.

4.4 Possible mechanisms of upwelling shadows events

The possible mechanisms that could explain the strong temperature contrast between the GA and PL during upwelling shadow events are discussed in this section. The surface cooling outside the GA can be explained directly by coastal upwelling at PL, where the Ekman transport generates the rise of colder waters (Wong et al., 2021). As has already been demonstrated, strong warming observed in the GA during these events occurs only near the surface. While the bottom temperatures remained almost constant, generating a more stable water column minimizing the vertical advection ($w\Delta T/\Delta z = 0$) compared to periods without upwelling shadow. Furthermore, zonal heat advection should not contribute to the warming of GA but, instead, to cooling induced by cold waters west of PL ($u\Delta T/\Delta x = 0$). Then, in the surface heat balance, the terms contributing to the observed warming within the GA could be the meridional heat advection or the ocean-atmosphere heat exchange (radiative or convective).

Wong et al. (2021) explored the role of the meridional surface heat transport from the north on the warming of the GA, highlighting the influence of the northerly wind during the relaxation periods of the coastal upwelling. However, the present study shows that the GA's surface warming begins even under the influence of southwesterly winds (Fig. 7ad and 8ad). On the other hand, a very rough estimate of a plausible meridional advection term ($v\Delta T/\Delta y$) with even slightly overestimated values observed in Figures 5 to 8 (v = -30 cm/s and dT/dy = 1°C/50 km) indicates a temperature change of about +0.5°C/day. Considering advection from the north of the warm front located around 34°S (300 km north of GA) and a temperature difference of 4°C (18°C - 14°C), the daily warming rate decreases to 0.25°C/day. Because the warming rates observed in C1 and C2 were greater than 1°C/day, and in some cases (e.g., December 26, 2016, not shown), this warming reached up to 2.5°C/day, horizontal advection could only explain a small fraction of the warming inside the GA.

Since SST is determined by the relative magnitude of the terms in the heat balance equation, these terms (radiative and convective fluxes) were also explored (Figure 10). Unfortunately, *in-situ* data is not available in this area to directly estimate or measure these fluxes, so the heat fluxes from the ERA5 reanalysis were used. However, available data from coastal meteorological stations at Coronel (close to Muelle Fin, inside GA) and Lebu (south of PL) were plotted as a reference only for case C2. The heat budget equation can

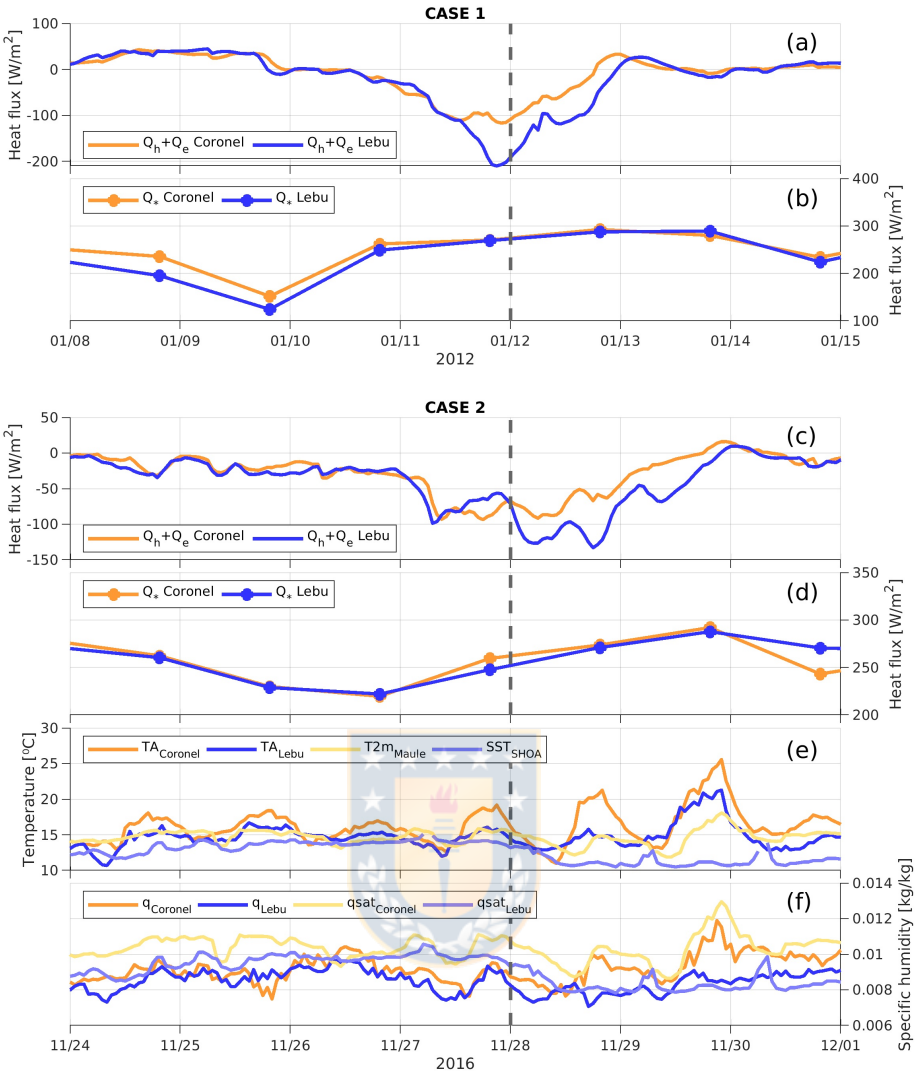

Figure 10. Surface heat fluxes for C1 (a,b) and C2 (c,d). In both cases, fluxes were obtained from ERA5 data. Q_* is represented by the daily mean and it is centered at 19 UTC (peak time) for facilitate the comparison. e) Sea surface temperature ($T2m_{Maule}$ and SST_{SHOA}) and air temperatures ($TA_{Coronel}$ and TA_{Lebu}) measurements inside (Coronel) and outside the Gulf (Lebu) during C2 event. f) Observed specific humidity (q) and estimated at saturation with SST (qsat) both inside and outside the Gulf during C2 event. Fluxes are positive downwards. Q_h: sensible heat, Q_e: latent heat, Q_*: net radiation

be written as $Q_* + Q_v = Q_h + Q_e + Q_t$, where Q_* is the net all-wave radiation, Q_v is the heat advected by currents (including vertical circulation), Q_h and Q_e are sensible and latent heat, respectively. The term Q_t represents the net amount of heat available to change the temperature. Before the events, the low net radiation (i.e., $\sim$ 500 - 750 W/m^2 in C1) was related to the cloudiness associated with the passage of extratropical cyclones (not shown). At the onset of events (vertical dashed line), with the typical clear skies during the coastal low development (R. Garreaud et al., 2002), the net radiation (Q_*) is again maximum, reaching values of $\sim$ 950 W/m^2 (Figs 10b and d). Also, net heat loss from sensible and latent heat fluxes occurs at the beginning of these events (negative $Q_h + Q_e$ in Figure 10a and c) due to the increase in the wind magnitude associated with the CLLJ. This net convective heat loss from the ocean (widely dominated by Q_e) was maximum around day 1 of both events but offset by the net radiative flux increase (Q_*). When wind relaxes between days 2 and 3, the net heat loss from convective fluxes approaches zero ($Q_h + Q_e \approx 0$). Positive or even zero warm advection by currents ($Q_v \geq 0$) generates more energy to raise the SST inside and outside the GA. A composite analysis of the surface heat flux (not shown) of the 40 events revealed a similar pattern to cases C1 and C2.

For C2, differences between SST and the air temperature (proportional to Q_h) suggest that the reduction in negative net convective flux on day 2, is also due to an increase in sensible heat flux from air to sea. Thus, Q_h tends to cancel a weakened latent heat flux (due to wind relaxation) (Figure 10). In other words, Q_h increased because the air temperature at Coronel and Lebu reached maximum values around November 30 (Day 3 for C2), increasing the temperature difference between air and sea surface. All of this is consistent with the moment when the coastal (thermal) low, precisely formed by the adiabatic heating of the lower troposphere (associated with an easterly downslope flow), is in its mature stage (Fig. 6h). This coastal low simultaneously reduces the wind magnitude and changes its direction near the surface inside the GA. In addition, previous works show that once the coastal low begins to dissipate, low -stratocumulus- clouds propagate poleward from northern Chile (R. Garreaud et al., 2002), which could also reduce the specific humidity difference between the air and sea surface (and therefore latent heat flux magnitude).

These radiative and convective fluxes suggest surface warming inside and outside the GA. However, the coastal upwelling forced by the CLLJ brings cold waters to the surface, resulting in a strong surface cooling at PL. In the meantime, high surface temperatures inside the GA do not reflect this subsurface advection of cold water due to the geometric

conditions of the GA. These geographical features have been discussed by Largier (2020) and Wong et al. (2021) in the case of GA. They refer to a headland (PL) of around 250 m high within the marine atmospheric boundary layer and Santa Maria Island (SMI). Both partially protect the GA from upwelling winds. SMI is also responsible for shallow depths in Boca Chica (less than 25 m), limiting water exchange between GA and the continental shelf to the west (Valle-Levinson et al., 2003). However, PL and SMI could facilitate forming a headland eddy that could bring shelf waters from the coastal upwelling into the bay (Largier, 2020; Leth & Middleton, 2004). The formation of these eddies depends on the flow speed, headland size, and lateral eddy flux (Largier, 2020) and are also related to wind relaxation periods that generate advection of waters from the north (Mesias et al., 2001). Besides, a decrease in wind velocities into the GA coincides with wind shadows found in other square bays as Monterey Bay (Largier, 2020), where the difference in wind magnitude between outside and inside winds results in an enhanced wind stress curl (Wong et al., 2021). These changes in the alongshore wind cause an alongshore pressure gradient that can intensify the re-circulation of the headland eddy (Roughan et al., 2005), causing surface warming inside the GA (Largier, 2020). Changes in wind forcing affect the strength and orientation of upwelling flow at PL (northward), which sometimes separate from the apex of headland or curve clockwise, affecting the north part of the GA with cold upwelling waters. If the flow is strong enough, it can go straight and cross isobaths (Largier, 2020).

4.5 Some ecological consequences

Based on this study and that of Wong et al. (2021), a typical upwelling shadow event in the GA could be linked to four stages of ecological relevance: i) SST increased for several days in the GA; ii) Decrease in the advective water exchange between GA and the oceanic zone; iii) Generation of a temporary retention area for plankton organisms inside of GA; iv) Export to the adjacent coastal zone, post-upwelling shadow event, of a differentiated water column (physical-chemical and biological) that would have consequences on biological productivity inside and outside coastal waters.

The GA is immersed in the Humboldt Current System (HCS), known for its high biological productivity. For instance, Daneri et al. (2000) reported high values of gross primary production for this zone of the HCS (20 and 26 g C m^{-2} d^{-1}) compared with other coastal areas and bays around the world (Chavez et al., 2008, 2011; Rain-Franco et al., 2018; Harding et al., 2020). A complex process of biological succession, driven by upwelling,

has been proposed for this zone of the HCS determining ultimately high values of primary productivity, phytoplankton and zooplankton abundances (Anabalón et al., 2007; Vargas et al., 2007; Morales & Anabalón, 2012; Sánchez et al., 2012; Anabalón et al., 2016; Jacob et al., 2018; Osma et al., 2020). Further, this high productivity produce some of the largest benthic, pelagic and demersal fisheries of the world (Cubillos et al., 1998; Thiel et al., 2007; Díaz et al., 2020; Hernández et al., 2021; Hernández & Tapia, 2021).

In the context of transport and dispersal of zooplankton, the GA has been recognized as an important area of retention for larval stages of several pelagic and benthic species. For instance, Landaeta and Castro (2006) identified high concentrations of Chilean hake Merluccius gayi eggs and larvae stages; Castro et al. (2007) studied the vertical distribution of copepods assemblages during an upwelling season finding high densities for several species. In addition, Yannicelli et al. (2006) found similar patterns of high densities of decapod crustacean larvae related to vertical patterns of distribution. On the other hand, in Monterey Bay, W. Graham et al. (1992) and Harvey et al. (2021) reported similar patterns of high planktonic organisms' densities (for a comparative study of this issue in various upwelling bays worldwide, see Largier, 2020).

Krautz et al. (2017) quantified the abundances and non-predatory mortality of various zooplankton taxa in PL and GA and compared them with Coliumo Bay and the mouth of the Itata River, located 50-100 km further north. In global terms, GA presented one order of magnitude higher in the total abundance of zooplankton, holoplankton, and meroplankton, mainly in summer, associated with upwelling shadows. Also, the maximums of primary productivity and seasonal reproductive activity occurred in this Gulf (Daneri et al., 2000; Landaeta & Castro, 2006; Yannicelli et al., 2006; Castro et al., 2007; Hernández-Miranda et al., 2009; Escribano & Morales, 2012). Furthermore, there authors evaluated the non-predatory mortality of zooplankton, registering the highest percentages in the head of GA and PL. These higher mortality percentages would be associated with the 2015-2016 El Niño event and secondarily with low salinity in the surface layer. According to Wong et al. (2021), in January 2015 - April 2016, the GA would have been immersed in a warm phase due to the southward displacement of the SPA, increasing the upwelling shadows events.

The coupling between each upwelling shadow event and the retention of phyto and zooplankton for periods of 3 to 9 days associated with the highest reproductive biological activity (i.e., reproductive seasonality) would be acting as a seasonal catalyst of the biologi-

cal productivity generated inside of the GA and its subsequent export to the adjacent coastal ocean. This seasonal physical-biological coupling could be defined as one of the underlying mechanisms of high fertilization in this coastal area, mediated by upwelling. This has been proposed for other upwelling shadow areas on the planet, for example, Monterrey Bay on the California coast (Largier, 2020; Harvey et al., 2021), Mejillones and Antofagasta bays in the north of Chile (V. H. Marín et al., 2001; V. Marín & Moreno, 2002; Escribano et al., 2002; Castilla et al., 2002; V. H. Marín et al., 2003). In the current scenario, comparative time analysis of Monterey Bay (Northern Hemisphere) with the Gulf of Arauco (Southern Hemisphere) could illuminate the influence of global climate change on the biological productivity of mid-latitude bays in both hemispheres of the globe.

5 Conclusions

This work provides new perspectives on how atmospheric systems whose formation responds to the circulation in the free troposphere (heights greater than 800 - 1000 m) can impact the coastal upwelling and consequently modify associated conditions such as upwelling shadows (US), generating new explanations for the variability of these processes.

US has been studied under different approaches such as wind variability, topography, and biological characteristics. This work focuses on a meteorological viewpoint, analyzing the relationship between atmospheric synoptic-scale patterns and the occurrence of upwelling shadows inside the Gulf of Arauco ($\sim 37°$S), an equatorward semi-enclosed embayment in the subtropical west coast of South America. An index developed by Wong et al. (2021) to define US days inside GA was used. An upwelling shadow event was set as three or more consecutive US days, finding 40 events during the austral summer from January 2011 to September 2019. Based on a composite analysis of SLP, SST, and near-surface winds for these events, added to the detailed study of two individual cases with in situ measurements, we suggested a mechanism for explaining the upwelling shadow process inside the Gulf, highly influenced by atmospheric conditions.

The CLLJ formation associated with the passage of a migratory anticyclone strongly intensifies the southerly winds near the surface, enhancing the coastal upwelling and cooling the area west of PL. This intense vertical advection of cold water dominates the radiative balance in the ocean's surface layer over any radiative or convective flux. On the other hand, the formation of a coastal low north of PL, due to the adiabatic warming in the lower

troposphere of easterly down-slope winds (also associated with the migratory anticyclone) give way to cloudless skies allowing more solar radiation to reach the ocean's surface layer. The combination between cold water west of PL with the enhanced surface warming and weak circulation inside GA results in a tremendous SST difference between PL and GA (>3°C), favoring the upwelling shadow. In addition, the CLLJ relaxation when migratory anticyclone moves eastward weakens the net convective fluxes, contributing to magnifying upwelling shadow signal.

Another process that could increase SST within the GA is the meridional advection of warm water from the north, which could explain likely temperature changes of about 0.25 - 0.5°C/day. However, the observed warming rates (>1°C/day that sometimes reaches up to 2.5°C/day) suggest that it could only partially explain the warming within the GA. On the other hand, the water exchange between PL and GA is limited due to shallow depths in Boca Chica. Therefore, a better estimation of radiative and convective fluxes through direct measurements is required to have more accurate conclusions. Also, this research will continue with high-resolution hydrodynamic modeling that allows a better understanding of the GA's internal circulation patterns and its water exchange with the adjacent ocean.

Considering that the wind variability directly influences the coastal upwelling and that the formation of migratory anticyclones is a common characteristic of mid-latitudes in both hemispheres (Klein, 1958), this study can help to explain how this last mechanism impacts coastal upwelling and subsequently upwelling shadows in similar bays around the world (e.g., Monterrey Bay at NH). In addition, an increase in the frequency of these migratory anticyclones (Aguirre et al., 2021), could influence the intensity and duration of the upwelling shadows. In a biological context, the increase of the SST, the weak circulation, and the stratification of the water column in the GA, associated to the presence of upwelling shadows, affect the biological productivity because of the decrease in the advective water exchange, generating a retention area of plankton inside the protected bay and limiting the transport with the oceanic zones. In this case, the presence of upwelling shadow in GA could be one reason why this gulf has registered one order of magnitude higher in the total abundance of zooplankton, holoplankton, and meroplankton, mainly in summer (Krautz et al., 2017). However, more studies with a biological focus are required to evaluate these changes.

Finally, direct measurements of radiative and convective fluxes will be required to have more accurate conclusions, and high-resolution hydrodynamic modeling will be necessary to

599 understand better the GA's internal circulation and its water exchange with the adjacent
600 ocean.

601 Acknowledgments

602 M.S. was partially supported by the Program for Ecosystem Studies in the Gulf of Arauco
603 (PREGA), which is funded by Celulosa Arauco y Constitucion S.A., by INCAR (FONDAP-
604 CONICYT No. 15110027), and by ANID FONDECYT No. 1190805. Z.W. was supported
605 by the Scholarship CONICYT-PCHA/Doctorado Nacional/2013-21130213 (No Folio Beca
606 63140267) and by Red Doctoral en Ciencia, Tecnología y Ambiente, REDOC CTA, Univer-
607 sity of Concepcion, and partially supported by PREGA. P.M. was partially supported by
608 PREGA. E.H. was partially supported by INCAR (FONDAP-CONICYT No. 15110027).
609 We acknowledge the Hydrographic and Oceanographic Service of the Chilean Navy (SHOA)
610 for SST data from Capitanía de Puerto Lebu and the Sea Temperature Monitoring Study
611 developed by the University of Concepción and funded by Colbún S.A. for providing tem-
612 perature data measured in Bahía Coronel (GA). We also acknowledge the European Centre
613 for Medium-Range Weather Forecasts (ECMWF), responsible for ERA5 reanalysis. Finally,
614 we thank the JPL OurOcean group for providing the G1SST dataset.

615 References

616 Aguirre, C., Flores-Aqueveque, V., Vilches, P., Vásquez, A., Rutllant, J. A., & Garreaud,
617 R. (2021). Recent changes in the low-level jet along the subtropical west coast of
618 south america. *Atmosphere*, *12*(4), 465.

619 Aguirre, C., Pizarro, O., Strub, P. T., Garreaud, R., & Barth, J. A. (2012). Seasonal dy-
620 namics of the near-surface alongshore flow off central Chile. *J. Geophys. Res. Oceans*,
621 *117*(C1), 1–17. doi: 10.1029/2011JC007379

622 Anabalón, V., Morales, C., Escribano, R., & Varas, M. A. (2007). The contribution of
623 nano-and micro-planktonic assemblages in the surface layer (0–30 m) under different
624 hydrographic conditions in the upwelling area off concepción, central chile. *Progress*
625 *in Oceanography*, *75*(3), 396–414.

626 Anabalón, V., Morales, C., González, H., Menschel, E., Schneider, W., Hormazabal, S.,
627 ... Escribano, R. (2016). Micro-phytoplankton community structure in the coastal
628 upwelling zone off concepción (central chile): Annual and inter-annual fluctuations in
629 a highly dynamic environment. *Progress in Oceanography*, *149*, 174–188.

Bravo, L., Ramos, M., Sobarzo, M., Pizarro, O., & Valle-Levinson, A. (2013). Barotropic and baroclinic semidiurnal tidal currents in two contrasting coastal upwelling zones of chile. *Journal of Geophysical Research: Oceans*, *118*(3), 1226–1238.

Castilla, J., Lagos, N., Guiñez, R., & Largier, J. (2002). Embayments and nearshore retention of plankton: the antofagasta bay and other examples. *The oceanography and ecology of the nearshore and bays in Chile*, 179–203.

Castro, L. R., Troncoso, V. A., & Figueroa, D. R. (2007). Fine-scale vertical distribution of coastal and offshore copepods in the Golfo de Arauco, central Chile, during the upwelling season. *Prog. Oceanogr.*, *75*(3), 486–500.

Chavez, F. P., Bertrand, A., Guevara Carrasco, R., Soler, P., & Csirke, J. (2008). The northern humboldt current system: Brief history, present status and a view towards the future. *Progress in Oceanography*, *79*(special issue 2-4), 95–105.

Chavez, F. P., Messié, M., & Pennington, J. T. (2011). Marine primary production in relation to climate variability and change. *Annual review of marine science*, *3*, 227–260.

Cubillos, L., Núñez, S., & Arcos, D. (1998). Producción primaria requerida para sustentar el desembarque de peces pelágicos en chile. *Investigaciones marinas*, *26*, 83–96.

Daneri, G., Dellarossa, V., Quiñones, R., Jacob, B., Montero, P., & Ulloa, O. (2000). Primary production and community respiration in the Humboldt Current System off Chile and associated oceanic areas. *Mar. Ecol. Progr. Ser.*, 41–49.

Díaz, P. A., Álvarez, G., Seguel, M., Marín, A., & Krock, B. (2020). First detection of pectenotoxin-2 in shellfish associated with an intense spring bloom of dinophysis acuminata on the central chilean coast. *Marine Pollution Bulletin*, *158*, 111414.

Escribano, R., Marín, V., Hidalgo, P., & Olivares, G. (2002). Physical-biological interactions in the pelagic ecosystem of the nearshore zone of the northern humboldt current system. *The oceanography and ecology of the nearshore and bays in Chile*, 145–175.

Escribano, R., & Morales, C. E. (2012). Spatial and temporal scales of variability in the coastal upwelling and coastal transition zones off central-southern Chile (35-40^{o}S). *Prog. Ocean.*, *92*, 1–7. doi: 10.1016/j.pocean.2011.07.019

Garreaud, R. (2000). Cold air incursions over subtropical south america: Mean structure and dynamics. *Monthly Weather Review*, *128*(7), 2544–2559.

Garreaud, R., & Muñoz, R. C. (2005). The low-level jet off the west coast of subtropical south america: Structure and variability. *Monthly Weather Review*, *133*(8), 2246–

2261.

Garreaud, R., & Rutllant, J. (2003). Coastal lows along the subtropical west coast of south america: Numerical simulation of a typical case. *Monthly Weather Review*, *131*(5), 891–908.

Garreaud, R., Rutllant, J., & Fuenzalida, H. (2002). Coastal lows along the subtropical west coast of south america: Mean structure and evolution. *Monthly Weather Review*, *130*(1), 75–88.

Garreaud, R. D., Gabriela Nicora, M., Bürgesser, R. E., & Ávila, E. E. (2014). Lightning in western patagonia. *Journal of Geophysical Research: Atmospheres*, *119*(8), 4471–4485.

Garreaud, R. D., Rutllant, J. A., Muñoz, R. C., Rahn, D. A., Ramos, M., & Figueroa, D. (2011). Vocals-cupex: the chilean upwelling experiment. *Atmospheric, Chemistry and Physics*.

Graham, W., Field, J., & Potts, D. (1992). Persistent "upwelling shadows" and their influence on zooplankton distributions. *Mar. Biol.*, *114*(4), 561–570.

Graham, W. M. (1993). Spatio-temporal scale assessment of an "upwelling shadow" in Northern Monterey Bay, California. *Estuaries*, *16*(1), 83–91. Retrieved from `http://dx.doi.org/10.2307/1352766` doi: 10.2307/1352766

Graham, W. M., & Largier, J. L. (1997). Upwelling shadows as nearshore retention sites: the example of northern Monterey Bay. *Cont. Shelf Res.*, *17*(5), 509–532.

Harding, L. W., Mallonee, M. E., Perry, E. S., Miller, W. D., Adolf, J. E., Gallegos, C. L., & Paerl, H. W. (2020). Seasonal to inter-annual variability of primary production in chesapeake bay: prospects to reverse eutrophication and change trophic classification. *Scientific reports*, *10*(1), 1–20.

Harvey, J. B., Ryan, J. P., & Zhang, Y. (2021). Influences of extreme upwelling on a coastal retention zone. *Frontiers in Marine Science*, *8*, 472.

Hernández, A., & Tapia, F. J. (2021). Connecting spatial structure in subtidal benthic communities with temporal variability in bottom temperature and dissolved oxygen along an upwelling coast. *Estuarine, Coastal and Shelf Science*, *250*, 107166.

Hernández, A., Tapia, F. J., Saldías, G. S., & Quiñones, R. A. (2021). Coastal geomorphology and oceanographic features shape subtidal benthic communities in management areas of central chile. *Aquatic Conservation: Marine and Freshwater Ecosystems*, *31*(1), 126–138.

Hernández-Miranda, E., Veas, R., Labra, F., Araneda, A., Carrasco, F., Salamanca, M., ... Quiñones, R. (2009). Biodiversidad del ecosistema costero adyacente a la desembocadura del río itata. *Ediciones Universidad de Concepciíon, Concepciíon, Chile*, 143–159.

Hersbach, H., Bell, B., Berrisford, P., Hirahara, S., Horányi, A., Muñoz-Sabater, J., ... others (2020). The era5 global reanalysis. *Quarterly Journal of the Royal Meteorological Society*, *146*(730), 1999–2049.

Hill, A., Hickey, B., Shillington, F., & Strub, P. (1998). *Eastern ocean boundaries coastal segment (e) in: Robinson ar, brink kh, editors. the sea. vol. 11.* New York, NY: John Wiley & Sons, Inc.

Jacob, B. G., Tapia, F. J., Quiñones, R. A., Montes, R., Sobarzo, M., Schneider, W., ... González, H. E. (2018). Major changes in diatom abundance, productivity, and net community metabolism in a windier and dryer coastal climate in the southern humboldt current. *Progress in Oceanography*, *168*, 196–209.

JPL-OurOcean-Project. (2011). *Ghrsst level 4 g1sst global foundation sea surface temperature analysis (gds version 1).* NOAA National Centers for Environmental Information. Dataset. https://www.ncei.noaa.gov/archive/accession/GHRSST-JPL_OUROCEAN-L4UHfnd-GLOB-G1SST. Accessed [2020-03-21].

Klein, W. H. (1958). The frequency of cyclones and anticyclones in relation to the mean circulation. *Journal of Atmospheric Sciences*, *15*(1), 98–102.

Krautz, M., Hernández-Miranda, E., Veas, R., Bocaz, P., Riquelme, P., & Quiñones, R. (2017). An estimate of the percentage of non-predatory dead variability in coastal zooplankton of the southern humboldt current system. *Marine environmental research*, *132*, 103–116.

Landaeta, M. F., & Castro, L. R. (2006). Spawning and larval survival of the Chilean hake Merluccius gayi under later summer conditions in the Gulf of Arauco, central Chile. *Fish. Res.*, *77*(1), 115–121.

Largier, J. L. (2020). Upwelling bays: How coastal upwelling controls circulation, habitat, and productivity in bays. *Annu. Rev. Mar. Sci.*, *12*.

Letelier, J., Pizarro, O., & Nuñez, S. (2009). Seasonal variability of coastal upwelling and the upwelling front off central Chile. *J. Geophys. Res. Oceans*, *114*(C12), 1–16. doi: 10.1029/2008JC005171

Leth, O., & Middleton, J. F. (2004). A mechanism for enhanced upwelling off central chile:

729 Eddy advection. *Journal of Geophysical Research: Oceans*, *109*(C12).

730 Lima, D. C., Soares, P. M., Semedo, A., & Cardoso, R. M. (2018). A global view of coastal
731 low-level wind jets using an ensemble of reanalyses. *Journal of Climate*, *31*(4), 1525–
732 1546.

733 Marengo, J., Cornejo, A., Satyamurty, P., Nobre, C., & Sea, W. (1997). Cold surges in
734 tropical and extratropical south america: The strong event in june 1994. *Monthly*
735 *Weather Review*, *125*(11), 2759–2786.

736 Marín, V., & Moreno, C. (2002). Wind driven circulation and larval dispersal: a review of
737 its consequences in coastal benthic recruitment. *The oceanography and ecology of the*
738 *nearshore and bays in Chile*, 47–63.

739 Marín, V. H., Delgado, L. E., & Escribano, R. (2003). Upwelling shadows at Mejillones Bay
740 (northern Chilean coast): a remote sensing in situ analysis. *Inv. Mar.*, *31*(2), 47–55.

741 Marín, V. H., Escribano, R., Delgado, L. E., Olivares, G., & Hidalgo, P. (2001). Nearshore
742 circulation in a coastal upwelling site off the northern Humboldt Current System.
743 *Cont. Shelf Res.*, *21*(13), 1317–1329.

744 Mesias, J. M., Matano, R. P., & Strub, P. T. (2001). A numerical study of the upwelling
745 circulation off central Chile. *J. Geophys. Res.: Oceans*, *106*(C9), 19611–19623. doi:
746 10.1029/2000JC000649

747 Montecinos, A., Munoz, R., Garreaud, R., Arriagada, A., Conejero, C., Morales, J., ...
748 Vizcarra, A. (2011). Experimiento de surgencia costera en el golfo de arauco (cupex-
749 ii). In *Segundo congreso de oceanografıa fısica, meteorologıa y clima.*

750 Montecinos, A., Muñoz, R. C., Oviedo, S., Martínez, A., & Villagrán, V. (2017). Climato-
751 logical characterization of puelche winds down the western slope of the extratropical
752 andes mountains using the ncep climate forecast system reanalysis. *Journal of Applied*
753 *Meteorology and Climatology*, *56*(3), 677–696.

754 Montes, C., Rutllant, J. A., Aguirre, A., Bascuñán-Godoy, L., & Juliá, C. (2016). Terral
755 de vicuña, a foehnlike wind in semiarid northern chile: Meteorological aspects and
756 implications for the fulfillment of chill requirements in deciduous fruit trees. *Journal*
757 *of Applied Meteorology and Climatology*, *55*(5), 1183–1196.

758 Morales, C. E., & Anabalón, V. (2012). Phytoplankton biomass and microbial abundances
759 during the spring upwelling season in the coastal area off concepción, central-southern
760 chile: Variability around a time series station. *Progress in Oceanography*, *92*, 81–91.

761 Muñoz, R. C., & Garreaud, R. (2005). Dynamics of the low-level jet off the west coast of

762 subtropical south america. *Monthly weather review*, *133*(12), 3661–3677.

763 Osma, N., Latorre-Melín, L., Jacob, B., Contreras, P. Y., von Dassow, P., & Vargas, C. A.
764 (2020). Response of phytoplankton assemblages from naturally acidic coastal ecosys-
765 tems to elevated pco2. *Frontiers in Marine Science*, *7*, 323.

766 Pawlowicz, R., Beardsley, B., & Lentz, S. (2002). Classical tidal harmonic analysis including
767 error estimates in matlab using t_tide. *Computers & Geosciences*, *28*(8), 929–937.

768 Rahn, D. A., & Garreaud, R. D. (2014). A synoptic climatology of the near-surface wind
769 along the west coast of South America. *Int. J. Climatol.*, *34*, 780–792. doi: 10.1002/
770 joc.3724

771 Rain-Franco, A., Rojas, C., & Fernandez, C. (2018). Potential effect of pesticides currently
772 used in salmon farming on photo and chemoautotrophic carbon uptake in central–
773 southern chile. *Aquaculture*, *486*, 271–284.

774 Ramp, S. R., Paduan, J. D., Shulman, I., Kindle, J., Bahr, F. L., & Chavez, F. (2005).
775 Observations of upwelling and relaxation events in the northern Monterey Bay during
776 August 2000. *J. Geophys. Res.*, *110*(C7), 1–21.

777 Renault, L., Dewitte, B., Falvey, M., Garreaud, R., Echevin, V., & Bonjean, F. (2009). Im-
778 pact of atmospheric coastal jet off central chile on sea surface temperature from satel-
779 lite observations (2000–2007). *Journal of Geophysical Research: Oceans*, *114*(C8).

780 Rosenfeld, L. K., Schwing, F. B., Garfield, N., & Tracy, D. E. (1994). Bifurcated flow from
781 an upwelling center: a cold water source for Monterey Bay. *Cont. Shelf Res.*, *14*(9),
782 931–964.

783 Roughan, M., Mace, A. J., Largier, J. L., Morgan, S. G., Fisher, J. L., & Carter, M. L.
784 (2005). Subsurface recirculation and larval retention in the lee of a small headland: a
785 variation on the upwelling shadow theme. *Journal of Geophysical Research: Oceans*,
786 *110*(C10).

787 Rutllant, J. (1993). Coastal lows and associated southerly winds events in north-central
788 chile. In *4th international conference on southern hemisphere meteorology and oceanog-*
789 *raphy. boston: American meteorological society* (pp. 268–269).

790 Rutllant, J. (1994). *On the generation of coastal lows in central chile* (Tech. Rep.). Inter-
791 national Centre for Theoretical Physics.

792 Rutllant, J., & Garreaud, R. (2004). Episodes of strong flow down the western slope of the
793 subtropical andes. *Monthly Weather Review*, *132*(2), 611–622.

794 Saavedra, N., & Foppiano, A. (1992). Monthly mean pressure model for chile. *International*

Journal of Climatology, *12*(5), 469–480.

Sánchez, G. E., Lange, C. B., González, H. E., Vargas, G., Muñoz, P., Cisternas, C., & Pantoja, S. (2012). Siliceous microorganisms in the upwelling center off concepción, chile (36° s): Preservation in surface sediments and downcore fluctuations during the past 150 years. *Progress in Oceanography*, *92*, 50–65.

Sherman, K., & Hempel, G. (2008). The unep large marine ecosystem report: A perspective on changing conditions in lmes of the world's regional seas. *np npub*.

Sobarzo, M., Saldías, G. S., Tapia, F. J., Bravo, L., Moffat, C., & Largier, J. L. (2016). On subsurface cooling associated with the Biobio River canyon (Chile). *J. Geophys. Res. Oceans*, *121*, 4568–4584. doi: 10.1002/2016JC011796

Strub, P. T., Mesĩas, J., Montecino, V., Rutlland, J., & Salinas, S. (1998). Coastal ocean circulation off western south America. In A. R. Robinson & K. H. Brink (Eds.), *The Sea: The Global Coastal Ocean, Regional Studies and Synthesis* (pp. 273–313). New York: John Wiley.

Thiel, M., Macaya, E., Acuña, E., Arntz, W. E., Bastías, H., & etal. (2007). The humboldt current system of northern and central chile: Oceanographic processes, ecological interactions and socioeconomic feedback. *Oceanog. and Mar. Biol.*, *45*, 195–344.

Valle-Levinson, A., Atkinson, L. P., Figueroa, D., & Castro, L. (2003). Flow induced by upwelling winds in an equatorward facing bay: Gulf of Arauco, Chile. *J. Geophys. Res. Oceans*, *108*(C2), 36-1–36-14. doi: 10.1029/2001JC001272

Vargas, C. A., Martínez, R. A., Cuevas, L. A., Pavez, M. A., Cartes, C., González, H. E., ... Daneri, G. (2007). The relative importance of microbial and classical food webs in a highly productive coastal upwelling area. *Limnology and Oceanography*, *52*(4), 1495–1510.

Vera, C. S., & Vigliarolo, P. K. (2000). A diagnostic study of cold-air outbreaks over south america. *Monthly Weather Review*, *128*(1), 3–24.

Wong, Z., Saldías, G. S., Largier, J. L., Strub, P. T., & Sobarzo, M. (2021). Surface thermal structure and variability of upwelling shadows in the gulf of arauco, chile. *Journal of Geophysical Research: Oceans*, e2020JC016194.

Woodson, C., Eerkes-Medrano, D., Flores-Morales, A., Foley, M., Henkel, S., Hessing-Lewis, M., ... others (2007). Local diurnal upwelling driven by sea breezes in northern Monterey Bay. *Cont. Shelf Res.*, *27*(18), 2289–2302.

Woodson, C., Washburn, L., Barth, J. A., Hoover, D., Kirincich, A. R., McManus, M., ...

828 Tyburczy, J. (2009). Northern Monterey Bay upwelling shadow front: Observations of
829 a coastally and surface-trapped buoyant plume. *J. Geophys. Res. Oceans*, *114*(C12),
830 1–15. doi: 10.1029/2009JC005623
831 Yannicelli, B., Castro, L. R., Valle-Levinson, A., Atkinson, L., & Figueroa, D. (2006).
832 Vertical distribution of decapod larvae in the entrance of an equatorward facing bay
833 of central Chile: implications for transport. *J. Plankton Res.*, *28*(1), 19–37.

5. DISCUSIÓN

El golfo de Arauco ha sido el centro de atención para distintos estudios oceanográficos y ambientales debido a sus particulares características físicas, biológicas, batimétricas, topográficas y, principalmente, por formar parte de una de las zonas de surgencia más importantes de los sistemas de corriente de borde oriental. Además, al ser un sector semicerrado, protegido de la influencia directa de los vientos favorables a surgencia, en su interior se desarrolla el proceso conocido como sombra de surgencia. Por lo anterior, esta tesis se orientó a comprender el mecanismo de formación de este proceso, forzantes involucrados y evolución en distintas escalas de variabilidad temporal.

Desde que Graham y Largier (1997) describieron y definieron el fenómeno de las sombras de surgencia, diversos investigadores de los sistemas de corrientes de borde oriental han estudiado este fenómeno con distintos enfoques. Los principales mecanismos físicos propuestos para explicar el calentamiento costero superficial durante un evento de relajación de la surgencia costera han sido la radiación solar entrante y la advección horizontal (Hamilton y Rattray Jr, 1978; Brink et al., 1981; Szoeke y Richman, 1981; Lentz, 1987; Dever y Lentz, 1994). Send et al. (1987) evaluaron los efectos topográficos de Point Reyes (38°N) y las variaciones espaciales en el campo de vientos favorables a surgencia sobre el calentamiento costero. Wang (1997) mostró que un rotor del viento positivo crea un fuerte gradiente de presión a lo largo de la costa con dirección hacia el polo. Este gradiente de presión induce una corriente costera hacia el polo dentro de la zona de surgencia durante la relajación, como fue observado por Send et al. (1987) y Largier et al. (1993). Otros estudios de sombras de surgencia se han enfocado en aspectos biológicos, dada la asociación de este proceso con la alta actividad biológica costera, incluyendo la dinámica de los bloom de algas nocivas (Graham et al., 1992; Graham y Largier, 1997; Marín et al., 2001; Pitcher et al., 2010; Torreblanca et al., 2016; Schulien et al., 2017). En el caso del GA, Letelier et al., (2009) reportaron sombras de surgencia asociadas con altas

concentraciones de clorofila-a, en tanto que Largier (2020) mencionó algunas características físicas que permiten clasificar al GA como una bahía de sombra de surgencia.

En este estudio se definió un índice de sombra de surgencia (USI) para la región costera donde se ubica el golfo de Arauco (Resultados: Capítulo 1), el cual permitió cuantificar la ocurrencia temporal, persistencia, e intensidad de estos eventos. Más del 89% de días con sombra de surgencia ocurrieron entre diciembre y marzo, con valores del USI mayores que 1.1$^°C. Estos eventos ocurrieron en condiciones de viento favorable a surgencia y bajo la influencia de un rotor negativo del viento (viento ciclónico). En la bahía de Monterey, Graham (1993) identificó sombras de surgencia durante primavera-verano, sugiriendo que este proceso es propio de épocas de surgencia en ambientes costeros de latitudes similares (Graham y Largier, 1997; Largier, 2020).

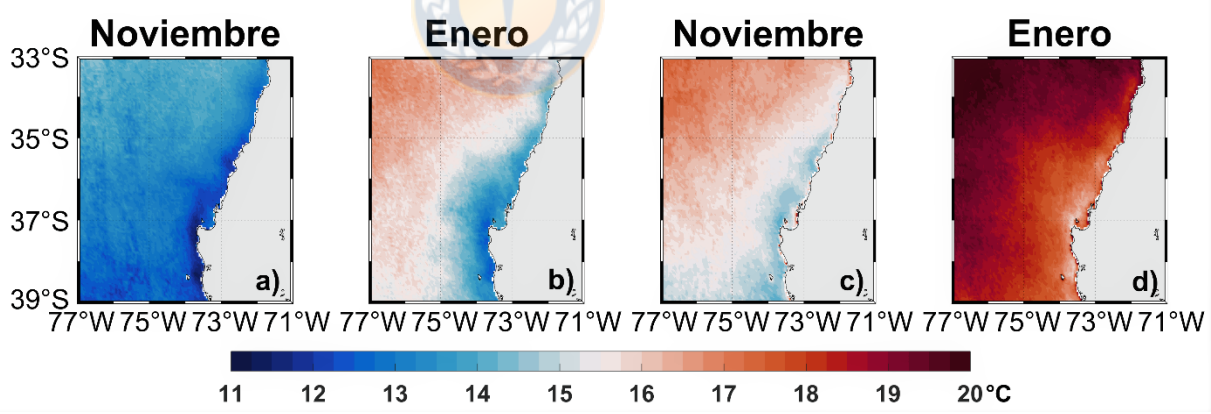

Figura 13. Promedio mensual de los valores mínimos (a y b) y máximos (c y d) de temperatura superficial del mar (TSM) del área de estudio para los meses de noviembre y enero (período 2002 - 2016). Datos: GOES-SST.

En Chile centro-sur la TSM tiene un ciclo estacional dependiente de la época del año (verano - otoño - invierno - primavera). Este trabajo demostró que la sombra de surgencia es más común en primavera-verano aun considerando que los promedios de la TSM varían según el mes (Figura 13). Estas diferencias en las condiciones térmicas

iniciales dan paso a dos escenarios distintos para el desarrollo de la sombra de surgencia: (i) sombras de surgencia en un ambiente frío (noviembre) y (ii) sombras de surgencia en un ambiente cálido (enero) (Resultados: Capítulo 1). Estas condiciones iniciales no habían sido estudiadas anteriormente.

El agua cálida superficial y la estratificación de la columna de agua dentro del golfo de Arauco durante la sombra de surgencia puede estar asociada a una débil circulación ciclónica debido a la presencia de PL (Penven et al., 2000; Pitcher et al., 2010; Largier, 2020). El estudio de corrientes al interior del golfo mostró que, en el sector de la cabecera, la circulación fluctúa desde 20 cm/s con dirección suroeste, antes de los eventos, a 5 cm/s con dirección noroeste en superficie y sur-sureste en profundidad durante la sombra de surgencia. En boca Chica, en tanto, fluctúa desde aproximadamente 20 cm/s con un flujo noroeste, a 10 cm/s con un flujo noroeste en superficie y hacia el este en el fondo, lo cual contribuye a la estratificación de la columna de agua especialmente en la cabecera del golfo. Por otra parte, el calentamiento superficial también puede estar relacionado con el calentamiento adiabático del aire que da paso a la formación de las BCD (Garreaud et al., 2002). Además, la lenta circulación sumada a la radiación solar entrante resulta en tiempos de residencia más largos dentro del GA. En la bahía de Monterey, también se observaron prolongados tiempos de residencia asociados a las sombras de surgencia Graham y Largier (1997); Ryan et al. (2014a,b).

De forma general la sombra de surgencia evoluciona en dos fases (Figura 14). La primera fase ocurre con la intensificación del estrés del viento hacia el Ecuador que incrementa el transporte de Ekman y genera la surgencia costera frente a PL. Contemporáneamente, al interior del GA el viento hacia el Ecuador es más débil debido a la presencia de la Cordillera de Nahuelbuta que se extiende hacia PL. Esta diferencia en la magnitud del estrés del viento facilita la generación de un rotor de viento ciclónico, favoreciendo la retención del agua dentro del GA y limitando el ingreso del agua fría de la surgencia, lo que contribuye con la diferencia térmica superficial entre PL y GA. La

segunda fase ocurre durante la relajación de los vientos favorables a surgencia. La duración de la relajación es crucial para el gradiente térmico zonal, porque puede causar el debilitamiento o destrucción de la sombra de surgencia (Figuras 9 y 10 del Capítulo 1 de Resultados).

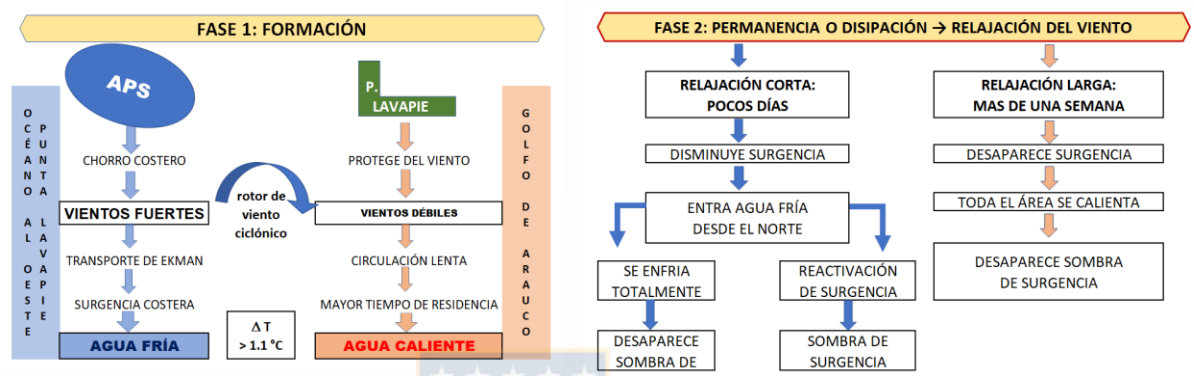

Figura 14. Bosquejo con las dos fases en la evolución de las sombras de surgencia en el golfo de Arauco.

Breves relajaciones (un par de días o menos) de los vientos favorables a surgencia promueven la advección desde el norte hacia el interior del golfo, de aguas superficiales frías de la surgencia, causando un enfriamiento superficial y un debilitamiento del gradiente térmico entre PL y GA. Este ingreso de agua fría superficial hacia el sistema semicerrado también se ha reportado para la bahía de Monterey (Tracy, 1990; Graham et al., 1992; Rosenfeld et al., 1994). Relajaciones de viento de más de una semana conllevan a la disolución del gradiente térmico entre PL y GA debido a la ausencia de agua fría de surgencia frente a PL. Los períodos de relajación también contribuyen con el incremento del tiempo de residencia del GA. En la bahía de Monterey, las relajaciones del viento fueron consideradas una fuente esencial de la variabilidad en la sombra de surgencia (Graham y Largier, 1997). Otro factor que podría aumentar el calentamiento dentro del GA es una inversión del viento dentro del golfo, facilitando la advección del agua cálida superficial desde el norte.

Si bien el APS es responsable de la variabilidad de vientos favorables a surgencia frente a las costas de Chile (Garreaud et al., 2002; Renault et al., 2012; Rahn y Garreaud, 2014; Ancapichun, 2015), el paso de anticiclones migratorios que derivan hacia el Este alrededor de los 40°S, genera un gradiente de presión meridional que modifica el patrón de vientos (Garreaud et al., 2002). La presencia de la cordillera de los Andes causa un desbalance de los vientos zonales en los niveles de baja altura lo que, por un lado, intensifica los vientos meridionales fortaleciendo el chorro costero hacia el Ecuador (Rahn y Garreaud, 2014; Aguirre et al., 2021) generando, consecuentemente, una intensificación de la surgencia costera (Aguirre et al., 2019) y, por otro lado, el aire que circula libremente desde el Este por sobre la cordillera comienza a descender cordillera abajo con dirección hacia el Oeste. Debido al aumento de la presión atmosférica con la disminución de la altura esta masa de aire experimenta calentamiento adiabático dando inicio a la formación de la baja costera (Garreaud et al., 2002). Este proceso de aumento de la temperatura superficial del aire contribuye al calentamiento superficial del golfo y fortalece la sombra de surgencia. Por otra parte, el descenso de este aire cálido y seco inhibe la formación de nubes dejando el cielo despejado y permitiendo que ingrese mayor radiación solar de onda corta en el área, lo que también favorecería el aumento de la TSM de la sombra de surgencia. La Figura 15 muestra un esquema del proceso descrito previamente.

Las diferencias relativas de TSM entre el GA y PL también varían a escala interanual. En el análisis de la TSM del Capítulo 1, se observó la presencia de una fase cálida y una fase fría. Durante la fase cálida (2002-2006) una anomalía positiva de alrededor de 1°C facilitó la ocurrencia de los eventos de sombra de surgencia debido a la predominancia de aguas cálidas que incrementaron el contraste entre las aguas frías frente a PL con las aguas cálidas en el GA. Saldías et al. (2016) y Schneider et al. (2017), atribuyeron este cambio de una fase cálida (2002 a 2006) a una fase fría (iniciando en 2007) al desplazamiento hacia el sur del sistema de alta presión del Pacífico sur durante los meses de invierno y a la influencia de la dinámica interanual del ENSO. La influencia de El Niño sobre la TSM también fue descrita por Graham y Largier (1997) en la bahía

de Monterey, pero con temperaturas más homogéneas horizontalmente durante el evento ENSO cálido de 1992, lo opuesto al caso del golfo de Arauco en el centro-sur de Chile.

Un factor que no queda claro aún, debido a la falta de información, es el rol de la Isla Santa María en favorecer o no el desarrollo de las sombras de surgencia en el GA. Si bien la presencia de esta isla explica que boca Chica sea un sector angosto y poco profundo, al punto de limitar el intercambio de agua entre el golfo y las aguas oceánicas (Valle-Levinson et al., 2003), también podría considerarse como una extensión geográfica de PL. Desde este punto de vista estaría incrementando potencialmente la circulación ciclónica dentro de GA. Sin embargo, la presencia de esta isla podría también causar un efecto opuesto, debilitando la circulación ciclónica dentro del golfo. Futuras investigaciones podrían contribuir al esclarecimiento del rol de esta isla en la dinámica del golfo de Arauco.

A partir de estas premisas se rechaza la primera hipótesis ya que la SS en el golfo inicia y se mantiene con la intensificación de los vientos provenientes del suroeste que generan la surgencia costera; y que, durante los periodos de relajación de estos vientos (o inversión de los mismos a viento norte) más que intensificar la SS, la debilita o disipa totalmente. Además, la lenta circulación al interior del GA y la estimación de la advección meridional de agua superficial durante la SS solo explicarían un bajo porcentaje del calentamiento superficial asociado a la SS.

Por otro lado, considerando que: a) el rotor del viento sumado a la radiación solar entrante pueden explicar entre el 40% y 70%, b) la lenta circulación al interior del golfo facilita la estratificación de la columna de agua y por ende un mayor calentamiento superficial, c) el patrón de anomalías de presión atmosférica a nivel del mar asociado al paso de ACM, que son procesos de escala sinóptica, es coherente con el patrón de anomalías de TSM que representa las SS y que, d) la estimación de los flujos radiativos

durante el desarrollo de las BC indican una mayor intensificación de las SS, se acepta la segunda hipótesis.

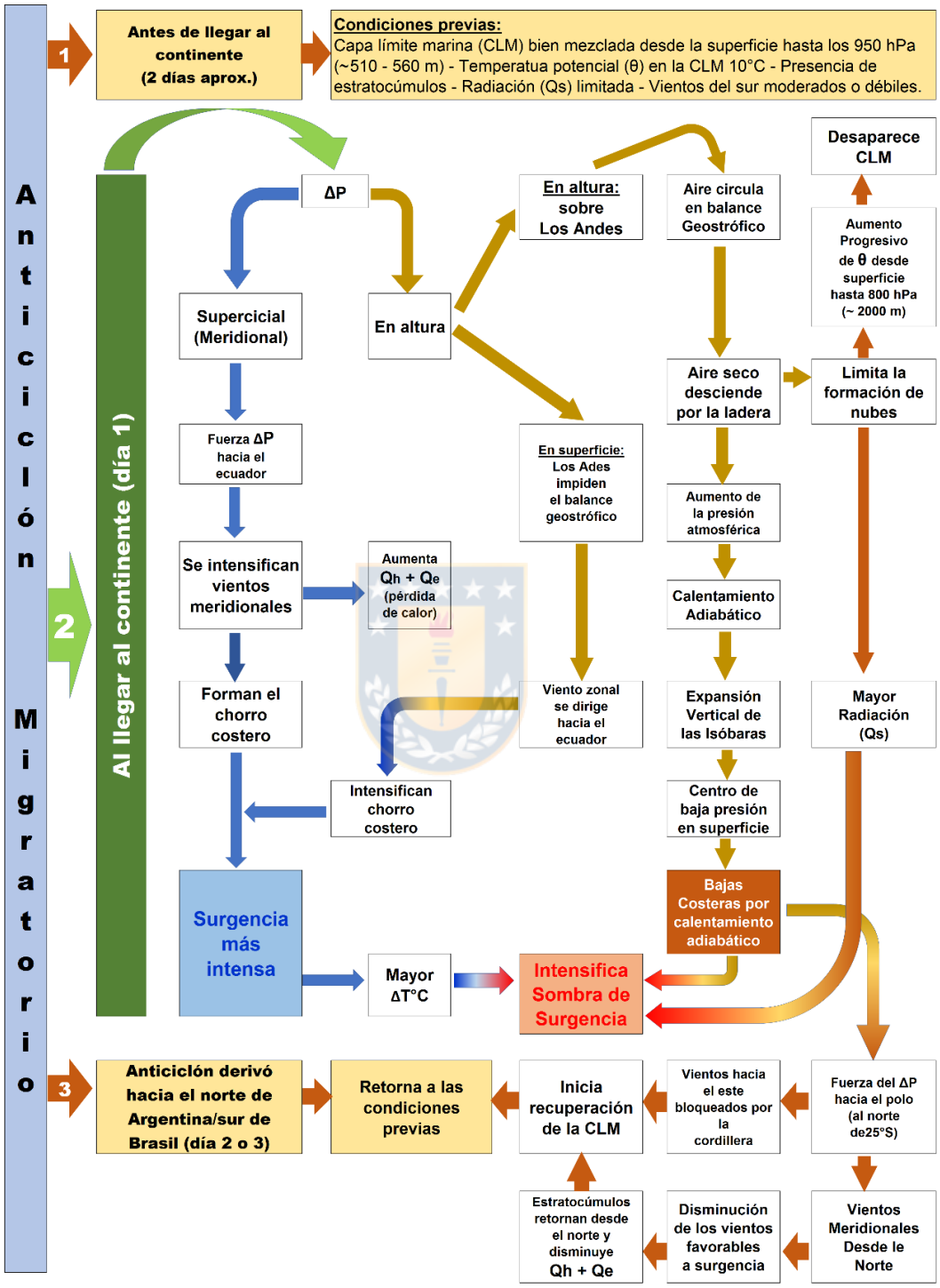

Figura 15. Esquema para representar el proceso de formación de las BC, durante el paso de un ACM en 3 etapas: 1) antes de llegar a la costa, 2) al llegar al continente y 3) una vez que el anticiclón ha avanzado hasta la parte norte de Argentina.

6. CONCLUSIONES

La presente tesis ha permitido ampliar el conocimiento sobre la formación y evolución de los eventos de sombra de surgencia, específicamente dentro del golfo de Arauco en el centro-sur de Chile, en una de las zonas de surgencia más importantes de los sistemas de corriente de borde oriental. Probablemente, este fenómeno representa uno de los mecanismos físicos en primavera verano más relevantes para la oceanografía superficial del GA con repercusiones ecológicas todavía no completamente dilucidadas. A continuación, se puntualizan las principales conclusiones de esta tesis:

1. A través del Índice de Sombra de Surgencia (USI) desarrollado en esta tesis, se encontró que en el golfo de Arauco (GA) las sombras de surgencia (SS) ocurren en promedio durante 37 días al año (~ 10.5%), y fueron más frecuentes entre el 2002 y 2006 (~ 16.5%, 60 días por año). Su presencia se restringe a la época de primavera-verano, siendo más frecuentes en los meses de diciembre (~ 50% del mes), enero (~ 25% del mes) y febrero (~ 25% del mes), en condiciones de vientos favorables a surgencia (magnitud > 5 m/s y estrés del viento de hasta 0.4 N m^{-2}). Debido a la aguda geometría de la línea de costa en punta Lavapié (PL), que protege al golfo de estos vientos, las SS también van acompañadas de un intenso rotor ciclónico del estrés del viento (alrededor de -20*10^{-7} Nm^{-3}).

2. La duración e intensidad de los eventos de sombras de surgencia depende de las condiciones térmicas iniciales (según la época del año) en el GA y de la persistencia e intensidad de los vientos hacia el Ecuador. Esto genera dos escenarios diferentes para el desarrollo de la sombra de surgencia: (i) sombras de surgencia en un ambiente frío (nov-dic) con una TSM regional promedio de ~ 15°C, valores de USI más bajos (~ 1.34°C en promedio) y con la sombra de surgencia restringida dentro del golfo con duraciones que no pasan de los 3 o 4 días consecutivos; y (ii) sombras de surgencia en un ambiente cálido (Ene-Feb) con una TSM regional promedio de ~ 17°C y con altos valores de USI (~ 1.42°C en promedio). En este escenario la sombra de surgencia puede extenderse desde el golfo

hacia el norte por decenas de kilómetros a lo largo de la costa. Bajo condiciones particulares, estos eventos pueden sobrepasar los 10 días consecutivos. Durante el periodo 2002 - 2016 (Capítulo 1 de Resultados) los eventos más largos se observaron en el mes de enero de los años 2004, 2005 y 2006 con una duración de 16, 11 y 30 días, respectivamente.

3. Los períodos de relajación de los vientos favorables a surgencia tienen un rol clave en la duración de la sombra de surgencia. Breves períodos de relajación de la surgencia (un par de días o menos) pueden disipar parcial o totalmente la sombra de surgencia debido al ingreso, desde el norte, de aguas de surgencia al golfo. Estos períodos de relajación favorecen el incremento del tiempo de residencia del GA y el posterior calentamiento debido a la radiación solar entrante y, consecuentemente, el fortalecimiento de la sombra. Por otro lado, períodos de relajación de más de una semana disipan totalmente el gradiente térmico debido al calentamiento general de la zona de estudio en estas condiciones.

4. Un patrón de anomalías positivas (4 hPa) de la presión atmosférica a nivel del mar entre 40°S y 50°S, y anomalías negativas (-2 hPa) al norte de 37°S es coherente con el patrón de anomalías positivas de TSM (2°C) y de vientos (1 m/s) al interior del GA y anomalías negativas de TSM (-1°C) y positivas de viento (4 m/s) al oeste de PL. Esto sugiere que las sombras de surgencia en el GA también están fuertemente influenciadas por condiciones atmosféricas locales como las BC (áreas de baja presión al norte del golfo) asociadas al paso de ACM. El paso de estos anticiclones más al sur de PL genera un gradiente de presión atmosférica meridional que promueve la intensificación de los vientos del chorro costero y por ende fortalecen la surgencia costera al oeste de PL, aumentando la diferencia de TSM entre PL y GA (3°C). A baja altura, el viento zonal es bloqueado por la cordillera de los Andes, siendo forzado a fluir hacia el Ecuador. Por otra parte, el viento en altura (que sí está en balance geostrófico) desciende por la cordillera y se calienta adiabáticamente debido al aumento de presión. Este calentamiento, además de

contribuir al incremento de la TSM dentro del golfo, favorece condiciones de cielo despejado permitiendo que ingrese mayor radiación solar al sistema, lo que también intensifica la sombra de surgencia. Hacia el norte de la BC se forma un gradiente meridional en sentido contrario al formado por el ACM lo que genera un débil viento norte que se opone a los vientos del chorro costero y que, junto con el ACM derivando hacia el norte de Argentina, hacen que todo el sistema vuelva a sus condiciones iniciales.

5. El estrés del viento y la radiación solar entrante en superficie pueden explicar hasta el 40% de la varianza del USI entre los meses de diciembre y marzo. En algunos años, este porcentaje fue incluso mayor que 70% durante los meses de diciembre y febrero. Esto sugiere que la radiación solar entrante es una de las variables que más aporta al calentamiento dentro del GA. Días nublados antes y después de los eventos de sombra de surgencia limitan la cantidad de radiación que llega a la superficie (ejemplo ~ 500 - 750 W/m^2 en C1, Capítulo 2 de Resultados). Periodos de relajación de los vientos disminuyen el intercambio de calor entre el océano y la atmósfera (Qh y Qe). La intensificación de los vientos del chorro costero fortalece los flujos convectivos, promoviendo la pérdida de calor por parte del océano (Qh + Qe =$ ~100 W/m^2). Sin embargo, cielos despejados asociados al desarrollo de las bajas costeras permiten el ingreso de una mayor radiación solar en superficie, lo que compensa la pérdida de calor de estos flujos, favoreciendo la sombra de surgencia al aumentar la diferencia de temperatura entre PL y GA (> 3°C).

6. La lenta circulación al interior de GA durante los eventos de SS que, en la cabecera del golfo presenta velocidades de alrededor de 5 cm/s con dirección norte y en Boca Chica velocidades de 10 cm/s saliendo del golfo, contribuye a la estratificación de la columna de agua limitando el intercambio vertical y promoviendo un mayor calentamiento superficial intensificando, así, la sombra de surgencia.

7. Una estimación de la advección meridional de agua cálida desde el norte sugiere cambios de temperatura al interior del golfo de alrededor de 0.25 - 0.5°C/día, explicando

solo parcialmente el calentamiento inicial de las sombras de surgencia ya que las tasas de calentamiento observadas fueron > 1$^°C/día y en algunos casos alcanzando hasta los 2.5°C/día.

8. Procesos a mayor escala como lo son el desplazamiento del sistema de alta presión del Pacífico Sur y la influencia de la dinámica interanual del ENSO, a los que se le atribuye el cambio de una fase cálida (2002-2006) a una fase fría (2007 - 2012), también tienen un impacto en los eventos de sombras de surgencia. Es así que, durante la fase cálida, anomalías positivas (~1°C) facilitaron una mayor ocurrencia de eventos de sombra de surgencia al interior del golfo, registrándose el 53% de los días con sombra de surgencia en esta fase (5 años) con valor de USI promedio de 1.43°C. El otro 47% (fase fría) se observó en los 10 años siguientes, con un USI promedio de 1.25°C. Los meses que presentaron una mayor disminución en la ocurrencia de sombras de surgencia fueron noviembre y febrero, con una reducción del 80% y 71%, respectivamente. A pesar de la baja correlación entre la TSM y las anomalías del estrés del viento (r=0.25 para el GA y r=0.35 para PL), las fases cálida y fría presentaron una similitud con la variabilidad interanual del estrés del viento a lo largo de costa, mostrando anomalías negativas (positivas) durante la fase cálida (fría) indicando vientos favorables a surgencia menos (más) intensos.

9. Considerando que la surgencia costera está directamente influenciada por la variabilidad del viento, y que la formación de los anticiclones migratorios (ACM) es una característica común de las latitudes medias en ambos hemisferios, esta tesis contribuye, además, a explicar cómo estos mecanismos impactan la surgencia costera y consecuentemente las sombras de surgencia en bahías similares alrededor del mundo (por ejemplo, bahía de Monterey en el HN). Variaciones en la frecuencia de los anticiclones migratorios (Aguirre et al., 2021), podrían afectar la intensidad o incluso duración de los eventos de sombras de surgencia lo cual requerirá estudios más detallados.

10. En un contexto biológico, el incremento de la TSM, la débil circulación, y la estratificación de la columna de agua asociada a la presencia de la sombra de surgencia afecta la productividad biológica debido a la disminución en el intercambio advectivo del agua, generando un área de retención del plancton dentro de las bahías protegidas, lo que también limita los transportes de intercambio de aguas costeras y oceánicas. En este caso, la presencia de las sombras de surgencia en el golfo podría ser la explicación de registros de un orden de magnitud más alto en cuanto a la abundancia de zooplancton, holoplancton y meroplancton, principalmente en verano Krautz et al. (2017). Estos cambios deben ser evaluados incluyendo los parámetros biológicos necesarios.

BIBLIOGRAFÍA

Aguirre, C., Flores-Aqueveque, V., Vilches, P., Vásquez, A., y Rutllant, José A y Garreaud, R. (2021). Recent changes in the low-level jet along the subtropical west coast of South America. Atmosphere, 12(4):465.

Aguirre, C., Pizarro, Ó., Strub, P. T., Garreaud, R., y Barth, J. A. (2012). Seasonal dynamics of the near-surface alongshore flow off central chile. J. Geophys. Res. Oceans, 117(C1).

Aguirre, C., Rojas, M., Garreaud, R. D., y Rahn, D. A. (2019). Role of synoptic activity on projected changes in upwelling-favourable winds at the ocean's eastern boundaries. npj Clim. Atmos. Sc., 2(1):1–7.

Aiken, C. M., Castillo, M. I., y Navarrete, S. A. (2008). A simulation of the Chilean Coastal Current and associated topographic upwelling near Valparaíso, Chile. Cont. Shelf Res., 28(17):2371–2381.

Ancapichun, Santiago y Garcés-Vargas, J. (2015). Variability of the Southeast Pacific Subtropical Anticyclone and its impact on sea surface temperature off north-central Chile. Cienc. Mar., 41(1):1–20.

Ancapichún, S. (2012). Variabilidad del anticiclón del Pacífico sur y su relación con la oscilación decadal del Pacífico: Implicancias oceanográficas a lo largo de la costa centro-norte de Chile. PhD thesis, Universidad Austral de Chile.

Bakun, A. (1973). Coastal upwelling indices, west coast of North America. US Department of Commerce. NOAA Technical Report, NMFS SSRF-671.

Bakun, Andrew y Nelson, C. S. (1991). The seasonal cycle of wind-stress curl in subtropical eastern boundary current regions. J. Phys. Oceanogr., 21(12):1815–1834.

Barrett, Bradford S y Hameed, S. (2017). Seasonal variability in precipitation in central and southern Chile: Modulation by the South Pacific high. Journal of Climate, 30(1):55–69.

Blanco, J. L., Carr, M.-E., Thomas, A. C., y Strub, P. T. (2002). Hydrographic conditions off northern Chile during the 1996–1998 La Niña and El Niño events. J. of Geophysical Research: Oceans, 107(C3):3–1.

Bravo, L., Ramos, M., Sobarzo, M., Pizarro, O., y Valle-Levinson, A. (2013). Barotropic and baroclinic semidiurnal tidal currents in two contrasting coastal upwelling zones of Chile. J. Geophys. Res.: Oceans, 118(3):1226–1238.

Brink, K., Jones, B., Van Leer, J., Mooers, C., Stuart, D., Stevenson, M., Dugdale, R., y Heburn, G. (1981). Physical and biological structure and variability in an upwelling center off Peru near 15°S during March, 1977. Coast. Upwell., 1:473–495.

Castilla, J., Lagos, N., Guiñez, R., y Largier, J. (2002). Embayments and nearshore retention of plankton: the Antofagasta bay and other examples. The oceanography and ecology of the nearshore and bays in Chile, pages 179–203.

Dever, E. P. y Lentz, S. (1994). Heat and salt balances over the northern California shelf in winter and spring. J. Geophys. Res.: Oceans, 99(C8):16001–16017.

Devis-Morales, A., Montoya-Sánchez, R., Bernal, G., y Osorio, A. (2017). Assessment of extreme wind and waves in the Colombian Caribbean sea for offshore applications. Appl. Ocean Res., 69:10–26.

Fahad, A. A., Burls, N. J., Swenson, E. T., y Straus, D. M. (2020). The influence of south pacific convergence zone heating on the south pacific subtropical anticyclone and southern hemisphere storm tracks. Earth and Space Science Open Archive ESSOAr.

Figueroa, D. y Moffat, C. (2000). On the influence of topography in the induction of coastal upwelling along the Chilean coast. Geophys. Res. Lett., 27(23):3905–3908.

Fonseca, T. (1985). Física de las aguas costeras de la zona central de Chile. Tralka, 4(2):337–354.

Garcés-Vargas, J. y Abarca-del Río, R. (2012). The surface heat fluxes along the Eastern Pacific coast from 10°N to 40°S. Australian Meteorological and Oceanographic Journal, 62(2):71.

Garreaud, RenéD y Rutllant, J. (2003). Coastal lows along the subtropical west coast of South America: Numerical simulation of a typical case. Monthly Weather Review, 131(5):891–908.

Garreaud, R., Rutllant, J., y Fuenzalida, H. (2002). Coastal lows along the subtropical west coast of South America: Mean structure and evolution. Monthly Weather Review, 130(1):75–88.

Graham, W., Field, J., y Potts, D. (1992). Persistent "upwelling shadows" and their influence on zooplankton distributions. Mar. Biol., 114(4):561–570.

Graham, W. M. (1993). Spatio-temporal scale assessment of an "upwelling shadow" in Northern Monterey Bay, California. Estuaries, 16(1):83–91.

Graham, W. M. y Largier, J. L. (1997). Upwelling shadows as nearshore retention sites: the example of northern Monterey Bay. Cont. Shelf Res., 17(5):509–532.

Hamilton, P. y Rattray Jr, M. (1978). A numerical model of the depth-dependent, wind-driven upwelling circulation on a continental shelf. J. Phys. Oceanogr., 8(3):437–457.

Holton, J. R. (1973). An introduction to dynamic meteorology. American Journal of Physics, 41(5):752–754.

Inzunza, J. (2012). Meteorología descriptiva. Departamento de Geofísica, Universidad de Concepción, Concepción, pages 225–260.

Kaplan, D. M., Largier, J. L., Navarrete, S., Guiñez, R., y Castilla, J. C. (2003). Large diurnal temperature fluctuations in the nearshore water column. Estuarine, Coastal and Shelf Science, 57(3):385–398.

Krautz, M., Hernández-Miranda, E., Veas, R., Bocaz, P., Riquelme, P., y Quiñones, R. (2017). An estimate of the percentage of non-predatory dead variability in coastal zooplankton of the southern humboldt current system. Marine environmental research, 132:103–116.

Landaeta, M. F. y Castro, L. R. (2006). Spawning and larval survival of the Chilean hake Merluccius gayi under later summer conditions in the Gulf of Arauco, central Chile. Fish. Res., 77(1):115–121.

Largier, J., Magnell, B., y Winant, C. (1993). Subtidal circulation over the northern California shelf. J. Geophys. Res.: Oceans, 98(C10):18147–18179.

Largier, J. L. (2020). Upwelling bays: How coastal upwelling controls circulation, habitat, and productivity in bays. Annu. Rev. Mar. Sci., 12.

Lentz, S. J. (1987). A heat budget for the northern California shelf during CODE 2. J. Geophys. Res.: Oceans, 92(C13):14491–14509.

Letelier, J., Pizarro, O., y Nuñez, S. (2009). Seasonal variability of coastal upwelling and the upwelling front off central Chile. J. Geophys. Res. Oceans, 114(C12):1–16.

Marín, V. H., Delgado, L. E., y Escribano, R. (2003). Upwelling shadows at Mejillones Bay (northern Chilean coast): a remote sensing in situ analysis. Inv. Mar., 31(2):47–55.

Marín, V. H., Escribano, R., Delgado, L. E., Olivares, G., y Hidalgo, P. (2001). Nearshore circulation in a coastal upwelling site off the northern Humboldt Current System. Cont. Shelf Res., 21(13):1317–1329.

Montecinos, A., Muñoz, R. C., Oviedo, S., Martínez, A., y Villagrán, V. (2017). Climatological characterization of puelche winds down the western slope of the extratropical andes mountains using the ncep climate forecast system reanalysis. J. Appl. Met. Climatol., 56(3):677–696.

Muñoz, R. C. y Garreaud, R. (2005). Dynamics of the low-level jet off the west coast of subtropical south america. Mont. Weather Rev., 133(12):3661–3677.

Pawlowicz, R., Beardsley, B., y Lentz, S. (2002). Classical tidal harmonic analysis including error estimates in matlab using t_tide. Computers & Geosciences, 28(8):929–937.

Penven, P., Claude, R., De Verdière, A. C., y Largier, J. (2000). Simulation of a coastal jet retention process using a barotropic model. Oceanol. Acta, 23(5):615–634.

Pitcher, G., Figueiras, F., Hickey, B., y Moita, M. (2010). The physical oceanography of upwelling systems and the development of harmful algal blooms. Prog. Oceanogr., 85(1-2):5–32.

Rahn, D. A. y Garreaud, R. D. (2014). A synoptic climatology of the near-surface wind along the west coast of South America. Int. J. Climatol., 34:780–792.

Ramp, S. R., Paduan, J. D., Shulman, I., Kindle, J., Bahr, F. L., y Chavez, F. (2005). Observations of upwelling and relaxation events in the northern Monterey Bay during August 2000. J. Geophys. Res., 110(C7):1–21.

Renault, L., Dewitte, B., Marchesiello, P., Illig, S., Echevin, V., Cambon, G., Ramos, M., Astudillo, O., Minnis, P., y Ayers, J. K. (2012). Upwelling response to atmospheric coastal jets off central Chile: A modeling study of the October 2000 event. J. Geophys. Res. Oceans, 117(C2).

Rosenfeld, L. K., Schwing, F. B., Garfield, N., y Tracy, D. E. (1994). Bifurcated flow from an upwelling center: a cold water source for Monterey Bay. Cont. Shelf Res., 14(9):931–964.

Rosman, J. H., Koseff, J. R., Monismith, S. G., y Grover, J. (2007). A field investigation into the effects of a kelp forest (Macrocystis pyrifera) on coastal hydrodynamics and transport. J. Geophys. Res. Oceans, 112(C2).

Rutllant, J. (1994). On the generation of coastal lows in central Chile. Technical report, International Centre for Theoretical Physics.

Rutllant, J. y Fuenzalida, H. (1991). Synoptic aspects of the central Chile rainfall variability associated with the southern oscillation. Int. J. Climatol., 11(1):63–76.
Rutllant, J. y Garreaud, R. (1995). Meteorological air pollution potential for Santiago, Chile: towards an objective episode forecasting. Env. Monit. Asses., 34(3):223–244.
Rutllant, J. y Garreaud, R. (2004). Episodes of strong flow down the western slope of the subtropical Andes. Mont. Weather Rev., 132(2):611–622.
Rutllant, J. A., Rosenbluth, B., y Hormazabal, S. (2004). Intraseasonal variability of wind-forced coastal upwelling off central Chile (30°s). Cont. Shelf Res., 24(7-8):789–804.
Ryan, J., Harvey, J., Zhang, Y., y Woodson, C. (2014a). Distributions of invertebrate larvae and phytoplankton in a coastal upwelling system retention zone and peripheral front. J. Exper. Mar. Biol. Ecol., 459:51–60.
Ryan, J., McManus, M., Kudela, R., Artigas, M. L., Bellingham, J., Chavez, F., Doucette, G., Foley, D., Godin, M., Harvey, J., et al. (2014b). Boundary influences on HAB phytoplankton ecology in a stratification-enhanced upwelling shadow. Deep-Sea Res. II, 101:63–79.
Saldías, G. S., Largier, J. L., Mendes, R., Pérez-Santos, I., Vargas, C. A., y Sobarzo, M. (2016). Satellite-measured interannual variability of turbid river plumes off central-southern Chile: Spatial patterns and the influence of climate variability. Prog. Oceanogr., 146:212–222.
Schneider, W., Donoso, D., Garcés-Vargas, J., y Escribano, R. (2017). Water column cooling and sea surface salinity increase in the upwelling region off central-south Chile driven by a poleward displacement of the South Pacific High. Prog. Oceanogr., 151:38–48.
Schulien, J. A., Peacock, M. B., Hayashi, K., Raimondi, P., y Kudela, R. M. (2017). Phytoplankton and microbial abundance and bloom dynamics in the upwelling shadow of Monterey Bay, California, from 2006 to 2013. Mar. Ecol. Progr. Ser., 572:43–56.
Send, U., Beardsley, R. C., y Winant, C. D. (1987). Relaxation from upwelling in the coastal ocean dynamics experiment. J. Geophys. Res. Oceans, 92(C2):1683–1698.
Sobarzo, M., Bravo, L., Donoso, D., Garcés-Vargas, J., y Schneider, W. (2007). Coastal upwelling and seasonal cycles that influence the water column over the continental shelf off central Chile. Prog. Oceanogr., 75:363–382.
Sobarzo, M. y Djurfeldt, L. (2004). Coastal upwelling process on a continental shelf limited by submarine canyons, Concepción, central Chile. J. Geophys. Res. Oceans, 109(C12):1–20.
Stewart, R. H. (2008). Introduction to physical oceanography. Robert H. Stewart.
Strub, P. T., Mesías, J., Montecino, V., Rutlland, J., y Salinas, S. (1998). Coastal ocean circulation off western south America. In Robinson, A. R. y Brink, K. H., editors, The Sea: The Global Coastal Ocean, Regional Studies and Synthesis, pages 273–313. John Wiley, New York.
Szoeke, R. D. y Richman, J. (1981). The role of wind-generated mixing in coastal upwelling. J. Phys. Oceanogr., 11(11):1534–1547.

Talley, L. D. (2011). Descriptive physical oceanography: an introduction. Academic Press.
Tomczak, M. y Godfrey, J. S. (2003). Regional oceanography: an introduction. Daya books.
Torreblanca, M. L., Pérez-Santos, I., San Martín, B., Varas, E., Zilleruelo, R., Riquelme-Bugueño, R., y Palma, Á. T. (2016). Seasonal dynamics of zooplankton in a northern Chile bay exposed to upwelling conditions. Rev. Biol. Mar Oceanogr., 51(2):273–291.
Tracy, D. E. (1990). Source of cold water in monterey bay observed by avhrr satellite imagery. Technical report, Naval Postgraduate School, Monterey, California.
Valle-Levinson, A., Atkinson, L. P., Figueroa, D., y Castro, L. (2003). Flow induced by upwelling winds in an equatorward facing bay: Gulf of Arauco, Chile. J. Geophys. Res. Oceans, 108(C2):36–1–36–14.
Wallace, J. M. y Hobbs, P. V. (2006). Atmospheric science: an introductory survey, volume 92. Elsevier.
Wang, D.-P. (1997). Effects of small-scale wind on coastal upwelling with application to Point Conception. J. Geophys. Res. Oceans, 102(C7):15555–15566.
Weidberg, N., Ospina-Alvarez, A., Bonicelli, J., Barahona, M., Aiken, C. M., Broitman, B. R., y Navarrete, S. A. (2020). Spatial shifts in productivity of the coastal ocean over the past two decades induced by migration of the Pacific Anticyclone and Bakun's effect in the Humboldt Upwelling Ecosystem. Global and Planetary Change, 193:103259.
Wong, Z., Saldías, G. S., Largier, J. L., Strub, P. T., y Sobarzo, M. (2021). Surface thermal structure and variability of upwelling shadows in the Gulf of Arauco, Chile. J. Geophys. Res. Oceans, page e2020JC016194.
Woodson, C., Eerkes-Medrano, D., Flores-Morales, A., Foley, M., Henkel, S., Hessing-Lewis, M., Jacinto, D., Needles, L., Nishizaki, M., O'Leary, J., et al. (2007). Local diurnal upwelling driven by sea breezes in northern Monterey Bay. Cont. Shelf Res., 27(18):2289–2302.
Woodson, C., Washburn, L., Barth, J. A., Hoover, D., Kirincich, A. R., McManus, M., Ryan, J. P., y Tyburczy, J. (2009). Northern Monterey Bay upwelling shadow front: Observations of a coastally and surface-trapped buoyant plume. J. Geophys. Res. Oceans, 114(C12):1–15.
Zhang, Y., Bellingham, J. G., Ryan, J. P., y Godin, M. A. (2015). Evolution of a physical and biological front from upwelling to relaxation. Cont. Shelf Res., 108:55–64.